The Cyprus Institute
RESEARCH·TECHNOLOGY·INNOVATION

BASIC GUIDELINES
FOR THE EXCAVATION AND STUDY OF HUMAN SKELETAL REMAINS

The Cyprus Institute
Science and Technology in Archaeology and Culture Research Center (STARC)

Guide No. 1

Authors:
Efthymia Nikita & Anna Karligkioti

Reviewers:
Kathryn Marklein, University of Louisville • Ioanna Moutafi, University of Cambridge • Christina Papageorgopoulou, Democritus University of Thrace • Niki Papakonstantinou, Aristotle University of Thessaloniki • Paraskevi Tritsaroli, University of Groningen

Version 1.0 Nicosia, 2019

BASIC GUIDELINES
FOR THE EXCAVATION AND STUDY OF HUMAN SKELETAL REMAINS

The Cyprus Institute
Science and Technology in Archaeology and Culture Research Center (STARC)

Guide No. 1

Authors:
Efthymia Nikita & Anna Karligkioti

Reviewers:
Kathryn Marklein, University of Louisville • Ioanna Moutafi, University of Cambridge • Christina Papageorgopoulou, Democritus University of Thrace • Niki Papakonstantinou, Aristotle University of Thessaloniki • Paraskevi Tritsaroli, University of Groningen

Version 1.0

Nicosia, 2019


This work has received funding from the European Union's Horizon 2020 research and innovation programme under grant agreement No 811068. In addition, this work was co-funded by the European Regional Development Fund and the Republic of Cyprus through the Research and Innovation Foundation (Project: EXCELLENCE/1216/0023).

Nicosia 2019 (Version 1.1, layout edited 2021)

ISBN 978-9963-2858-4-6

CONTENTS

PREFACE

This document is the first in a series of guides aimed at promoting best practice in different aspects of archaeological science, produced by members of the Science and Technology in Archaeology and Culture Research Centre (STARC) of The Cyprus Institute.

The current document was largely developed in the context of two projects: *People in Motion* and *Promised*. The implementation of *People in Motion* involved the study of large skeletal assemblages from Byzantine sites across the Mediterranean. Osteological work on these assemblages was co-funded by the European Regional Development Fund and the Republic of Cyprus through the Research and Innovation Foundation (Project: EXCELLENCE/1216/0023). In addition, *Promised* aims at promoting archaeological sciences in the Eastern Mediterranean, with funding from the European Union's Horizon 2020 research and innovation programme under grant agreement No 811068.

The aim of this guide is to cover the main aspects of the excavation and macroscopic study of human skeletal remains. The focus is on bioarchaeological/human osteoarchaeological assemblages, rather than forensic anthropological material, though many of the practices described are shared between these two disciplines. It cannot be overemphasized that each skeletal assemblage will pose different challenges and any approach to field recovery and laboratory procedures will have to be adapted to these. Therefore, the current guide is meant to serve only as a general outline of best practices and the described field and lab-based methods should be modified depending on individual circumstances, such as the sample size, preservation of the material, research questions and other parameters. References are given throughout the document, but our aim is by no means to provide an exhaustive account of the literature.

This document is an open resource and it is anticipated to be updated at regular intervals. We would greatly appreciate any feedback and recommendations for future improvement.*

Efthymia Nikita

Anna Karligkioti

*For suggestions about how to improve this guide, please contact Efthymia Nikita: e.nikita@cyi.ac.cy

EXCAVATION

The stratigraphy of mortuary contexts may be very simple in cases of single undisturbed inhumations or particularly complex when the burial includes the remains of multiple individuals, especially in cases where the same burial site had been used for an extensive period of time (Hochrein 2002). This section provides basic guidelines to the excavation of skeletal remains. These guidelines are to be adapted on a site by site basis pending on the character of each archaeological assemblage and the available resources. The following guidelines have been drawn from a number of sources, primarily Barker (2003), Bartelink et al. (2016), Carver (2013), Cheetham et al. (2008), Dirkmaat (2012), Dupras et al. (2012), Haglung (2002), Haglund et al. (2001), and Hunter and Cox (2005), as well as the authors' personal experience in excavating human skeletal remains.

SITE LOCATION AND INITIAL DOCUMENTATION

In certain cases, the location of a burial site will be easily observable; for example, in tholos tombs or other monumental burial constructions. In such cases, there is no need to apply the site location and delineation methods briefly presented in this section, and the first step will be to document the site and then proceed to excavate it. However, in cases where the skeletal remains lie in a pit or other feature not clearly visible on the ground surface, different methods may be used to locate the burial site. Non-invasive methods include air imagery and geophysical survey. The former can reveal ground disturbance that affects soil, vegetation, and other parameters, while the latter may locate geophysical anomalies, resulting from the different physical properties of the materials within the ground substrate.

Invasive methods include trenching and area (or surface) stripping. These methods are adopted when there is some indication as to the approximate location of the burial site and allow the delineation of this site. As these methods are invasive, that is, they involve soil removal, a preliminary important step is to survey the site so that any surface findings (including human skeletal remains) are collected, sorted, mapped and inventoried. In addition, the site should be documented by means of written descriptions, a sketch map, and photography. Once documentation is complete, soil removal may begin.

Trenching involves cutting a narrow trench across the area of interest (Figure 1) with the aim of identifying the boundaries of the burial site based on soil differences and human or other remains. The use of several closely spaced trenches is advised so that the location and size of the burial site are accurately identified. An alternative method is area or surface stripping (Figure 2). This method involves removing surface soil layers until the boundaries of the burial site are identified by soil changes or other characteristics. In our experience, area stripping generally works better for burial grounds, since the compartmentalisation caused by trenching complicates the subsequent excavation. Once defined, the burial site outline should be photographed, measured, and described in notes before further excavation ensues.

Both in trenching and in area stripping, the soil removed should be sieved. The size of the sieve will depend upon the soil type, but as a general rule, a 2mm sieve works well in most contexts. If possible, a double sieving process can be followed whereby the soil goes through a 4-5mm sieve initially and then through a 2mm sieve. All findings, including human skeletal remains, should be sorted and allocated an inventory number. In addition, all findings should be accompanied by an indication that they came from sieving, thus no accurate location information is available.

GRID CONSTRUCTION

Once the exact location and size of the burial site have been determined, a reference grid should be constructed in order to document in detail the site per se and the excavation activities that will follow. The first step in creating the grid is setting a datum. A datum is a fixed point, such as a specific point placed on a large tree, which will act as a reference point for mapping the excavation site (Bartelink et al. 2016; Christensen et al. 2014; Connor 2007; Dupras et al. 2012). The location of the datum should be recorded using a Global Positioning System (GPS). In case no datum is readily available, one can be constructed (for example, Sideris et al. 2017 used concrete pillars). A subdatum is located closer to the remains at

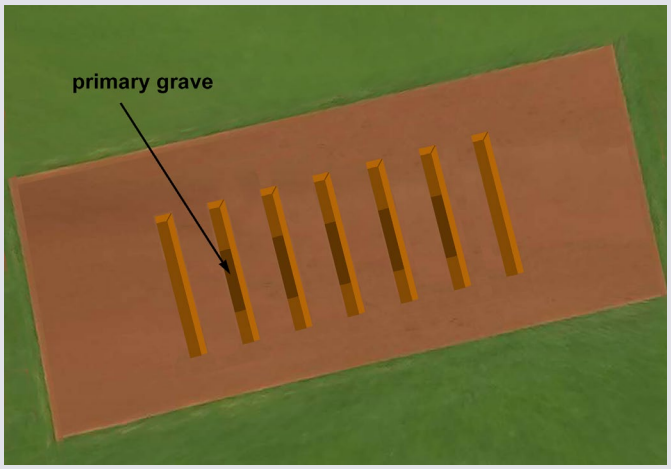

Figure 1. Trenching

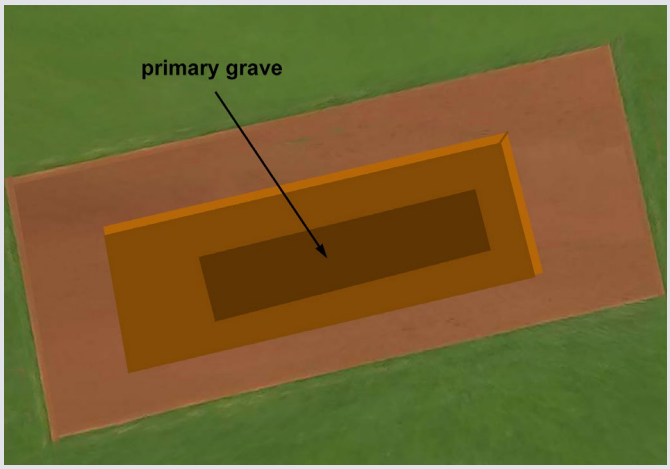

Figure 2. Area stripping

a specified distance from the datum, while baselines are lines running east-west or north-south through the subdatum. The grid should extend beyond the excavation area in order to capture all features (Figure 3). The grid is subdivided into square units (e.g. 5m x 5m squares) numbered in a systematic manner (e.g. Square 5/6 is the fifth square east and the sixth square north from a specific subdatum) (Nawrocki 1996). Additionally to the large grid of the excavation area, micro-grids may be used to divide each of the square units.

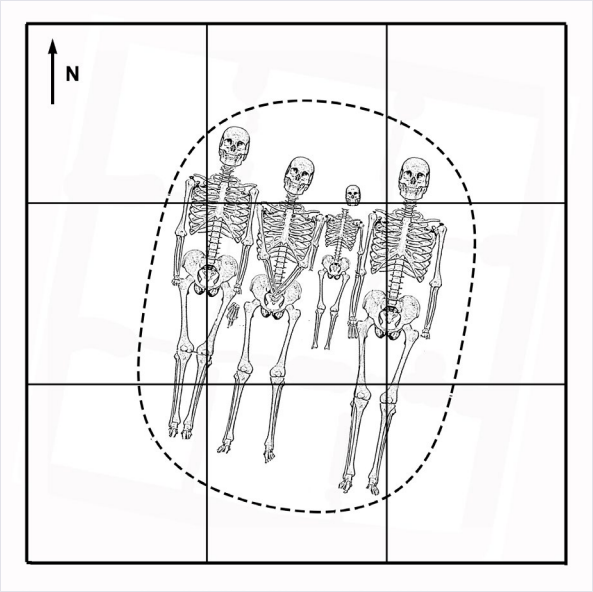

Figure 3. Example of reference grid constructed on top of the hypothetical burial of four individuals

Marking the location of points without a grid

Easy methods of mapping the location of different features, objects, skeletal elements etc. are baseline perpendicular measurements and triangulation from a baseline. However, these do not provide sufficient accuracy and level of detail. A more efficient way to record distances and angles is using a surveyor's level. This method requires two datum points, which provide a baseline to which all points can be referenced, and a surveyor's (dumpy) level to record bearing, distance and height. Finally, a total station may be used for remote, rapid 3D surveying. Readers interested in a more detailed account on how these approaches may be used in burial investigations can consult Cheetham et al. (2008) and Dupras et al. (2012).

DOCUMENTATION OF THE BURIAL SITE

Prior to removing any additional soil from the burial, it is important to document the site in more detail than already done, using the newly established reference grid. A site plan should be produced to depict all features in relation to each other and in relation to the datum. The plan should be at a scale that will effectively capture all the key information: the standard for most burials is a ratio of 1:10 cm; however, a scale of 1:20 cm may be best for drawing multiple burials, and a scale of 1:50 cm or even 1:100 cm may be used for drawing widely scattered remains. Alternatively, or additionally, site photographs may be printed and used for on-site notes, while tablets can also be employed in site documentation. Additional photographs and brief notes should be taken. It is important that any materials identified from different grid squares are kept separate.

EXPOSURE OF THE HUMAN REMAINS

The next step is to remove the soil surrounding the human remains. Two excavation methods are commonly employed: the stratigraphic method and the arbitrary level method (pedestal method) (Evis et al. 2016; Tuller 2012). The stratigraphic method should be the one preferred for reasons explained below, unless there is sufficient justification to opt for an alternative approach (Tuller and Đurić 2006).

Stratigraphic excavation

This method emphasizes the need to define stratigraphy in a grave in order to understand the chronological sequence of the events that led to its formation (Harris 1989) (Figure 4). The entire grave is viewed as an archaeological feature and its walls are preserved so that the grave contents are kept ***in situ***, provided that there are no health and safety concerns (Hochrein 2002; Hunter 1996). Stratigraphic layers are excavated successively and the layer from which each find originates is recorded (Carver 2013). It is important to stress that skeletal (and other) remains found within the same stratigraphic deposit share an association; however, there may be no relationship between remains in different layers. Therefore, when examining disarticulated skeletons, one should first look for possible matches within the same layer. The identification of individual stratigraphic units is sometimes clear, but at other times it can be very difficult. Evidence that may assist in the identification of distinct layers includes bulks of soil between deposits of remains, the orientation of the bodies and/or the presence of different types of deposits (primary vs. secondary) in successive layers (Tuller and Hofmeister 2014). In addition, the input of experienced archaeologists, who are familiar with the general area and stratigraphy, can be invaluable.

The advantages and weaknesses of stratigraphic excavation are presented in detail in Tuller and Đuric (2006). In summary, potential problems of this method include insufficient water drainage, limited access to the skeletal remains due to the maintenance of the burial walls, difficulties in identifying stratigraphic units, walking/standing on the skeletal remains during excavation, and considerable time investment. The advantages include the three dimensional reconstruction of the grave and the chronological reconstruction of the events that formed the burial site. As stressed above, despite its limitations, the stratigraphic method should be the one adopted because the information gained from this type of excavation outnumbers any difficulties in its implementation (Evis et al. 2016).

Figure 4. Step 1

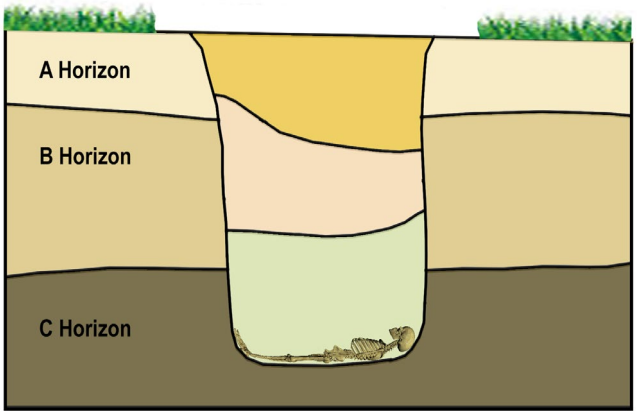

Figure 4. Step 2

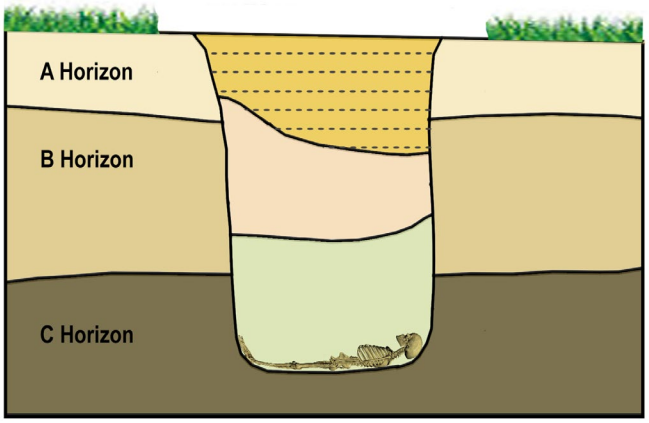

Figure 4. Step 3

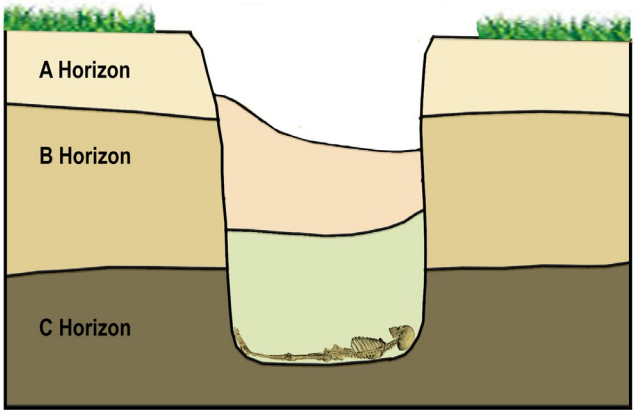

Figure 4. Step 4

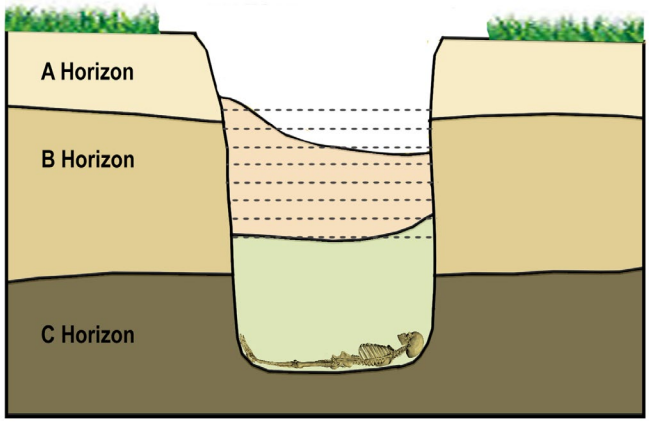

Figure 4. Step 5

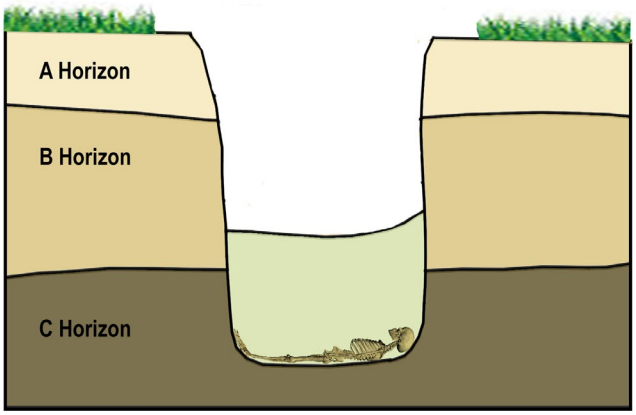

Figure 4. Step 6

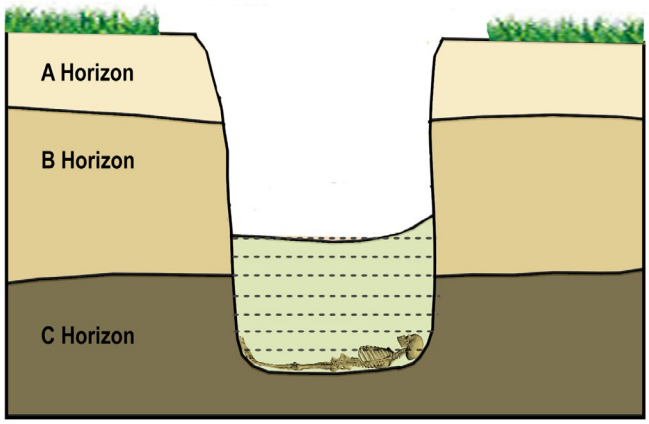

Figure 4. Step7

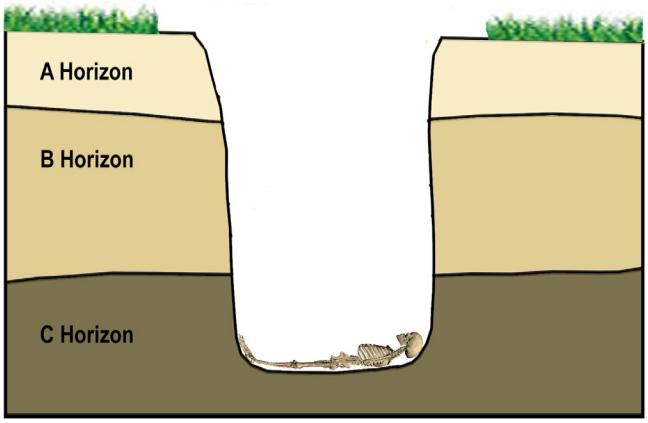

Figure 4. Steps in stratigraphic excavation | Adapted from Evis et al. 2016

Arbitrary level excavation

In arbitrary level excavation (Figure 5), soil is removed in successive levels of specific depth (e.g. 0.05m, 0.10m, 0.20m), without considering the existence of stratigraphic layers (Hanson 2016; Hester et al. 1997). Any findings are usually left upon a soil pedestal until the excavation of the level has been completed and then they are documented and removed, together with the pedestal (Oakley 2005; Stover and Ryan 2001; Ubelaker 1989). In cases of mass burials, to gain better access to the remains, trenches are often dug perimetrically, destroying the grave walls (Haglund et al. 2001; Joukowsky 1980).

The advantages and weaknesses of the arbitrary level excavation method are also presented in detail in Tuller and Đuric (2006). In summary, the advantages include better control of soil removal, easier access to the remains, more effective water drainage, and limited time standing on the remains during excavation. The problems with this method include the destruction and non-consideration of stratigraphic layers within the grave, the lack of stratigraphic origin for the different

findings, the mixing of strata and artefacts from the grave structure and natural strata through which the grave was dug, and the incomplete documentation of the grave cut. A possible compromise between the two excavation approaches would be to follow the stratigraphic method at least until reaching the remains and then, if absolutely necessary, to destroy the pit walls in order to facilitate excavation/recovery of the bones. Nonetheless, this may create problems if there are more than one "floor" layers in the grave and you must continue digging lower.

Figure 5. Step 1

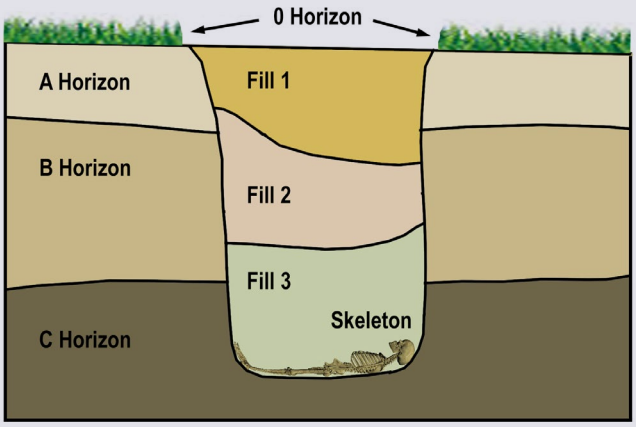

Figure 5. Step 2

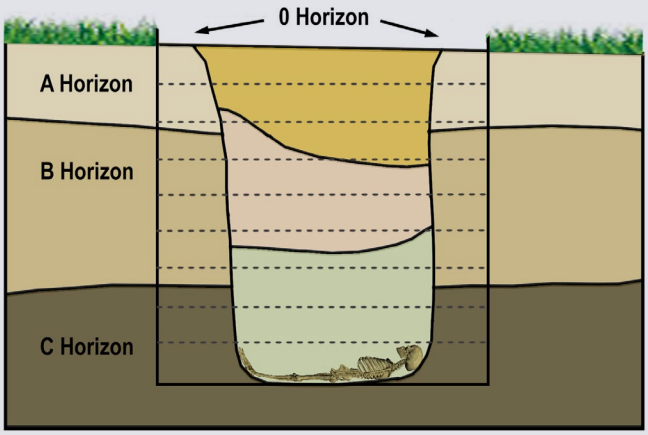

Figure 5. Step 3

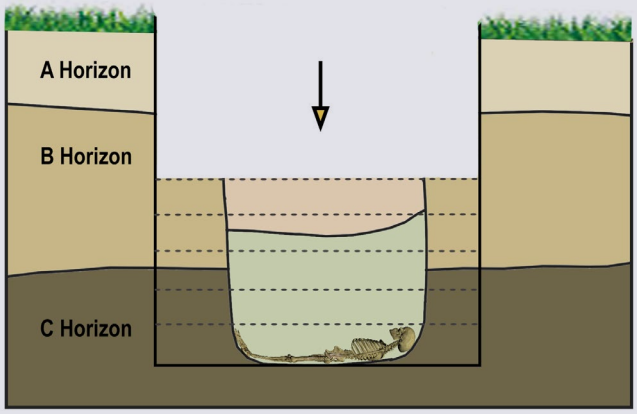

Figure 5. Step 4

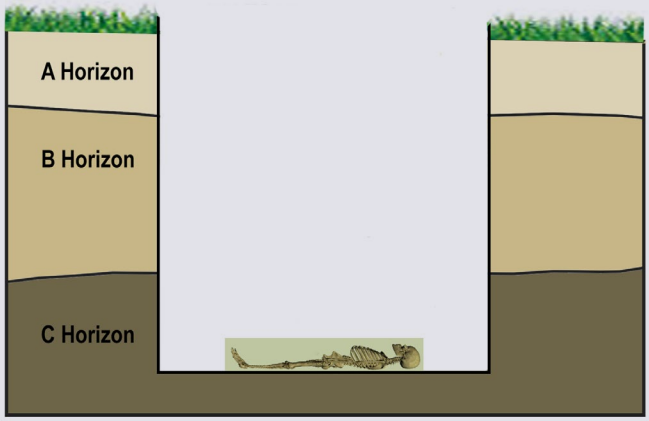

Figure 5. Step5

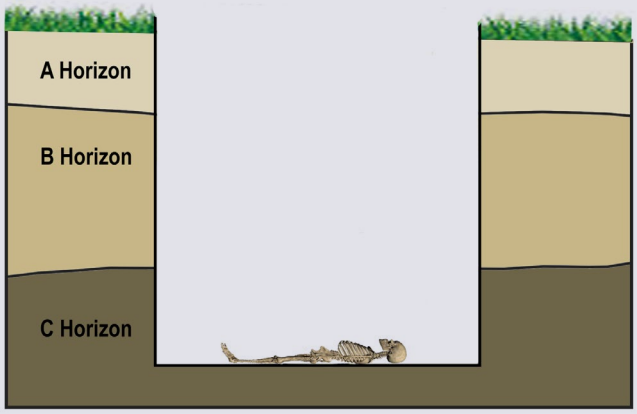

Figure 5. Steps in arbitrary level excavation | Adapted from Evis et al. 2016

General instructions

Irrespective of the excavation method adopted, soil removal should take place at sub-layers 2-5cm deep. As seen in Figures 4 and 5, in the stratigraphic method these sub-layers will follow the stratigraphic layers, whereas in the arbitrary level excavation, they will not take stratigraphy into account. By using sub-layers, each bone layer can be revealed and recorded more accurately. Any skeletal remains should be exposed at the same level. If the bones continue deeper than the selected layer, layer documentation should be completed before digging deeper. In addition, skeletal remains should be collected and inventoried by grid square and by micro-grid location per square in order to achieve maximum degree of spatial control within each burial context.

Each soil type encountered and its composition should be described in the field notes. The color of the soil may be evaluated using the Munsell color system or any other commercially available color reference system. Soil texture, that is, the relative proportion of clay grains (less than 0.002 millimeters), silt grains (0.002 to 0.05 millimeters), and sand grains (0.5 to 2 millimeters) contained in the soil, should also be noted, as should soil consistency (Roskams 2001).

All soil from each layer removed should be screened per micro-grid square. The size of the mesh will depend upon the soil type (e.g. sandy or clay) and the elements one wishes to capture (e.g. fetal bones, ear bones). It would be ideal to adopt a nested screen design so that soils and other materials are separated based on their different particle sizes (Bartelink et al. 2016). In case of wet soil or mud, wet flotation may be necessary instead of sieving (Atici 2014).

When excavating around the abdominal and pelvic region of female skeletons, attention should be paid to the possible presence of fetal bones. In addition, soil samples should be collected in order to recover archaeobotanical remains from different areas of the grave/deposit including the corners of the grave (in case of a rectangular grave). Soil samples can also be collected from the chest/thorax or hands. Sediment samples should be taken from the anterior surface of the sacrum for evidence of intestinal parasites, while sediments from inside the cranium and near the feet should be taken as controls (Anastasiou et al. 2018; Reinhard et al. 1986).

BURIAL DOCUMENTATION

Once the remains per layer have been exposed, they should be mapped on graph paper, photographed, and documented with notes prior to their collection (SWGANTH 2013). Using standardized recording forms is highly advisable (e.g. Courtaud 1996). Such forms should be developed before the recovery and adapted to the specific conditions during the recovery stage, if necessary (Bartelink et al. 2016).

The position of each bone must be documented (graphically and numerically) on a plan using the reference grid. As stated above, the scale of the plan will depend on the size of the burial site and the detail required, but the most common scales are 1:10 cm and 1:20 cm. A simple way of making accurate plans is by obtaining a photograph of each bone layer and superimposing tracing paper over the photograph to outline each bone (Cabo et al. 2012). An alternative or rather complementary approach is to individually number all bones and tag them on digital photos (Moutafi and Voutsaki 2016). In case of primary extended burials, the orientation of the skeletons should be mentioned by stating the skull first; for example, a north-south orientation indicates that the skull is at the north.

Photographs of the overall view of each layer should be taken, with north point and scale clearly visible, followed by close-up images of the bones in each grid square. Close-up images should also document any noteworthy features (e.g. unusual burial position, pathological lesions). In addition, it is important to obtain close-ups of the joints, which will be used for archaeothanatology-oriented analyses (e.g. to assess through state of labile joints the condition of body decomposition in open or filled space, cf. Duday 2009). In addition, it may be useful to obtain record shots from a specific fixed point in order to document each step of the excavation. Once the excavation is completed, these photographs can be viewed in reverse order and show how the grave deposit was formed and reconstruct the environment of decomposition of the body. Finally, even if not full photogrammetric recording is available, the inclusion of fixed points in the photos (e.g. points placed at each corner of the burial) and an effort to take a complete series of photos from all around and a few vertical orthophotos from above, provide easily the necessary means to create a photogrammetric model of the burial later.

Whenever the necessary equipment is available, the grave may be documented by 3D laser scanning (Gaudio et al. 2015; Vosselman and Maas 2010) or photogrammetry (Howland et al. 2014; Levy et al. 2014; Sideris et al. 2017). Contrary to drawings and photographs, which provide a 2D image of individual stratigraphic layers and profiles, such techniques visualise the 3D structure of the archaeological site (De Reu et al. 2013). The data obtained from scanners and photogrammetry can easily be combined and produce detailed excavation plans as well as virtual animations, where different contextual information may be combined to reconstruct the site (Siebke et al. 2018).

Important Note

After the removal of the soil in each layer/sub-layer and the exposure of the bones, and before the collection of any material:

1. Photos should be obtained. Bones that were displaced during excavation should not be placed back on the skeleton in order to take nice photos. Very often these bones are not placed in their original position (e.g. patella or small bones of hands and feet) and the photo is not correct to be used after the excavation to collect additional information for the interpretation of mortuary practices. Any displacement of bone during excavation should be noted on the recording form or the field notes
2. Elevations should be taken, in particular at the skull, pelvis and feet
3. Numbering of bones and other findings should be completed
4. All elevations and bone/artifact numbering should be noted on the sketch

Drawing to scale using grid-system mapping
(Dupras et al. 2012)

1. Draw the limit of the grave on the graph paper, mark the location of the datum and baseline, and label the grid squares
2. Record the position of every bone and other findings using the distance from the corner of the square that is closest to the datum along the grid square's two lines that run parallel to the baseline and the reference number line
3. Plot the point just measured on the graph paper and repeat for all points per bone (e.g., for a long bone, find the position of the proximal and distal ends and the midshaft)
4. Record the depth or elevation of the mapped bone using the datum line
5. Proceed throughout the grid until all bones and other findings have been recorded

Producing an overlay for plan drawings
(Dupras et al. 2012)

1. After plotting the first excavation layer, draw a set of cross-hairs outside the previously recorded data
2. Place a sheet of tracing paper over the original graph paper and trace the cross-hairs onto the tracing paper so that it can be realigned with the original drawing later on
3. Map the next layer of data on the tracing paper, on top of the data recorded on the underlying graph paper
4. Following the above process, add as many overlays as necessary to capture the different excavation layers

Section drawings
(Dupras et al. 2012)

1. On graph paper, mark the position of the datum. If you want to draw depths, the datum should be placed at the top of the graph paper; if you are recording elevations, it should be placed at the bottom
2. From the datum point draw the surface horizon line
3. Below/above the horizon line, mark the depths/elevations of all mapped bones, objects and stratigraphic layers

BONE COLLECTION

To minimise damage to the skeletal remains, these should be removed from the site as soon as possible after their excavation. Before excavated bone is bagged, it must be cleaned as much as possible from adherent soil. The one exception is the cranium: soil removed from the cranial cavity in the field may result in the cranial bones of younger individuals (with unfused sutures) coming apart making laboratory reconstruction difficult, cleaning the nasal apertures and the eye orbits may destroy delicate bones, while cleaning the area around the maxilla and mandible may result in the loss of loose teeth. In case there is no time to clean the bones on site, these should be wrapped in acid-free paper and then foil to maintain their structure before they are transported to the lab.

Self-sealing polythene bags should be used and the site name, context number, excavation date, and skeletal remains contained in each bag should be clearly marked using permanent ink. Bags should originally be left partially open so that humidity is not trapped inside. Alternatively, when bones are very moist, they should be initially bagged in acid-free paper bags and after they are air-dried under shade, they should be transferred to polythene bags.

When multiple bags are kept in a box, heavier and more robust bones should be placed at the bottom. Bubble wrap may be used for extra protection, if necessary. Special care is needed when neonatal remains, poorly preserved or pathological bone is bagged. Such bone should be wrapped in acid-free paper and then bagged and boxed.

Bones should be bagged by side and element, according to the following system:

- Cranium
- Mandible
- Loose teeth
- Sternum and hyoid
- Left/right ribs
- Left/right shoulder (scapula, clavicle)
- Left/right arm (humerus, ulna, radius)
- Left/right hand (carpals, metacarpals, phalanges)
- Vertebrae
- Pelvic bones (os coxae, sacrum)
- Left/right leg (femur, tibia, fibula)
- Left/right foot (tarsals, metatarsals, phalanges)

Small bone fragments can be bagged as a group by grid/micro-grid quadrant. Every bone removed should be inventoried, so that a depositional map can be produced in the future (Nawrocki 1996; Osterholtz et al. 2014).

Taking bone/tooth samples for later ancient DNA and isotope analysis during bone collection from the field should minimize contamination variables; however, it will preclude the macroscopic study of the sampled elements. Any samples obtained, should be registered at the sample log and documented on site photographically and with notes.

FINAL CLEAN UP

Once all skeletal remains have been lifted, the remaining soil in the grave should be removed and screened to recover any remaining elements, and a final photograph should be taken (Nawrocki 1996).

To ensure that no deeper deposits are present, even if you are certain you have reached the bottom of the burial, it is advisable to remove the soil stratum below the estimated floor of the deposit.

LABORATORY ANALYSIS

Each assemblage reaching the lab will have specific properties depending on the sample size, state of preservation and other parameters. Figure 6 summarises the general procedure that may be followed when studying human skeletal remains, but this shall be adapted depending on the nature of each assemblage under examination.

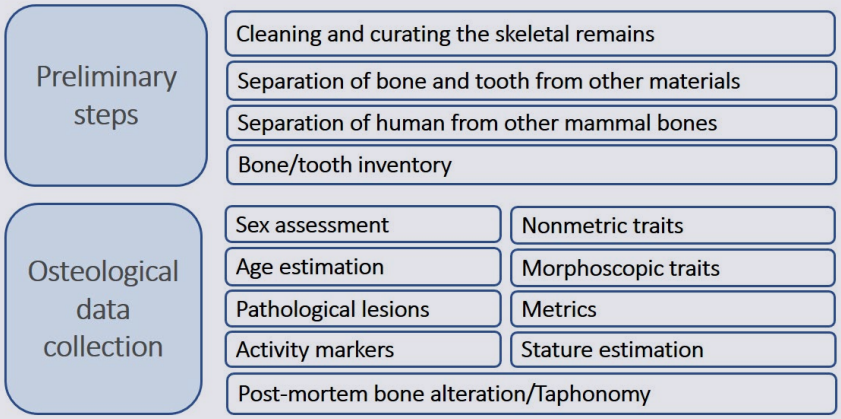

Figure 6. General procedure in the study of human skeletal remains

CLEANING AND CURATING THE SKELETAL REMAINS

Before data collection can start, bones and teeth need to be cleaned. The state of preservation of the skeletal remains will dictate the optimum cleaning method but washing gently with tepid or cold water is the most commonly adopted approach. The bones should not be immersed into deionised water to avoid dissolving the bone mineral, while the water should be changed regularly and soil remnants should be sieved to capture small bones or bone fragments. Bones should be left to dry naturally and not in direct sunlight. If washing is not an option, the alternative is dry brushing using a very soft brush over a sieve. When cleaning teeth, it is important not to create artificial microwear patterns or remove dental calculus deposits.

Before the skeletal remains are stored, they should be fully dried, to prevent mould growth. Most remains are placed in plastic bags per anatomical area (see section Bone Collection) and multiple bags are placed inside boxes. Padding (acid-free tissue paper or bubble wrap) may be placed at the bottom of the boxes and/or between different layers of bags to provide additional protection.

If the remains are particularly fragile, they may require conservation. However, the use of consolidants and reconstruction materials may compromise future biomolecular and chemical analyses, thus minimum intervention is recommended and only when important information can be gained, such as reconstructing long bone lengths or cross-sections (Cassman and Odegaard 2007; France et al. 2015).

SEPARATION OF BONE AND TOOTH FROM OTHER MATERIALS

Taphonomic factors, such as thermal alteration, may make the distinction between bone/tooth and other materials, such as wood, stone or pottery, difficult. The first step is to focus on the **gross morphology** of each item. Cortical and trabecular bone have a distinct morphology (Currey 2002) that should allow their separation from most non-osseous materials, which are usually solid in cross-section. In addition, bone surfaces have muscle attachment sites and foramina, which can help distinguish them from non-biological materials. If the macroscopic study is insufficient, **microscopy** may allow detection of structure unique to bone and tooth.

In cases where bone and tooth fragments have been altered to the extent that gross morphology and microscopy cannot assist in their identification, **chemical analysis** may be useful. In their seminal paper, Ubelaker et al. (2002) adopted **scanning electron microscopy/energy dispersive spectroscopy** (SEM/EDS) as a tool that presents not only a highly magnified surface image, but can also identify

chemical composition. Even though this method shows potential, it is largely based on the relative proportion of Ca/P found in the bone, which prevents certain non-bone materials from being discriminated from bone and teeth (e.g. mineral apatite, ivory) (Zimmerman et al. 2015a). The use of X-ray fluorescence (XRF) for distinguishing bone/teeth from non-skeletal materials of similar chemical composition suffers from the same limitation (Christensen et al. 2012). However, the combination of the above analytical techniques with multivariate statistical analysis has been shown to improve their potential in distinguishing groups of bone/teeth and non-skeletal materials with a similar chemical composition to bone (see Zimmerman et al. 2015b for X-ray fluorescence and Meizel-Lambert et al. 2015 for SEM/EDS).

SEPARATION OF HUMAN FROM OTHER MAMMAL BONES

Once bone and tooth remains have been separated from other materials, it is important to distinguish human remains from those of other animal species. In many cases, this will not be an issue as only human remains will be present in the assemblage; however, there are cases where animals have been buried with humans, sacrificed as part of the mortuary ritual, or ended up in the tomb post-depositionally (e.g., animals that burrowed into the tomb and died there). In the following paragraphs we provide some very general guidelines that may assist in the separation of human remains from those of other mammals. For a more thorough account, see Adams et al. (2008), Barone (1976), France (2009), Hillson (1992, 2005), Pales and Garcia (1981), Schmid (1972) and Thenius (1989) for general atlases, as well as identification atlases for specific parts of the world (e.g. Gilbert 1973 for North American mammals; Walker 1985 for African fauna; ***Beginner's Guide to Identifying British Mammal Bones*** by the Natural History Museum: http://www.nhm.ac.uk/content/dam/nhmwww/take-part/identify-nature/british-mammal-bones-ID-guide.pdf). In any case, it is always best to have a zooarchaeologist help to confirm nonhuman mammalian bones from human bones.

Morphological assessment is the initial method of choice if the materials present diagnostic information. Differences in the skeletal anatomy between humans and other mammals are endless, depending on the local fauna. General guidelines are provided in **Tables 1-3**. In addition, Figures 7-13 visually compare human to other mammal skeletons.

Table 1. Differential cranial anatomy between humans and other mammals (Watson and McClelland 2018)

Human	Quadrupedal mammals
Small face and large vault	Large face and small vault
More curved cranial bones	Less curved cranial bones
Not developed muscle markings (rather smooth vault)	Pronounced muscle markings
Smooth interior vault surfaces (occasionally showing meningeal grooves)	More complex interior vault surfaces
Inferiorly placed foramen magnum	Posteriorly placed foramen magnum
Chin present	No chin
Anteriorly placed orbits, superior to the nasal aperture	Laterally placed orbits, posterior to the nasal aperture
Minimal midface projection	Significant midface projection
U-shaped mandible, not separated at the midline	V-shaped mandible, separated at the midline

Table 2. Differential dental anatomy between humans and other mammals (Watson and McClelland 2018)

Human	Quadrupedal mammals
Mix of slicing (incisors), puncturing (canines), and grinding (molars) teeth	**Carnivores:** prominent canines, more shearing teeth with sharp ridges **Herbivores:** more grinding teeth (flat topped cheek teeth with characteristic pattern of ridges), gap between mandibular incisors and cheek teeth
Dental formula 2:1:2:3* * these represent the number of teeth per type (incisors, canines, premolars, molars) in each quadrant	Equidae: $\frac{3:1:4-3:3}{3:1:4-3:3}$ Canidae: $\frac{3:1:4:2}{3:1:4:3}$ Bovidae: $\frac{0:0:3:3}{3:1:3:3}$ Ursidae: $\frac{3:1:4-1:2}{3:1:4-1:3}$ Cervidae: $\frac{0:1:3:3}{3:1:3:3}$ Rodentiae: $\frac{1:0:1-3:3}{1:0:1-3:3}$ Suidae: $\frac{3:1:4:3}{3:1:4:3}$ Leporidae: $\frac{2:0:1-3:3}{1:0:1-3:3}$
Large maxillary incisors	Small maxillary incisors (except for horses)
Small canines	**Carnivores:** large canines **Herbivores:** small or no canines
Rounded cusps separated by grooves on the premolar and molar crowns	**Carnivores:** sharp premolars and molars **Herbivores:** broad and flat premolars and molars with parallel grooves and ridges

Table 3. Differential post-cranial anatomy between humans and other mammals (Watson and McClelland 2018)

Human	Quadrupedal mammals
Spinal curvature	No spinal curvature
Relatively large vertebral bodies and short spinous processes	Small vertebral bodies and elongated spinous processes
Triangular sacrum, composed of 5 fused vertebrae	Elongated sacrum, composed of 3-4 fused vertebrae
More gracile upper limbs	More robust upper limbs
Triangular-shaped scapula	Rectangular-shaped scapula
Clavicle present	Clavicle often absent
Radius and ulna are individual bones	Radius and ulna are often fused
Tibia and fibula are individual bones	Tibia and fibula are often fused
Femur is the largest skeletal element	Femur is equal in length to other limb bones
Elongated foot	Broad foot

A special case: Immature bones

The bones of infants or very young children may be mistaken for animal bones because they have not yet assumed the morphology of mature human bones. In such cases, it may be helpful to corroborate the macroscopic analysis with microscopic and/or chemical analysis.

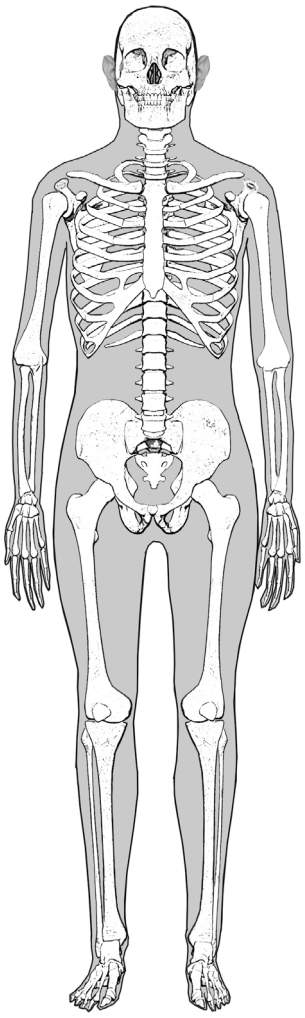

Figure 7. Human skeleton

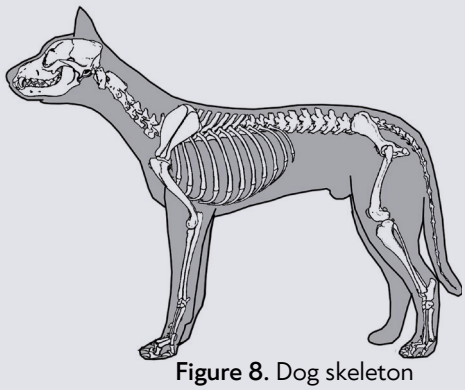

Figure 8. Dog skeleton

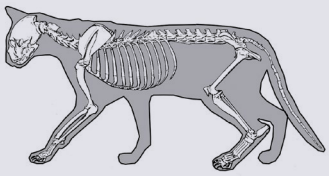

Figure 9. Cat skeleton

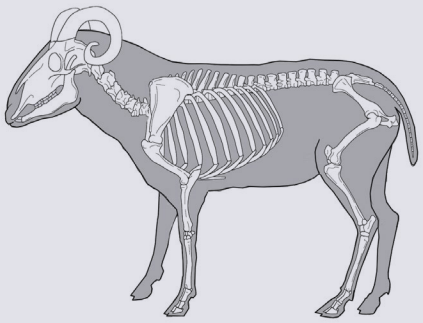

Figure 10. Goat skeleton

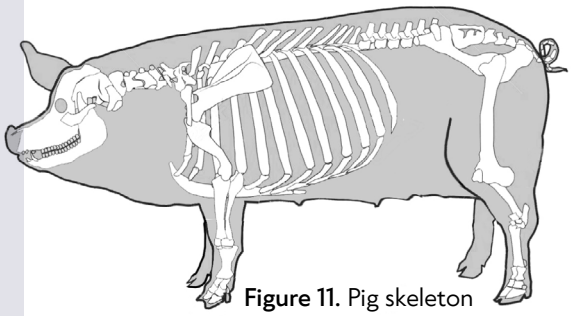

Figure 11. Pig skeleton

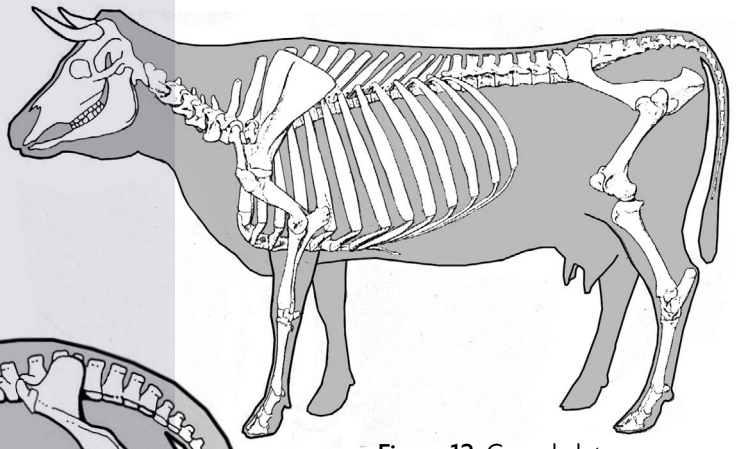

Figure 12. Cow skeleton

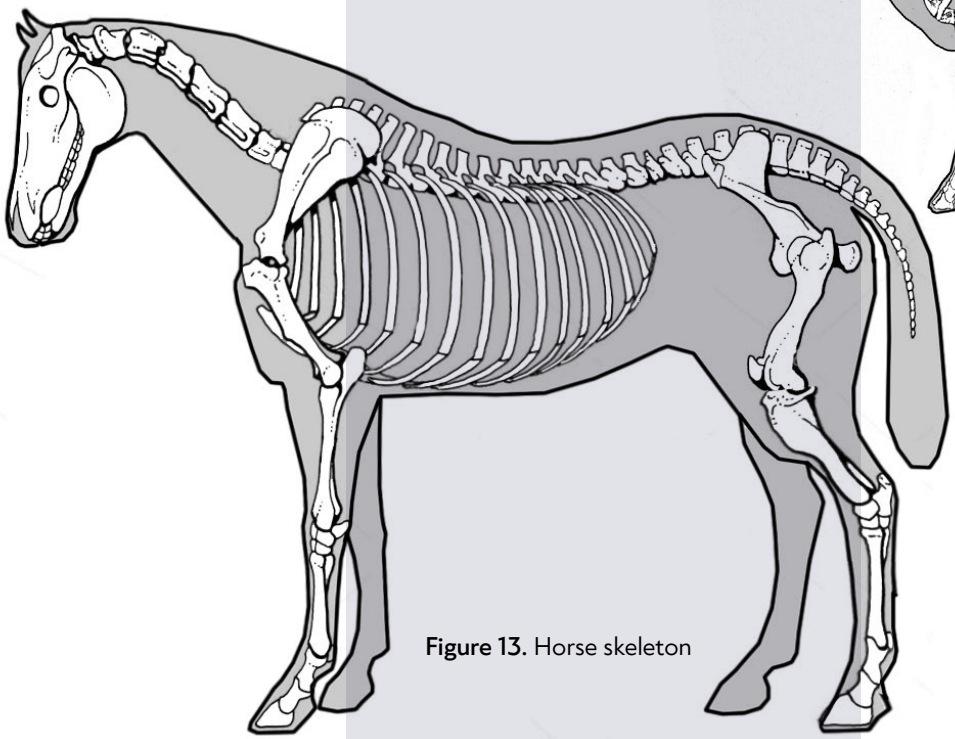

Figure 13. Horse skeleton

Bone macrostructure also differs between humans and most non-human animals. Some basic differences in animal and human bone macrostructure are given in **Table 4.**

Table 4. Differential bone macrostructure between humans and other mammals (Watson and McClelland 2018)

Human	Nonhuman mammals
Less dense (more porous) cortical bone	Less porous (more dense) cortical bone
Humeral and femoral cortical thickness about ¼ of the total diaphyseal diameter	Proximal limb bones cortical thickness about ½ of the total diaphyseal diameter
Cranial vault bones exhibiting thick diploë	More compact cranial vault bones

The **microscopic structure** of cortical bone is often diagnostic between humans and animals, even in cases of highly taphonomically altered remains, such as burned bones (Cattaneo et al. 1999). In their review paper, Hillier and Bell (2007) highlight that the two main types of bone tissue within the cortical bone of many mammalian species are Haversian bone tissue and plexiform bone tissue. Humans exhibit only Haversian bone tissue, whereas large mammals exhibit both Haversian and plexiform bone tissue. Note that humans also exhibit plexiform bone tissue, but only during early fetal development and in response to injury or inflammation. Plexiform bone tissue may not survive due to postmortem damage; hence, when using this as a criterion to differentiate human from nonhuman remains, it is important to pay attention to the preservation of the bone fragment under study. The Haversian bone tissue may be differentiated between humans and nonhuman mammals on the ground of its overall appearance. Osteons in human cortical bone are scattered whereas in many animals, there is osteon banding, that is, osteons align in rows (Mulhern and Ubelaker 2001). Histomorphometry may also be successfully applied as the size of Haversian systems and canals differs among different species; however, there is considerable overlap (Whitman 2004).

Different **analytical chemistry techniques** have been proposed for use in differentiating human and nonhuman bone and teeth including near-infrared (NIR) Raman spectroscopy (McLaughlin and Lednev 2012), Fourier transform (FT) Raman spectroscopy (Brody et al. 2001; Edwards et al. 2006), NIR-FT Raman spectroscopy (Shimoyama et al. 1997), laser induced breakdown spectroscopy (LIBS) (Vass et al. 2005), and SEM/EDX (Meizel-Lambert et al. 2015). Even though several studies have suggested that bones and teeth differ in elemental composition among different species (Aerssens et al. 1998; Beckett et al. 2011; Biltz and Pellegrino 1969; Bratter et al. 1977; Rautray et al. 2007), the hydroxyapatite structure of human and nonhuman bone are very similar (Christensen et al. 2012; Ubelaker et al. 2002), and there is a strong overlap between the trace elements exhibited in different species due to similarities in diet and environment. These issues limit the discriminatory potential of chemical analysis (Zimmerman et al. 2015a).

BONE/TOOTH INVENTORY

Once the human skeletal remains have been separated from all other materials/remains in the assemblage, the first step in their analysis is the construction of a careful inventory. During inventorying, it is imperative to retain all contextual information (archaeological site, context number, inventory number given in the field etc.). The extent and nature of the inventory are problem-driven but any inventory should document in appropriate detail what bones or parts of bone are present per individual. In more detailed studies, the Anatomical Preservation Index (Andrews and Bello 2006; Bello and Andrews 2006) could be used per element or even per zone to document bone completeness. In case of intact bones, each skeletal element will be a separate entry. In case of fragmentary remains, different approaches may be used. Diagnostic Zones are based on counting recognizable parts or zones of a particular bone. A commonly used zonation system is the one devised by Knüsel and Outram (2004), which is an adaptation of the method proposed by Dobney and Rielly (1988) for faunal remains. Figures 14-23 present the different zones per skeletal element (Knüsel and Outram 2004). Zones are scored as present even if only a small part is observed. The recording of nonadult material should follow the zone conventions for the adult skeleton but clarify if a specific zone is unfused or fragmented, as appropriate.

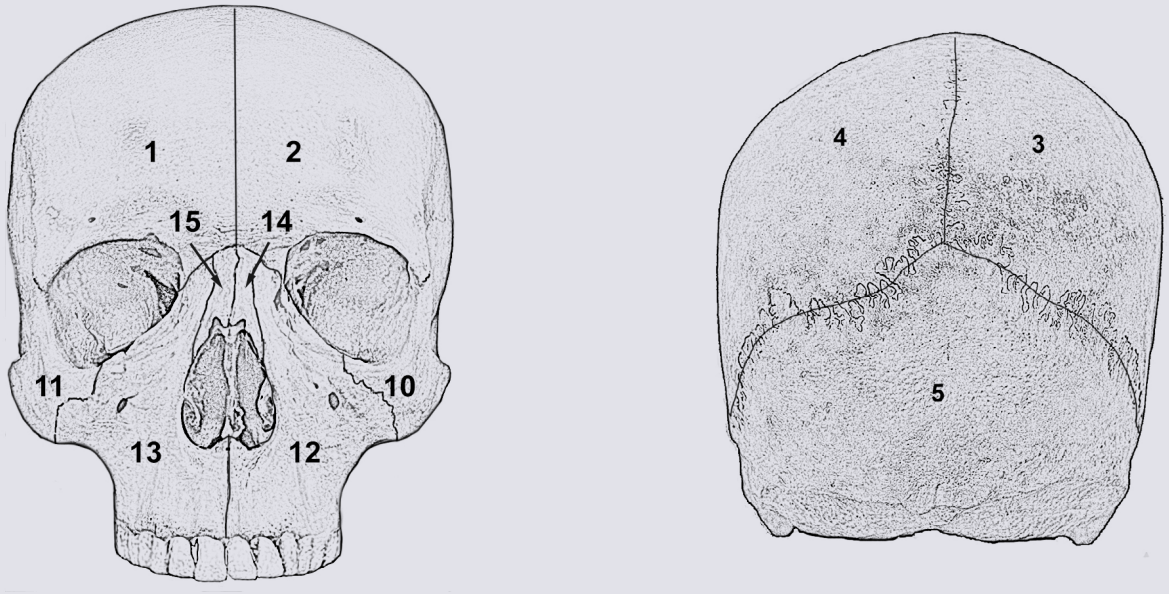

Figure 14. Zones of the anterior and posterior cranium | Adapted from Knüsel and Outram 2004 and Nikita 2017

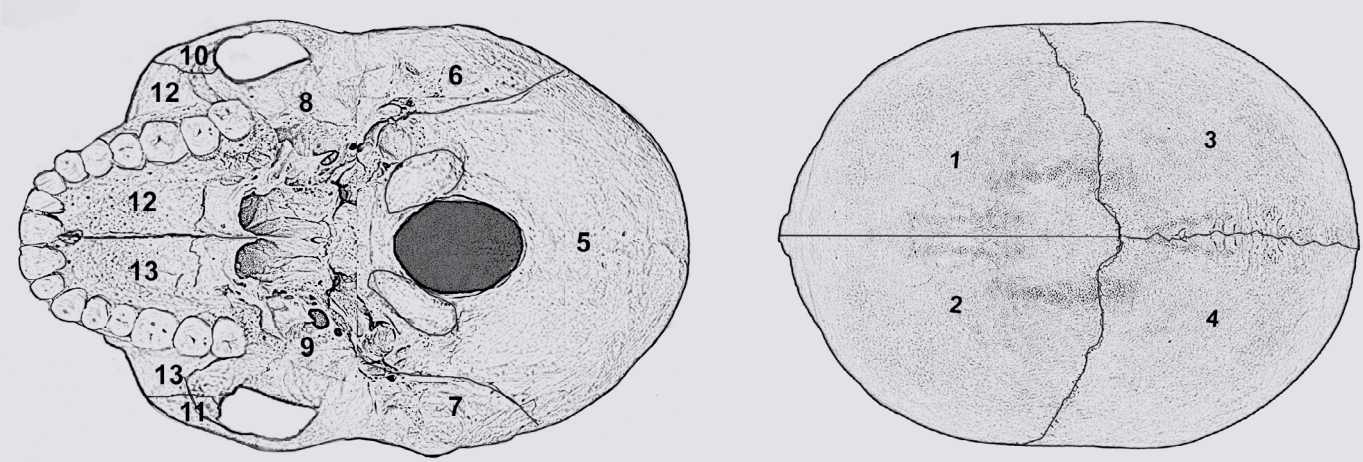

Figure 15. Zones of the inferior and superior cranium | Adapted from Knüsel and Outram 2004 and Nikita 2017

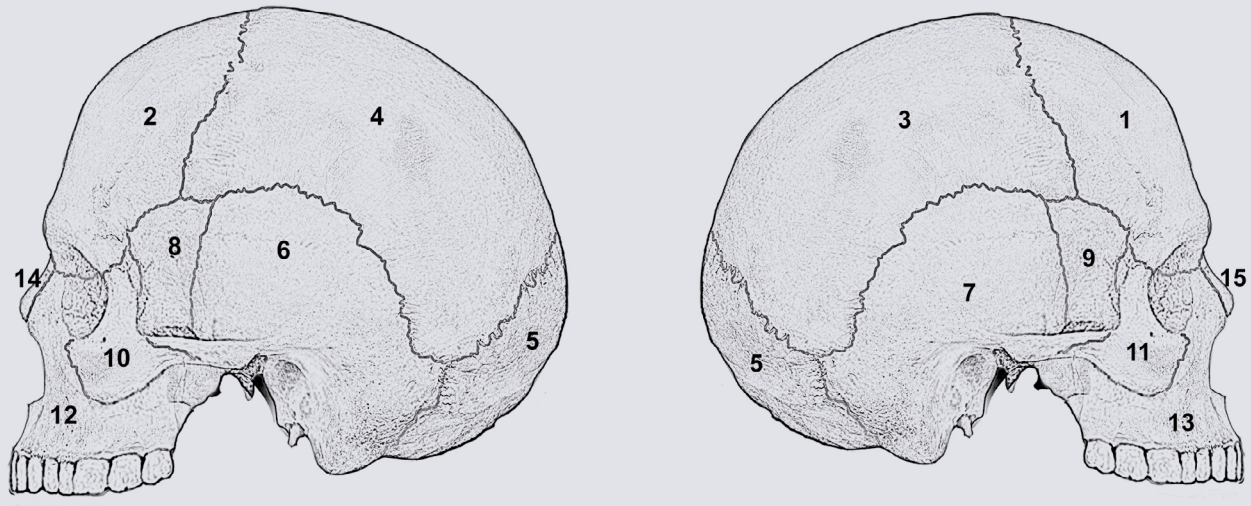

Figure 16. Zones of the lateral cranium | Adapted from Knüsel and Outram 2004 and Nikita 2017

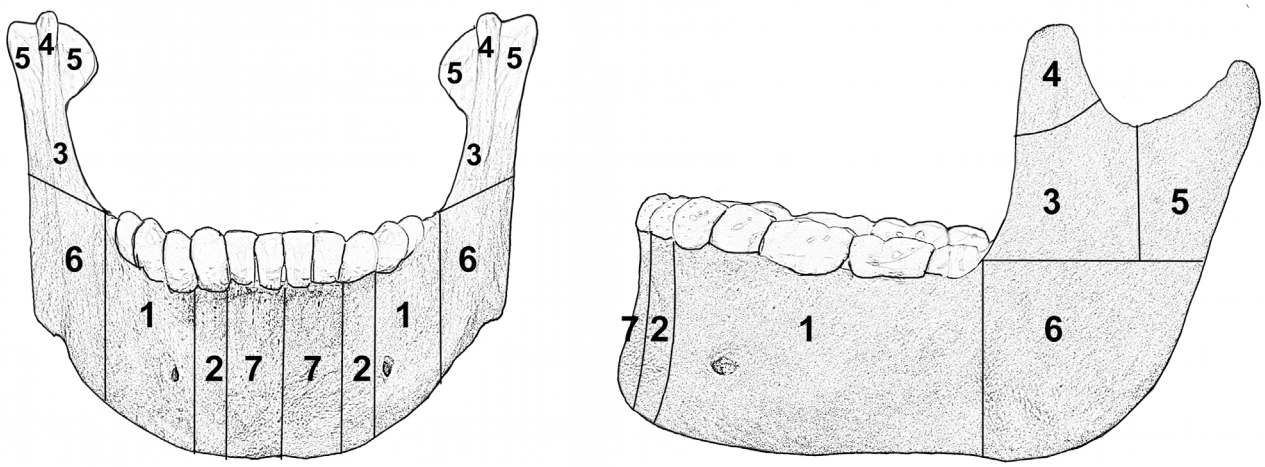

Figure 17. Zones of the mandible | Adapted from Knüsel and Outram 2004 and Nikita 2017

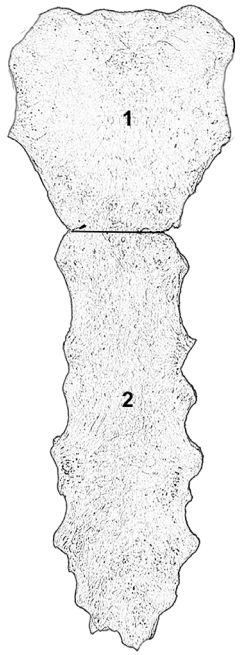

In case the xiphoid process is preserved, it should receive a score of 3

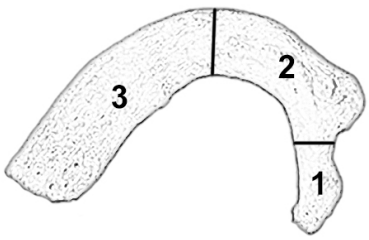

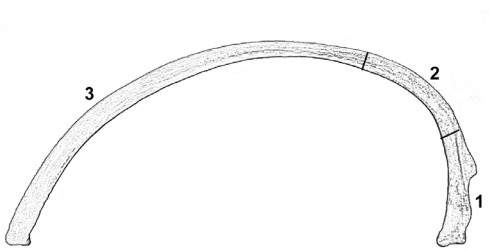

Figure 18. Zones of the sternum and ribs | Adapted from Knüsel and Outram 2004 and Nikita 2017

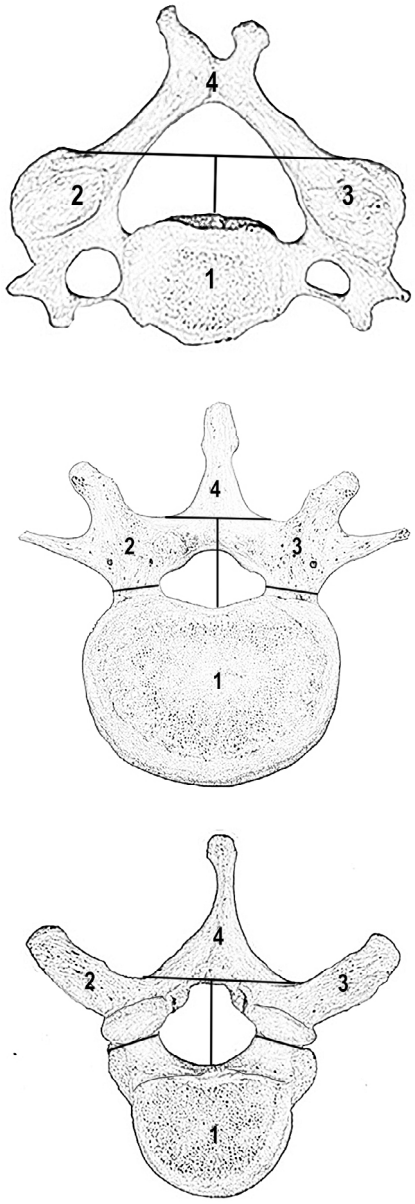

Figure 19. Zones of the vertebrae | Adapted from Knüsel and Outram 2004 and Nikita 2017

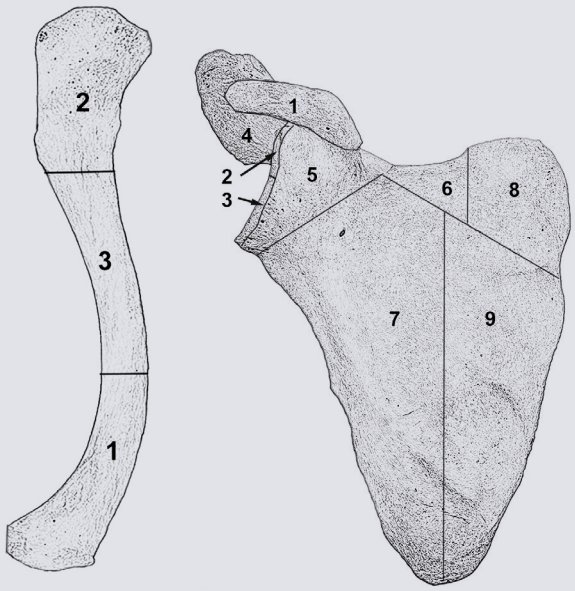

Figure 20. Zones of the clavicle and scapula | Adapted from Knüsel and Outram 2004 and Nikita 2017

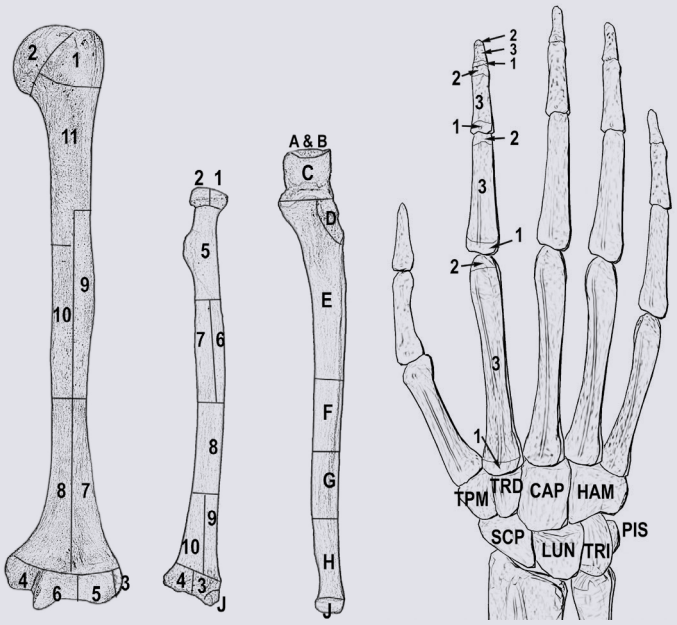

Figure 21. Zones of the upper limb bones | Adapted from Knüsel and Outram 2004 and Nikita 2017

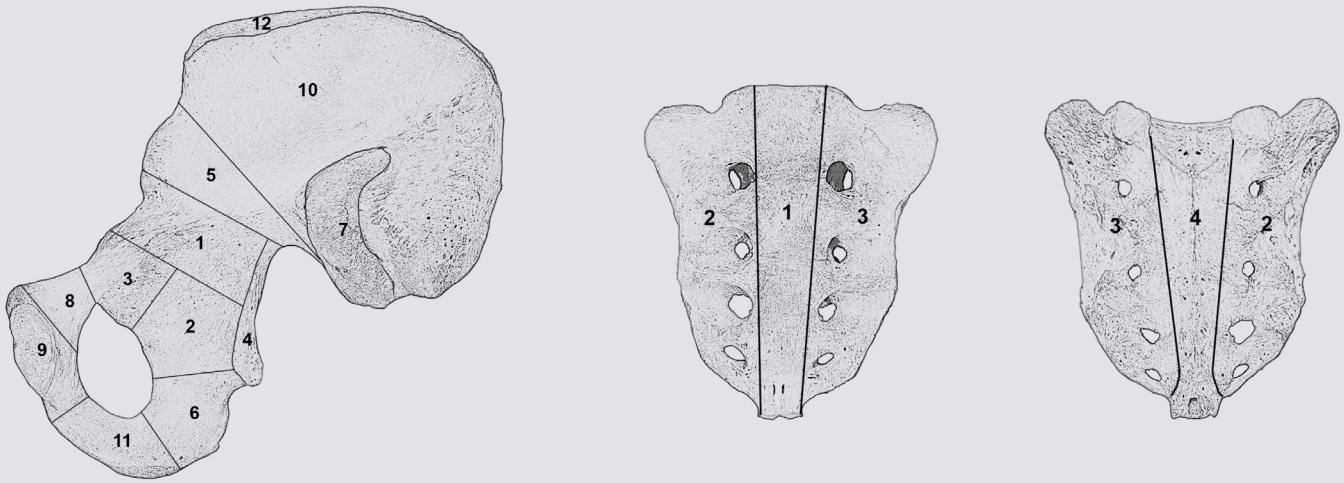

Figure 22. Zones of the os coxa and sacrum | Adapted from Knüsel and Outram 2004 and Nikita 2017

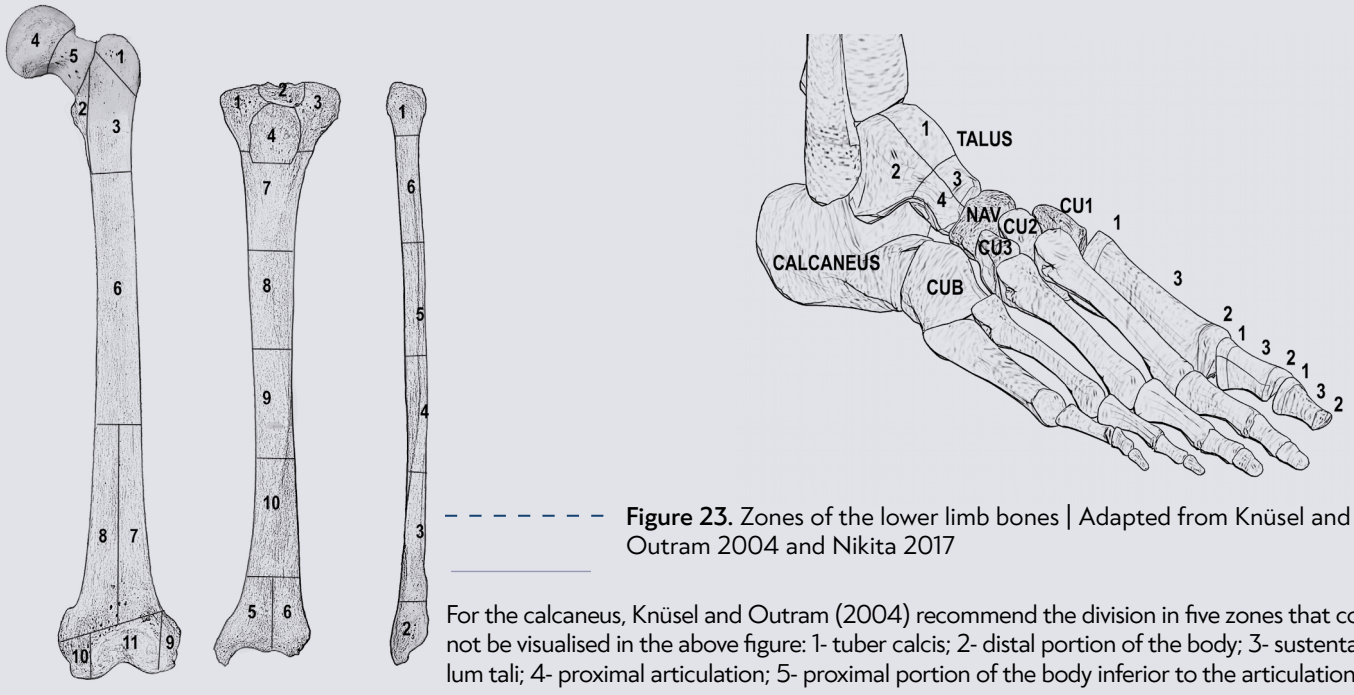

Figure 23. Zones of the lower limb bones | Adapted from Knüsel and Outram 2004 and Nikita 2017

For the calcaneus, Knüsel and Outram (2004) recommend the division in five zones that could not be visualised in the above figure: 1- tuber calcis; 2- distal portion of the body; 3- sustentaculum tali; 4- proximal articulation; 5- proximal portion of the body inferior to the articulations.

A simpler zonation system has been proposed by Osterholtz (2018, 2019) and is given in Figures 24-29. Even simpler zones may be used, depending on the degree of fragmentation of the assemblage and the research questions, such as the division of long bones in equal sections along their length (e.g. Kendell and Willey 2014).

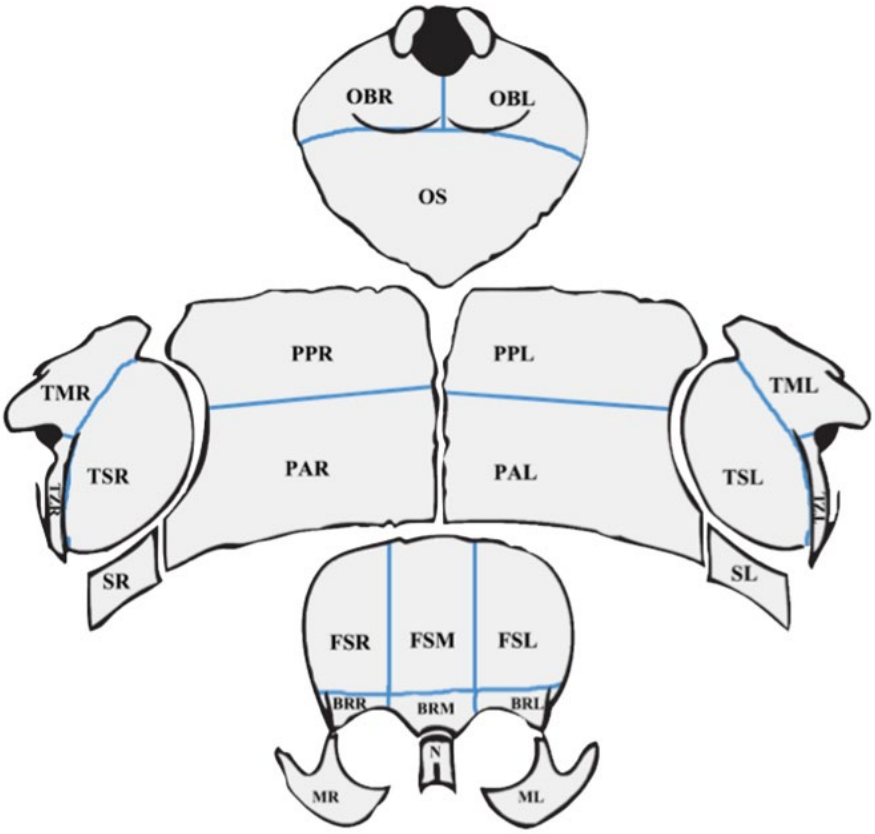

Figure 24. Zones of the cranium (Osterholtz 2018)

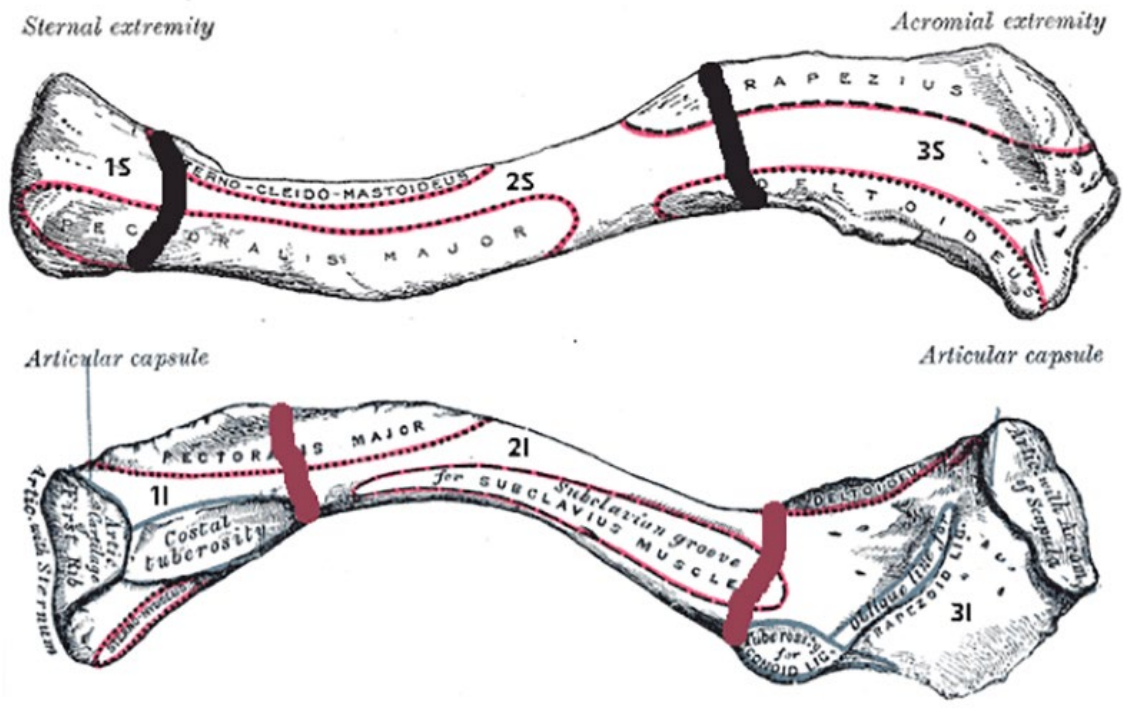

Figure 25. Zones of the clavicle (Osterholtz 2018)

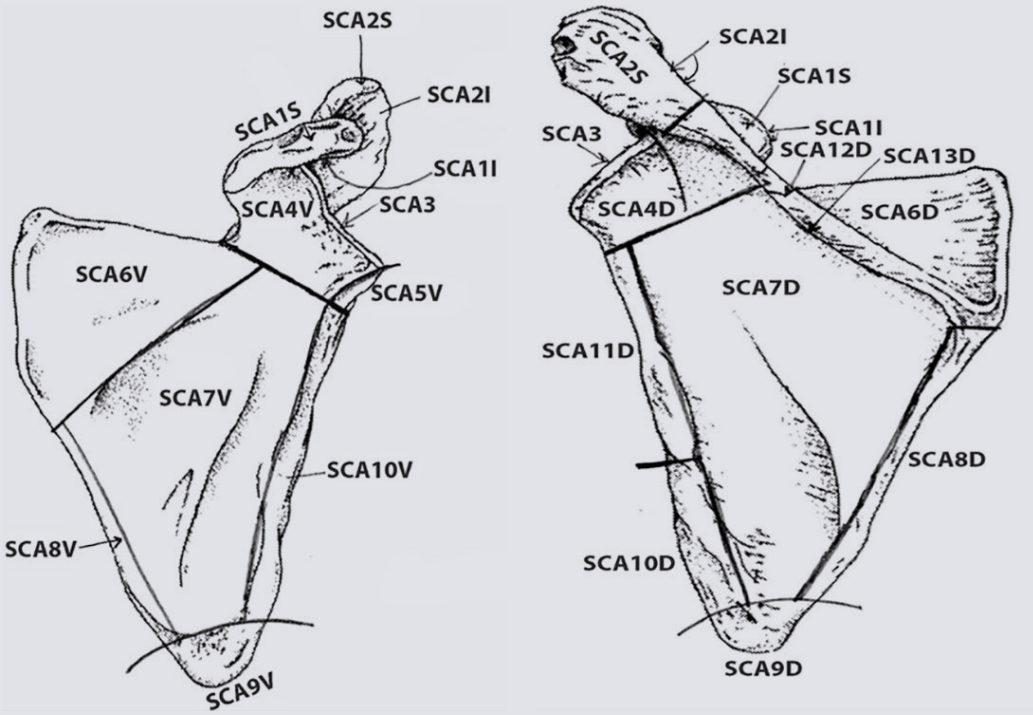

Figure 26. Zones of the scapula (Osterholtz 2018)

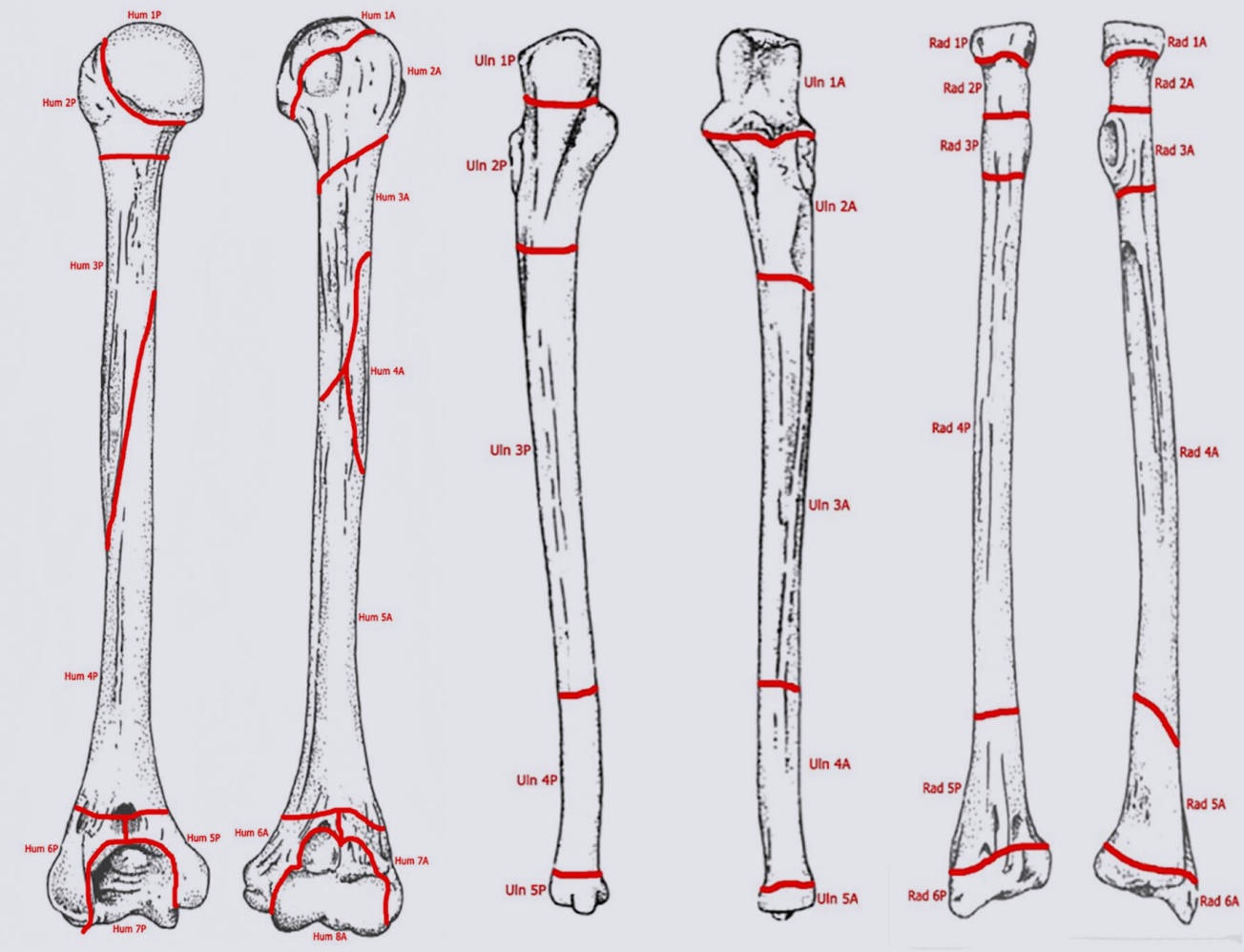

Figure 27. Zones of the upper limb long bones (Osterholtz 2018)

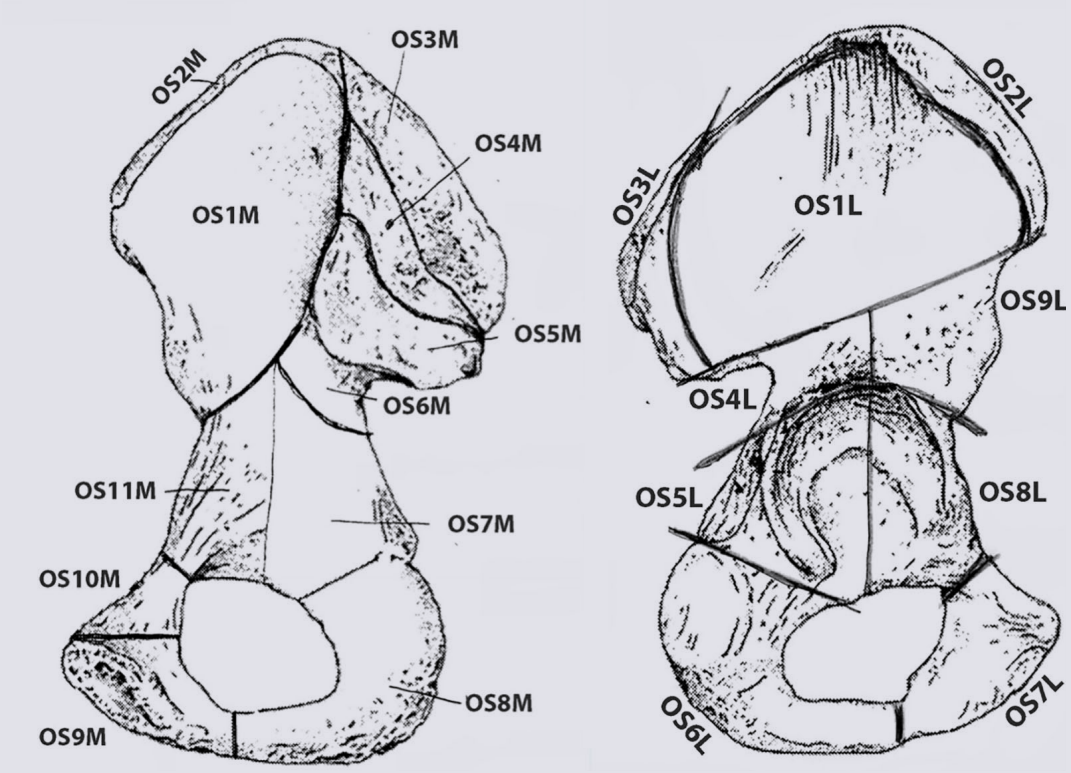

Figure 28. Zones of the os coxa (Osterholtz 2018)

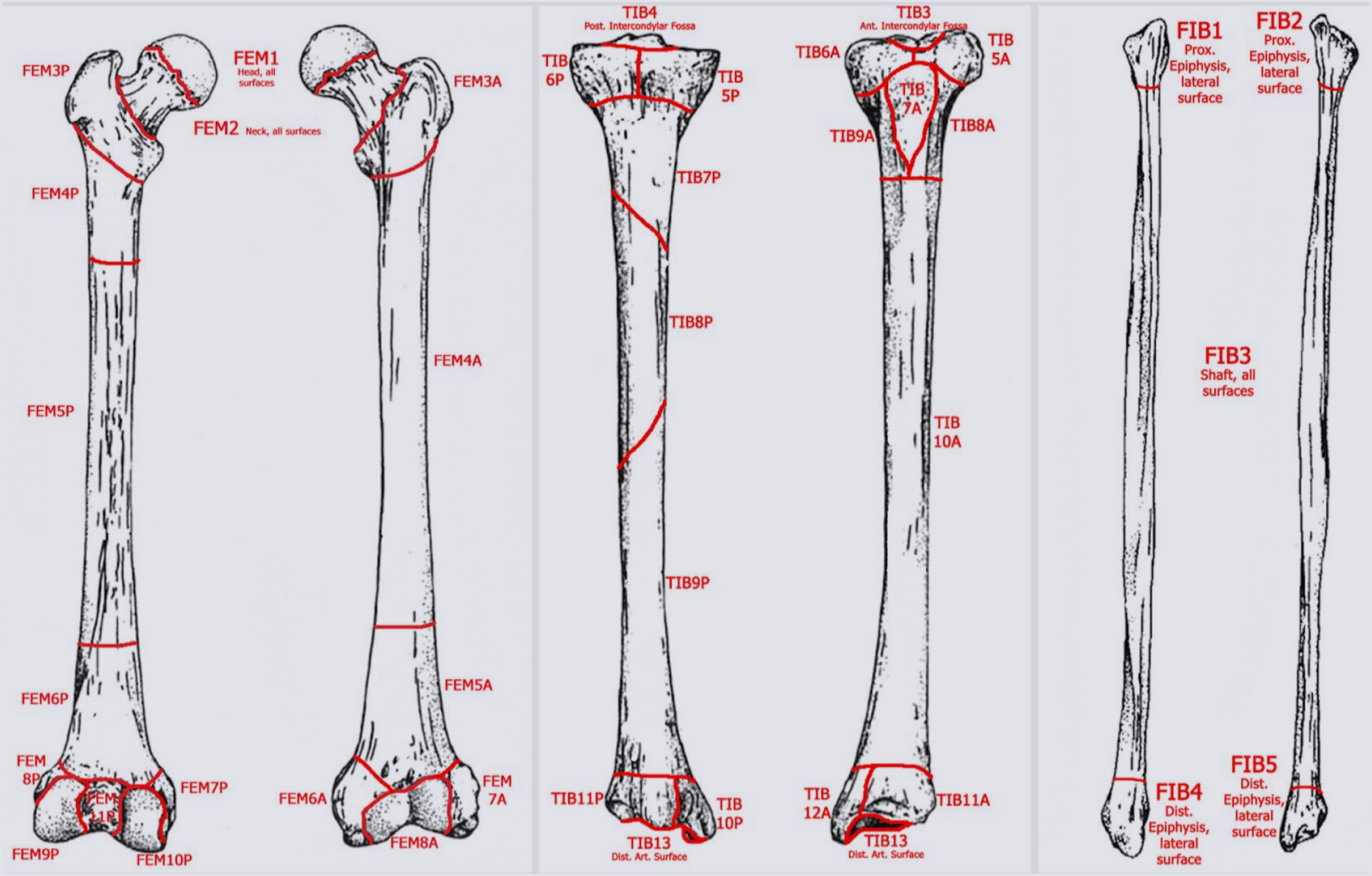

Figure 29. Zones of the lower limb long bones (Osterholtz 2018)

Instead of zones, other scholars have used **landmarks**, that is, standard anatomical features. **Table 5** lists the landmarks for the anterior cranium and the scapula from Mack et al. (2016). For the landmarks used for the remaining skeleton, as well as for relevant illustrations, see the original publication. For each element, the landmarks are coded as present or absent, whereby a landmark is considered present if more than 50% of it is observed.

Bone fragments that are too small to identify should be divided in broad categories (e.g. cortical bone/trabecular bone, cranial bone/post-cranial bone, axial skeleton/appendicular skeleton), sorted by size class based on maximum dimension, counted and weighted (Outram 2001). The size classes will depend on the assemblage (e.g., 0–10, 11–20, 21–30, 30+ mm). The above process should be performed per burial section in order to obtain some quantification of the material available and its distribution.

When inventorying teeth, for each maxilla/mandible with preserved alveoli and/or teeth, the categories given in **Table 6** should be used. Loose teeth should simply be recorded as present along with their degree of development (see section 'Age-at-death' for dental development standards). Different systems have been proposed for coding each permanent and deciduous tooth (e.g. Zsigmondy, Buikstra and Ubelaker 1994, Fédération Dentaire International) and it is up to each scholar to decide which one he/she finds easier to implement. We recommend avoiding numerical systems whereby each tooth is coded by a number (e.g. Buikstra and Ubelaker 1994) and instead opt for a more descriptive coding scheme that allows immediate identification of each tooth. For example, use 'U' for the upper and 'L' for the lower jaw, 'L' and 'R' to distinguish left and right, and identify teeth by their initials (e.g. I1 for central incisors, M2 for second molars etc). In a system as such, the maxillary left central incisor would be coded as ULI1.

In case any intrusive bones/teeth are identified, they should be noted in the inventory as such and be clearly separated from the skeletal remains of the primary burial. If such a separation cannot be performed due to the morphological similarity of the remains and/or their preservation, a relevant note must be made.

SEX ASSESSMENT

Sex assessment focuses principally on the morphology of the pelvis and secondarily on the cranium. Note that whereas pelvic sexually dimorphic traits are not generally population-specific (e.g., Klales et al. 2012; Oikonomopoulou et al. 2017), this does not apply to cranial traits. This is due to the fact that cranial sexual dimorphism is related to the greater robusticity that characterises males compared to females but robusticity largely reflects load-bearing activity, which depends upon the cultural norms of each population (Barker et al. 2008a). Morphological traits that may be useful in sex assessment are given in **Table 7**, while Figures 30 and 31 visualise the location of these traits.

Table 5. Selected landmarks (Mack et al. 2016)

Anterior cranium	Scapula
Left superciliary arch	Acromion
Right superciliary arch	Coracoid process
Left supraorbital margin	Spinoglenoid notch
Right supraorbital margin	Glenoid fossa
Frontal crest	Superior border
Left nasal bone	Scapular neck
Right nasal bone	Scapular spine
Vomer	Body
Left infraorbital foramen	Medial border
Right infraorbital foramen	Lateral border
Left zygomatic	Inferior angle
Right zygomatic	

Table 6. Dental recording (Buikstra and Ubelaker 1994)

Code	Definition
1	Present, not in occlusion
2	Present, development completed, in occlusion
3	Missing, no associated alveolar bone
4	Missing, antemortem loss
5	Missing, postmortem loss
6	Missing, congenital absence
7	Present, damage renders measurement impossible
8	Present, unobservable

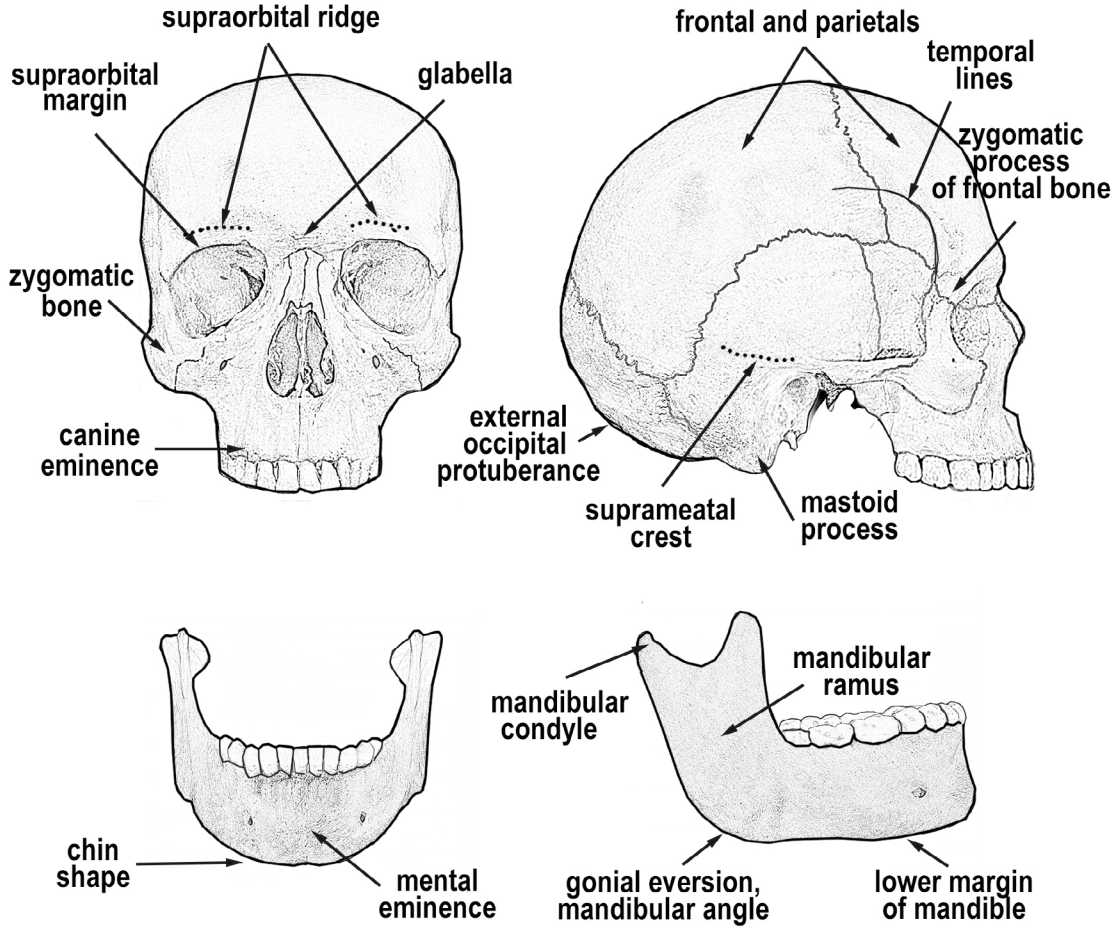

Figure 30. Cranial and mandibular sexually dimorphic anatomical areas

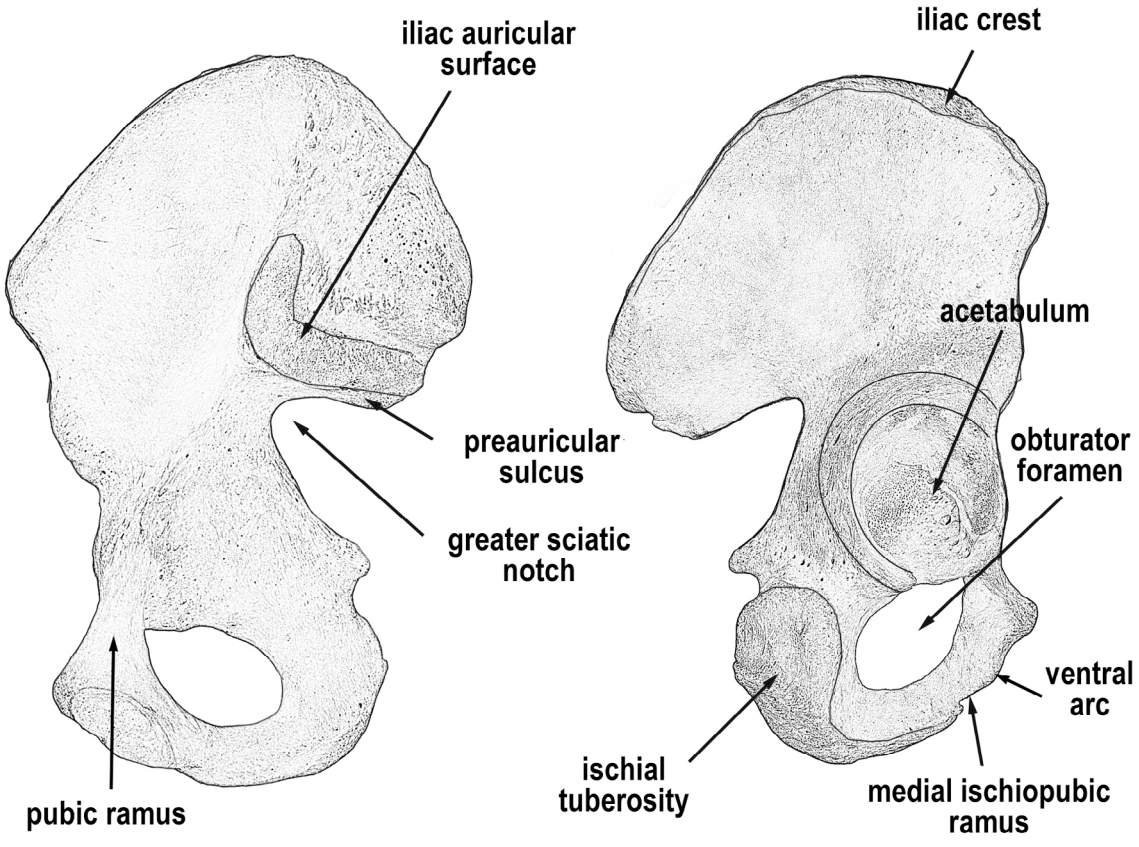

Figure 31. Pelvic sexually dimorphic anatomical areas

Table 7. Sexually dimorphic traits (Bass 1995; Buikstra and Ubelaker 1994; Ferembach et al. 1980; Krogman and İşcan 1986; Loth and Henneberg 1996; Nikita 2017; Phenice 1969; Schwartz 1995)

Anatomical area	Trait	Female expression	Male expression
Pelvis	Iliac auricular surface	Elevated from surrounding bone	Not elevated
	Iliac crest	Sinuous and smooth	Angulated
	Greater sciatic notch	Wide and shallow	Narrow and deep
	Preauricular sulcus	Present	Absent or very small and shallow
	Subpubic concavity	Present	Absent
	Subpubic arch	Broad U shaped	V shaped
	Ventral arc	Present	Absent
	Medial ischiopubic ramus	Narrow and sharp, often a ridge is present	Wide and dull
	Pubic rami	Long	Short
	Ischial tuberosity	Small	Large
	Obturator foramen	Small and triangular	Large and ovoid
	Acetabulum	Small, antero-laterally directed	Large, laterally directed
	Sacrum	Short, wide, less curved	Long, narrow, curved
Skull	Supraorbital margin	Sharp	Blunt
	Supraorbital ridges/glabella	Less pronounced	More pronounced
	Orbital outline	Circular	Squared
	Temporal lines	Slight	Marked
	Frontal and parietals	More bossed	Less bossed
	Mastoid process	Small	Large
	Suprameatal crest	Short, does not extend past the auditory meatus	Extends past the auditory meatus
	External occipital protuberance	Small	Well developed
	Occipital condyles	Small	Large
	Nuchal lines	Less pronounced	More pronounced
	Palate	Small, short, parabolic arch	Large, long, U-shaped arch
	Canine eminence	Indistinct	Distinct
	Chin shape	Round, pointed midline	Square
	Mental eminence	Less pronounced	More pronounced
	Mandibular ramus	No or very slight flexure	Flexure
	Mandibular ramus	Narrow	Broad
	Gonial eversion	Minimal	Pronounced
	Lower margin of mandible	Thin	Thick
	Mandibular angle	Obtuse	Perpendicular
	Mandibular condyles	Slight	Large
	Zygomatic process of frontal bone	Thin	Thick
	Zygomatic bone	Low and smooth	High and rough

When assessing sex, it is important to use different categories to determine how confident the assessment is, as shown in **Table 8**.

Metric analysis can also be used in sex estimation adopting measurements of the cranial and postcranial skeleton. An important aspect of metric methods is that they are population-specific. For American Whites and Blacks, Spradley and Jantz (2011) proposed the sex classification equations of **Table 9** and the cut off points of **Table 10**. Individuals with values higher than the sectioning point are considered male, whereas those with values smaller than the sectioning point are considered female. For other groups, see Nikita (2017) and references therein. When using metric methods, note also that secular change has been suggested to play an important role in the size of various groups (e.g., Hoppa and Garlie 1998), which may affect the reliability of methods applied to individuals from different time periods.

Table 8. Sex assessment categories

Sex category	Characteristics
Female	Exhibiting all skeletal traits indicating female sex
Probable Female	Exhibiting some of the skeletal traits indicating female sex
Ambiguous	Exhibiting either a mixture of male and female traits or traits that show an intermediate expression between male and female
Probable Male	Exhibiting some of the skeletal traits indicating male sex
Male	Exhibiting all skeletal traits indicating male sex
Indeterminate	Sex cannot be estimated either because of the poor preservation of the remains or because the individual is non-adult

Table 9. Sex classification functions for Americans (all measurements in cm; for measurement definitions, see section Metrics) | Drawn from Tables 3 and 4 in Spradley and Jantz 2011

Bone	Ethnic group	Equation
Cranium	Black	(0.71406*bizygomatic breadth) + (0.43318*mastoid height) + (-0.59308*biauricular breadth) + (0.34451*upper facial height) + (-0.14842*minimum frontal breadth) + (0.53049*foramen magnum breadth) + (-0.60805*orbital height) + (0.32505*nasal height) + (-54.2458)
	White	(0.50255*bizygomatic breadth) + (-0.07786*basion-nasion length) + (0.24989*mastoid height) + (0.19553*nasal height) + (0.24263*basion-bregma height) + (-0.15875*minimum frontal breadth) + (-0.13224*biauricular breadth) + (0.21776*glabella occipital length) + (-0.09443*frontal chord) + (-0.08327*parietal chord) + (-0.13411*occipital chord) + (-81.1812)
Mandible	Black	(0.13874*bigonial width) + (0.19311*bicondylar breadth) + (-34.6986)
	White	(0.15798*maximum ramus height) + (0.21951*bigonial width) + (0.06335*mandibular length) + (-35.0107)
Clavicle	Black	(0.2877*maximum length) + (0.9636*sagittal diameter at midshaft) + (1.1065*vertical diameter at midshaft) + (-66.6844)
	White	(0.23645*maximum length) + (0.88675*sagittal diameter at midshaft) + (0.60941* vertical diameter at midshaft) + (-51.7722)
Scapula	Black	(0.25647*height) + (0.2157*breadth) + (-60.55)
	White	(0.19365*height) + (0.25609*breadth) + (-55.6564)
Humerus	Black	(0.42616*epicondylar breadth) + (0.92*head diameter) + (0.49507*maximum diameter at midshaft) + (-74.5878)
	White	(0.04008*maximum length) + (0.4011*epicondylar breadth) + (0.26862*maximum vertical head diameter) + (0.62205*maximum diameter at midshaft) + (-59.6723)

Bone	Ethnic group	Equation
Radius	Black	(0.12149*maximum length) + (0.65603*sagittal diameter at midshaft) + (0.60906* transverse diameter at midshaft) + (-47.8611)
	White	(0.11151*maximum length) + (1.17296*sagittal diameter at midshaft) + (0.7476* transverse diameter at midshaft) + (-51.8801)
Ulna	Black	(0.07912*maximum length) + (0.8104*dorso-volar diameter at midshaft) + (0.74434* transverse diameter at midshaft) + (-44.2026)
	White	(0.1189*maximum length) + (0.98611*dorso-volar diameter at midshaft) + (0.89642* transverse diameter at midshaft) + (-0.09097*minimum circumference) + (-54.2634)
Sacrum	Black	(0.09686*transverse diameter of segment 1) + (-4.69561)
	White	(0.23919*anterior breadth) + (-0.03177*transverse diameter of segment 1) + (-8.09535)
Os Coxa	Black	(0.21749*height of os coxa) + (-0.11432*iliac breadth) + (-0.16143*pubis length) + (0.37051*ischium length) + (-45.1877)
	White	(0.15836*height) + (-0.08458*breadth) + (-0.12135*pubis length) + (0.1338*ischium length) + (-21.4996)
Femur	Black	(0.41661*epicondylar breadth) + (0.59516*maximum diameter of head) + (-58.836)
	White	(0.3644*epicondylar breadth) + (0.52629*maximum diameter of head) + (0.02826*bicondylar length) + (-65.70614)
Tibia	Black	(0.42495*maximum proximal epiphyseal breadth) + (0.34828*maximum distal epiphyseal breadth) + (-48.2631)
	White	(0.02828*length) + (0.6134*maximum proximal epiphyseal breadth) + (0.424*maximum diameter at nutrient foramen) + (-0.13118*circumference at nutrient foramen) + (-58.633)
Fibula	Black	(0.073*maximum length) + (0.09111*maximum diameter at midshaft) + (-29.4408)
	White	(0.07437*maximum length) + (0.14191*maximum diameter at midshaft) + (-29.5745)

Key: Sectioning point is 0, negative values signify females and positive values males

Table 10. Univariate sectioning points and classification rates | Drawn from Tables 7 and 8 in Spradley and Jantz 2011

AMERICAN BLACKS			AMERICAN WHITES		
Measurement	**Sectioning point**	**Classification rate**	**Measurement**	**Sectioning point**	**Classification rate**
Fem. Epicondylar Br.	78	0.89	Tib. Prox. Epiphyseal Br.	74	0.90
Tib. Prox. Epiphyseal. Br.	74	0.88	Scapula Height	153	0.89
Scapula Height	150	0.87	Fem. Epicondylar Br.	80	0.88
Fem. Max. Head Diam.	44	0.86	Fem. Max. Head Diam.	45	0.88
Humerus Epicondylar Br.	60	0.86	Humerus Epicondylar Br.	60	0.87

Measurement	Sectioning point	Classification rate	Measurement	Sectioning point	Classification rate
Humerus Head Diameter	44	0.86	Radius Max. Length	241	0.86
Scapula Breadth	103	0.86	Os Coxa Height	212	0.85
Radius Max. Length	253	0.85	Scapula Breadth	102	0.84
Clavicle Max. Length	150	0.84	Ulna Max. Length	258	0.84
Calcaneus Max. Length	81	0.83	Humerus Head Diameter	46	0.83
Fem. AP Subtroch Diam.	27	0.83	Clavicle Max. Length	148	0.82
Ischium Length	83	0.83	Humerus Max. Length	320	0.82
Ulna Max. Length	271	0.83	Hum. Min. Diam. MS	17	0.82
Ulna Phys. Length	240	0.83	Ulna Phys. Length	229	0.82
Fibula Maximum Length	384	0.82	Fem. Bicondylar Length	451	0.82
Fem. Bicondylar Length	465	0.81	Tibia Circum. Nut. For.	92	0.81
Humerus Max. Length	325	0.81	Fibula Maximum Length	369	0.81
Os Coxa Height	202	0.81	Femur Max. Length	455	0.80
Tib. Diameter Nut. For.	35	0.8	Tibia Length	375	0.79
Calcaneus Mid. Breadth	41	0.79	Fem. Circum. Midshaft	87	0.78
Fem. Circum. Midshaft	87	0.79	Tib. Dist. Epiphyseal Br.	49	0.78
Femur Max. Length	469	0.79	Tib. Diameter Nut. For.	34	0.76
Tibia Circum. Nut. For.	95	0.79	Calcaneus Max. Length	82	0.76
Tibia Length	393	0.79	Calcaneus Mid. Breadth	42	0.76
Bizygomatic Breadth	127	0.78	Fem. Trans. Diam.	26	0.75
Bicondylar Breadth	32	0.77	Bizygomatic Breadth	125	0.75
Cranial Maximum Length	182	0.76	Ischium Length	85	0.74
Hum. Min. Diam. MS	18	0.76	Bigonial Diameter	94	0.74
Tib. Dist. Epiphyseal Br.	48	0.75	Cranial Base Length	103	0.73
Hum. Max. Diam. MS	22	0.74	Radius Sag. Diam. MS	12	0.73
Clavicle Sag. Diameter	13	0.73	Ulna Trans. Diam.	15	0.73
Fem. Trans. Diam.	26	0.73	Cranial Maximum Length	183	0.73
Radius Sag. Diam. MS	12	0.72	Basion-Bregma Height	138	0.72
Radius Trans. Diam. MS	15	0.72	Hum. Max. Diam. MS	22	0.72
Bigonial Diameter	42	0.72	Radius Trans. Diam. MS	15	0.72

Measurement	Sectioning point	Classification rate	Measurement	Sectioning point	Classification rate
Height at Mental Foramen	21	0.71	Fem. AP Diam. Midshaft	29	0.72
Basion-Bregma Height	134	0.71	Upper Facial Breadth	103	0.71
Upper Facial Height	70	0.71	Fem. Trans. Subtroch.	30	0.71
Maximum Ramus Height	25	0.71	Bicondylar Breadth	114	0.71
			Biauricular Breadth	120	0.70
			Ulna Min. Circum.	35	0.70

Key: The classification rate indicates the correctly sexed individuals; e.g. 0.89 suggests that 89% of the individuals examined by Spradley and Jantz (2011) were assigned to the correct sex

Sex estimation in nonadults

Even though a number of methods have been proposed for sex assessment in juveniles (e.g. Bilfeld et al. 2015; Boucher 1955; Cardoso 2008; Coquerelle et al. 2011; Fazekas and Kósa 1978; Stull and Godde 2013; Viciano et al. 2013), these have been used to a limited extent because levels of testosterone are very low in males before puberty. Thus, skeletal differences between males and females are minimal prior to adolescence (Berg 2012).

AGE-AT-DEATH ESTIMATION

Skeletal age-at-death estimation methods for adults are based on physiological changes occurring in certain parts of the skeleton and link these to chronological age-at-death. Although chronological age-at-death represents a constant progression, this does not apply to skeletal age-at-death. This basic disparity is further complicated by the fact that adult ageing methods focus on degenerative skeletal changes, the rate of which differs at an intra- and inter-population level (Lampl et al. 1992). The estimation of age-at-death for juveniles is more accurate than for adults because it is based on developmental criteria occurring over a shorter time span. However, skeletal maturation and, to a lesser degree, dental development are still subject to the influences of intrinsic and extrinsic factors.

Because age-at-death estimation from the skeleton suffers from inherent inaccuracies, each skeleton is assigned to an age class rather than be given a strict age. Age classes become increasingly broad as the individual grows older. Such categories are given in **Table 11**.

Table 11. Age-at-death classes (Buikstra and Ubelaker 1994)

Categories	Age range
fetus	before birth
infant	0-3 years old
child	3-12 years old
adolescent	12-18 years old
young adult	18-35 years old
middle adult	35-50 years old
old adult	50+ years old
nonadult	<18 years old
adult	18+ years old
indeterminate	unable to estimate age-at-death

NONADULTS (AND YOUNG ADULTS)

Age-at-death estimation in nonadults is based on two broad approaches:

1. Mineralisation and eruption of the dentition
2. Development and maturation of skeletal remains, fusion of the ossification centres, and size and morphology of the individual skeletal elements

The dentition is less affected by adverse environmental circumstances, such as disease or malnutrition, compared to the skeleton, thus it is the preferred method, if available (Cardoso 2007).

Dental development

Each individual has two sets of teeth: deciduous and permanent. The deciduous teeth start to mineralise in utero (Hillson 1996), they are roughly half-formed by birth, and erupt in the mouth during the next 2 to 3 years. Permanent teeth also start to form in utero and gradually replace the deciduous ones.

Three main approaches are available for estimating age-at-death based on dental development:

1. Dental atlases that visualise the stage of dental development of the entire dentition at different ages, such as the London atlas (Figure 32)
2. Developmental stage of individual teeth (Figures 33-34)
3. Metric methods based on the length of individual teeth (**Table 12**)

Many more methods than those given in the figures and tables of this section are available and the reader is advised to consult the literature as these are often population-specific.

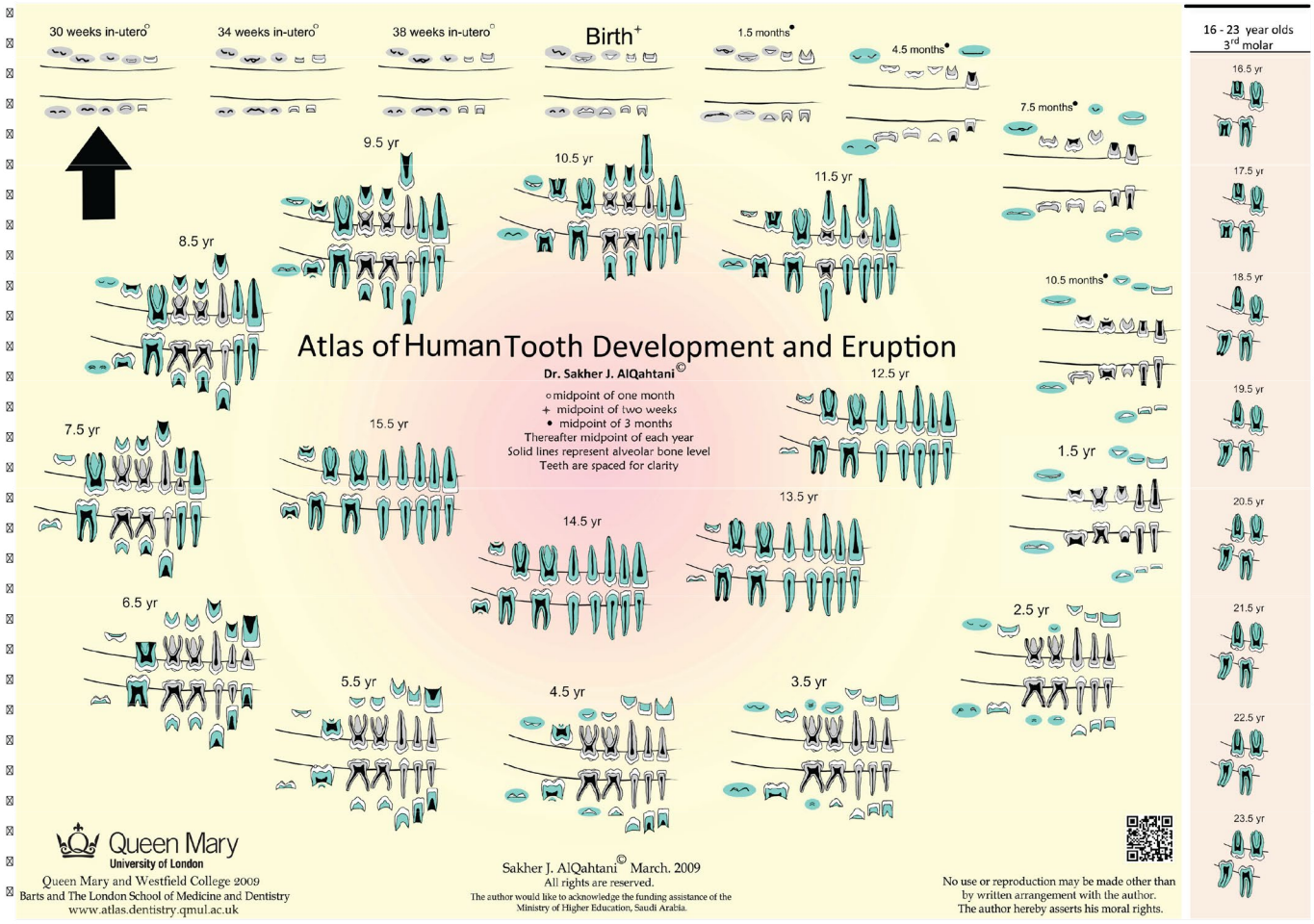

Figure 32. London atlas (AlQahtani et al. 2010; Downloadable at: https://www.qmul.ac.uk/dentistry/media/dentistry/images/atlas/atlas_of_tooth_development_in_English.pdf)

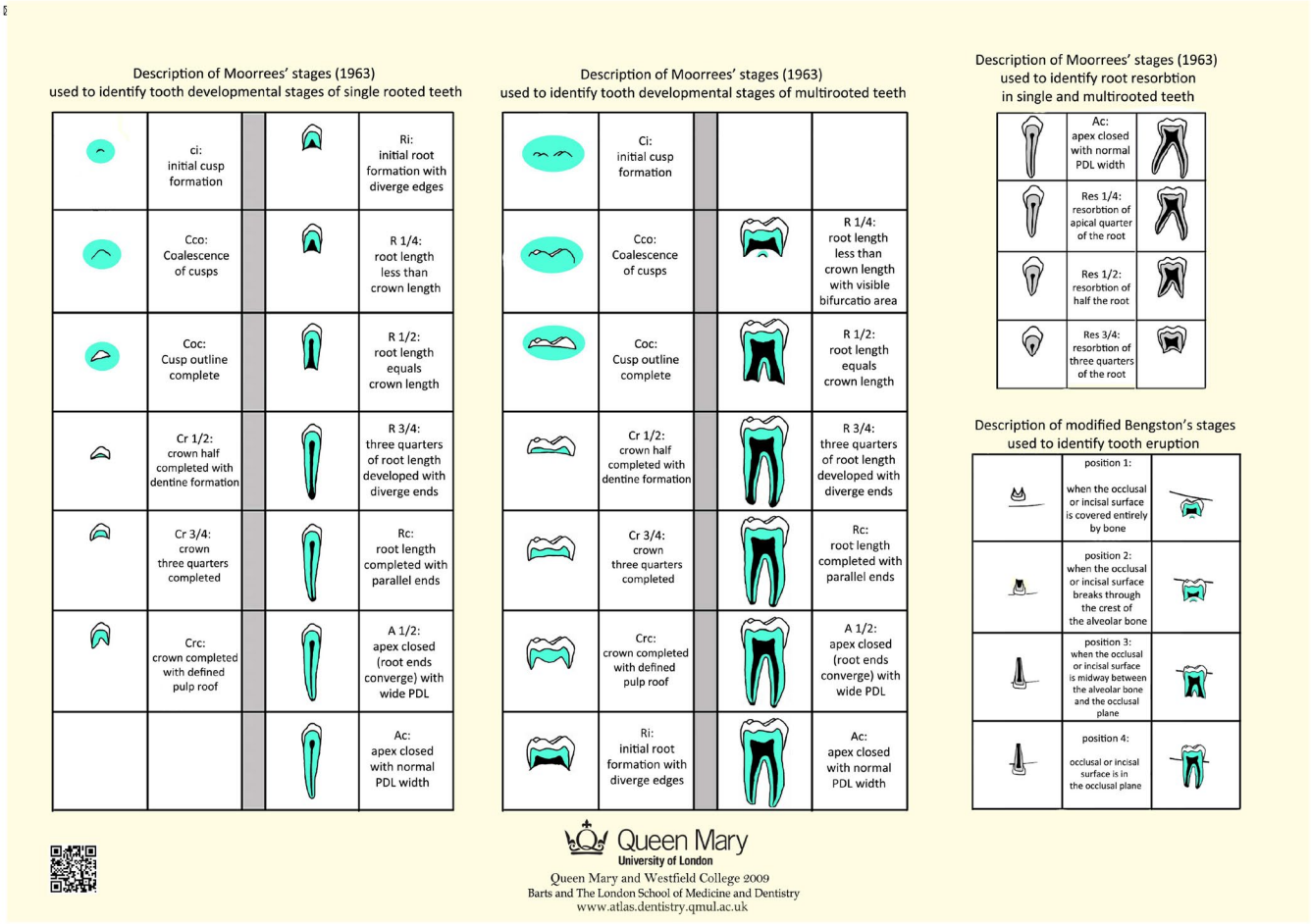

Figure 33. Tooth development stages based on Moorrees et al. (1963a, 1963b) | Redrawn by AlQahtani et al. 2010; Downloadable at: https://www.qmul.ac.uk/dentistry/media/dentistry/images/atlas/atlas_of_tooth_development_in_English.pdf

Table 12. Age-at-death estimation from tooth length (data for maxillary and mandibular teeth are combined except for I^2 and I^2) | Drawn from Liversidge et al. 1993

Tooth	Equation
di1	0.144 × length - 0.653
di2	0.153 × length - 0.581
dc	0.210 × length - 0.656
dm1	0.222 × length - 0.814
dm2	0.292 × length - 0.904
I1	0.052 - 0.060 × length + 0.035 × length^2
I^2	-0.166 + 0.533 × length + 0.003 × length^2
I_2	0.411 - 0.035 × length + 0.050 × length^2
C	-0.163 + 0.294 × length + 0.028 × length^2
M	-0.942 + 0.441 × length + 0.010 × length^2

Key:
d = deciduous tooth
i/I = incisor
c/C = canine
m/M = molar
length = for single-cusped or single-rooted teeth distance from cusp tip or mid-incisal edge to developing edge of crown or root in the midline parallel to the long axis of the tooth, in multi-cusped or multi-rooted teeth maximum tooth length; all distances in mm

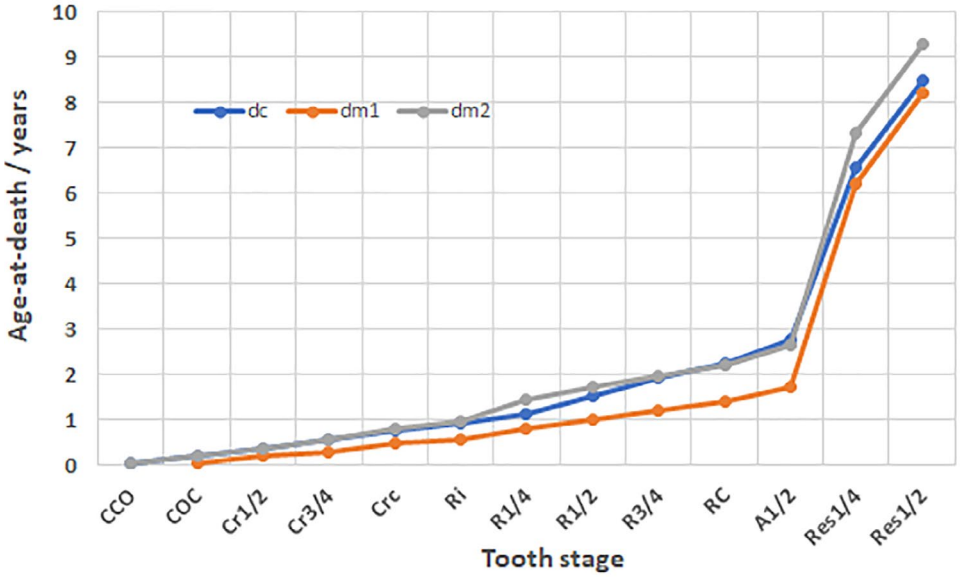

Figure 34A. Estimation of age-at-death (in years) based on individual tooth development stages for the deciduous canines and molars | Drawn from Table 6-5 in Cunningham et al. 2016; based on data from Shackelford et al. 2012

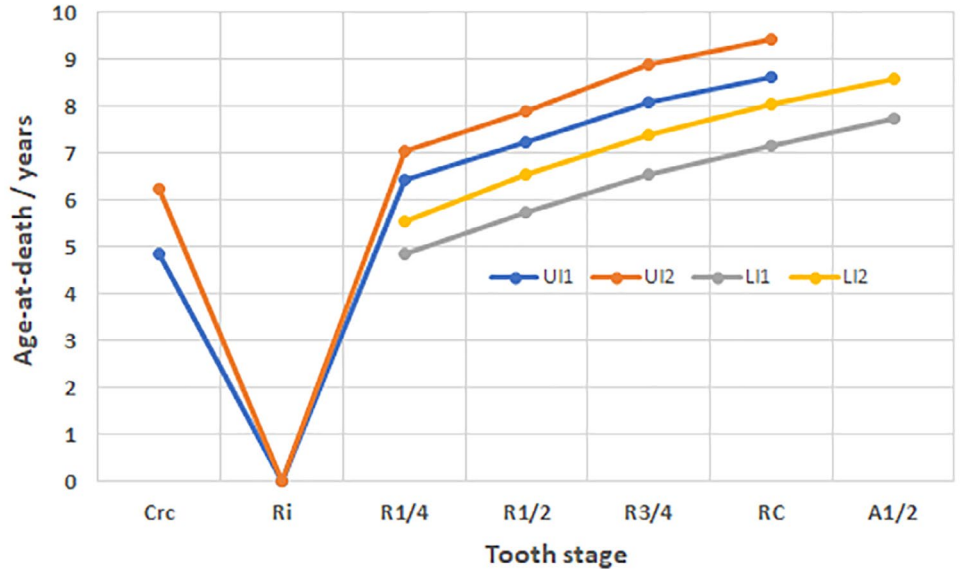

Figure 34B. Estimation of age-at-death (in years) based on individual tooth development stages for the permanent incisors | Drawn from Table 6-5 in Cunningham et al. 2016; based on data from Shackelford et al. 2012

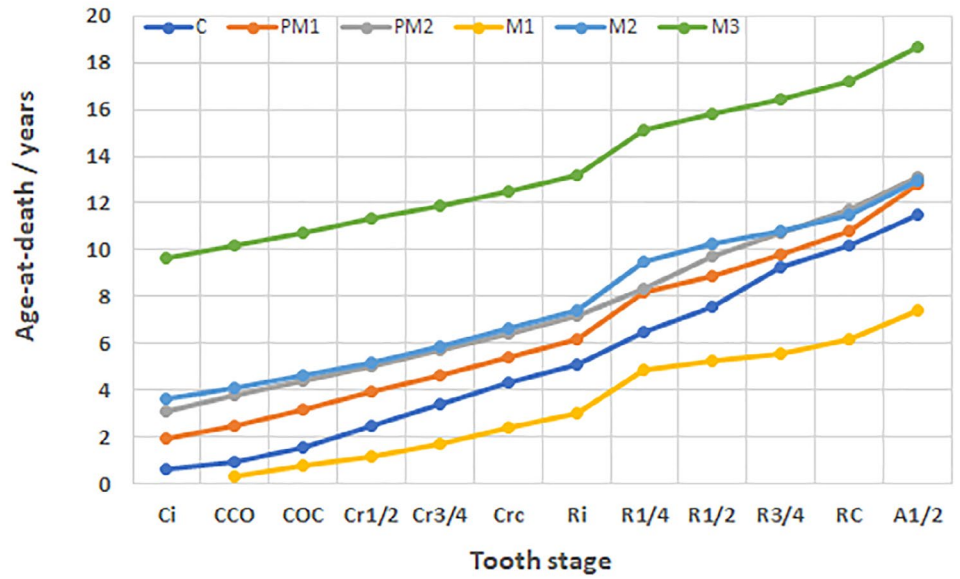

Figure 34C. Estimation of age-at-death (in years) based on individual tooth development stages for the permanent canines, premolars and molars Drawn from Table 6-5 in Cunningham et al. 2016; based on data from Shackelford et al. 2012

Appearance of ossification centres

The appearance of primary and secondary ossification centres may be used to estimate a minimum and a maximum age-at-death. However, most ossification centres appear in utero and will be difficult to identify accurately as their shape is still forming. Therefore, this method will not be described here because it is considered of rather limited applicability compared to the other approaches presented in this guide. Interested readers can consult Cunningham et al. (2016).

Union of ossification centres

Age-at-death estimates have also been developed based on the fusion of primary and secondary ossification centres (**Table 13**, Figures 35-45). This method is mostly useful when elements are in the process of fusing. When using this method, it must be noted that some elements fuse at an earlier age than the standard, while others may fail to fuse at all. Therefore, unless population-specific tests have been undertaken to confirm its accuracy, this method should only be used as a guide.

Table 13. Age of fusion of selected primary ossification centres (Cunningham et al. 2016)

Skeletal Element	Anatomical Parts	Age of Fusion
Frontal bone	Metopic suture	By 2nd- 4th year
Occipital bone	Squamous part – lateral parts	1st-4th year
	Basilar part – lateral parts	3rd-7th year
Sphenoid bone	Greater wing – body	By end of 1st year
Sphenoid-Occipital	Spheno-occipital synchondrosis	11th-17th year in females, 13th-19th year in males
Temporal bone	Petrous part – squamous part	By end of 1st year
Mandible	Mental symphysis	By end of 1st year

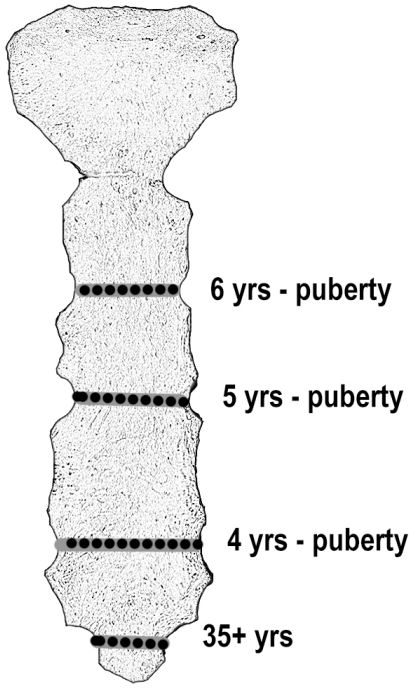

Figure 35. Fusion time of sternal ossification centres
Adapted from Cunningham et al. 2016 and Nikita 2017

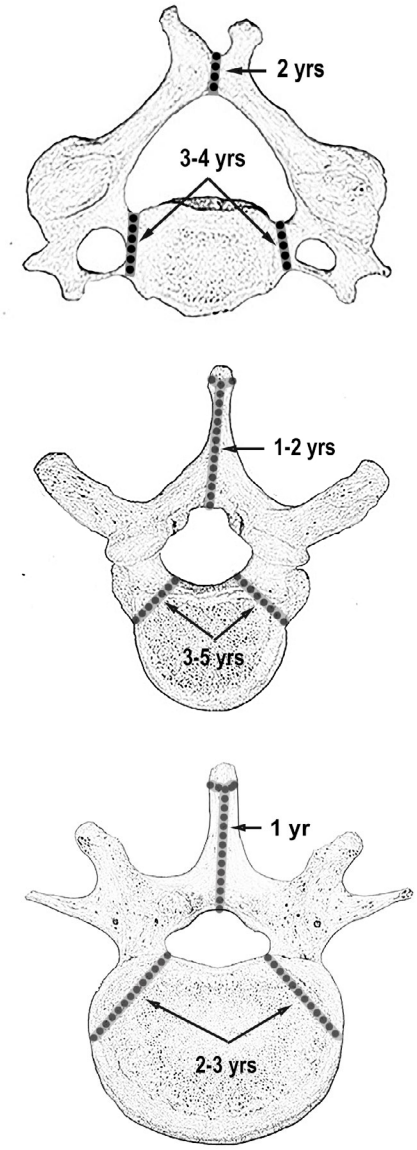

Figure 36. Fusion time of vertebral ossification centres
Adapted from Cunningham et al. 2016 and Nikita 2017

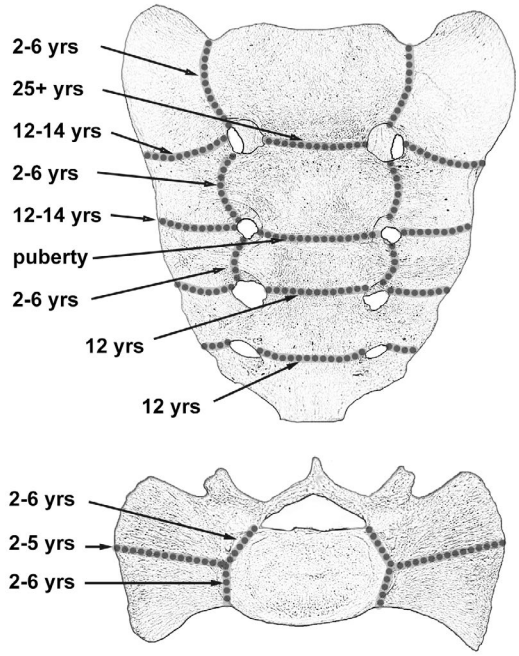

Figure 37. Fusion time of sacral ossification centres | Adapted from Cunningham et al. 2016 and Nikita 2017

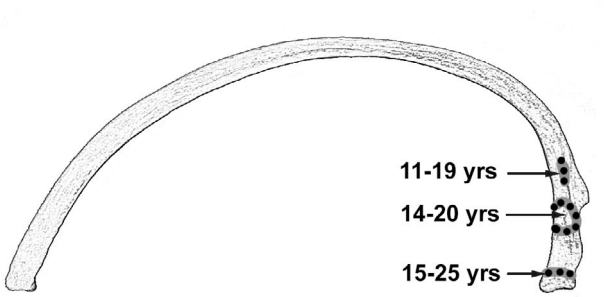

Figure 38. Fusion time of costal ossification centres
Adapted from Cunningham et al. 2016 and Nikita 2017

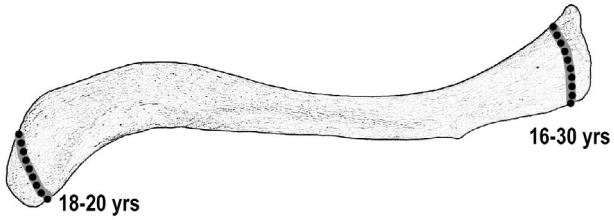

Figure 39. Fusion time of clavicular ossification centres
Adapted from Cunningham et al. 2016 and Nikita 2017

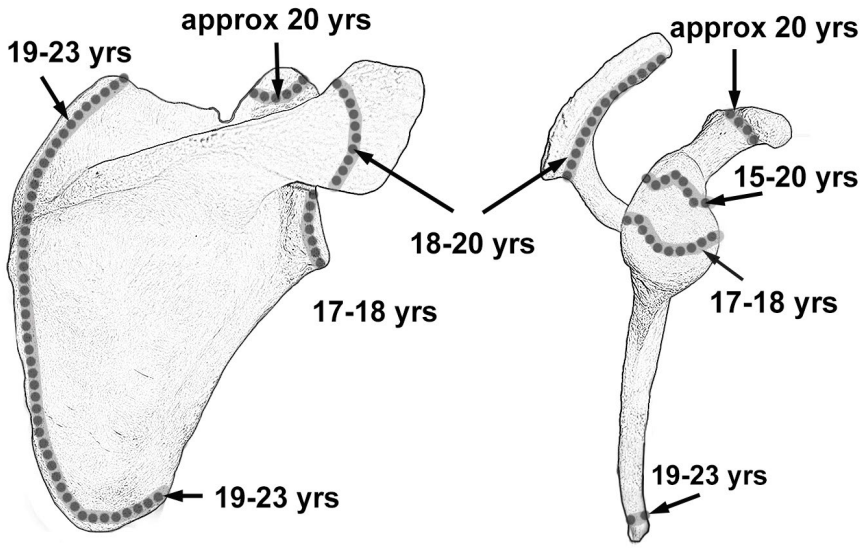

Figure 40. Fusion time of scapular ossification centres | Adapted from Cunningham et al. 2016 and Nikita 2017

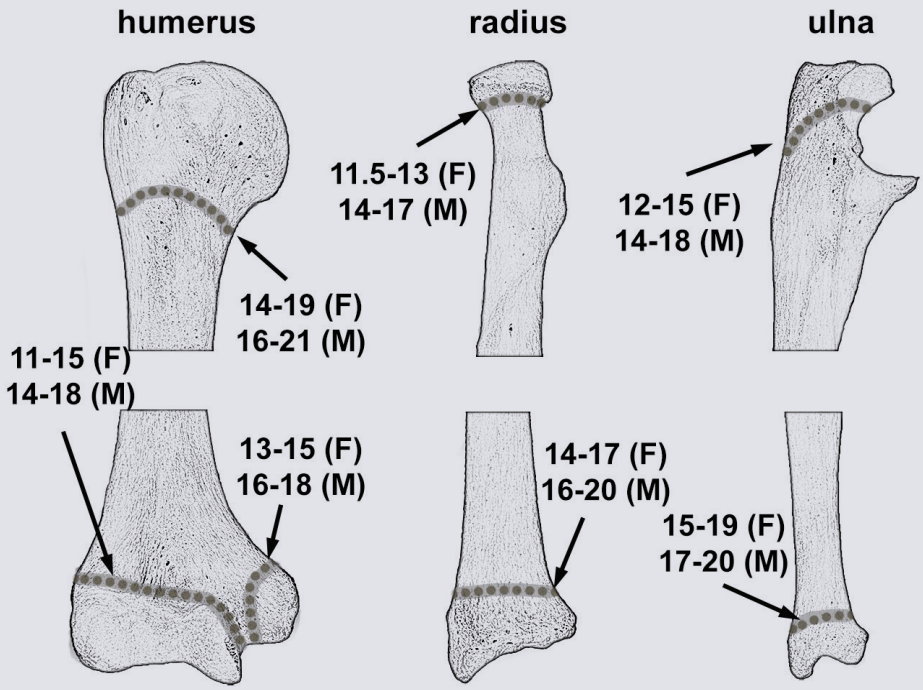

Figure 41. Fusion time of upper limb long bone ossification centres | Adapted from Cunningham et al. 2016 and Nikita 2017

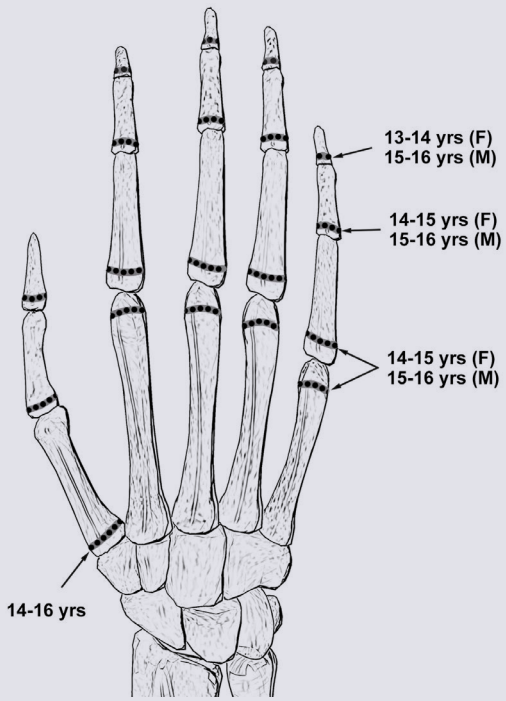

Figure 42. Fusion time of hand ossification centres
Adapted from Cunningham et al. 2016 and Nikita 2017

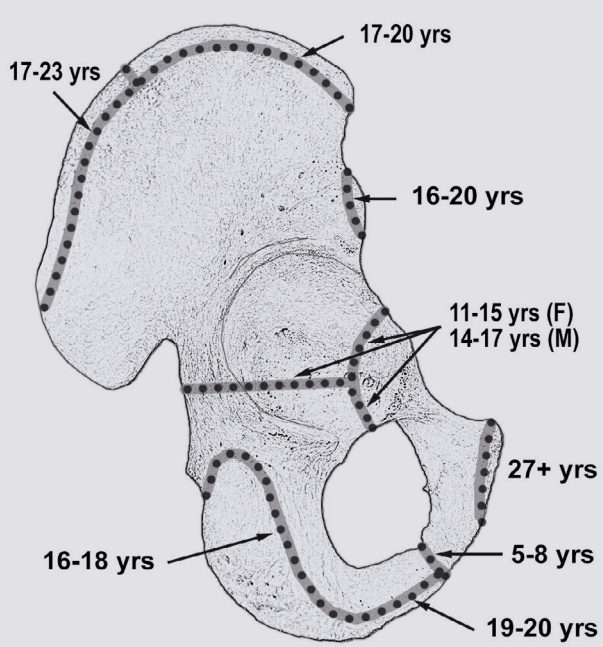

Figure 43. Fusion time of os coxal ossification centres
Adapted from Cunningham et al. 2016 and Nikita 2017

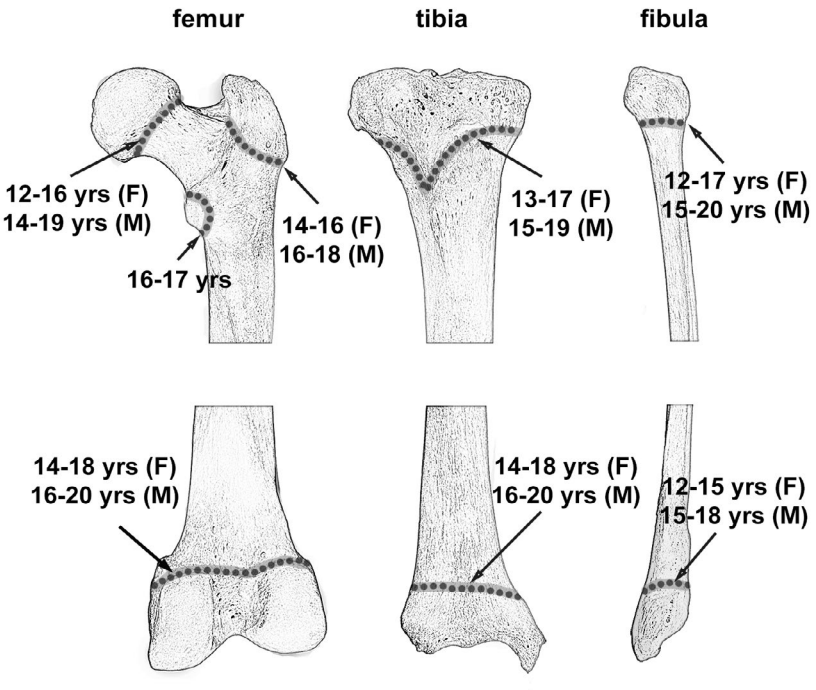

Figure 44. Fusion time of lower limb long bone ossification centres | Adapted from Cunningham et al. 2016 and Nikita 2017

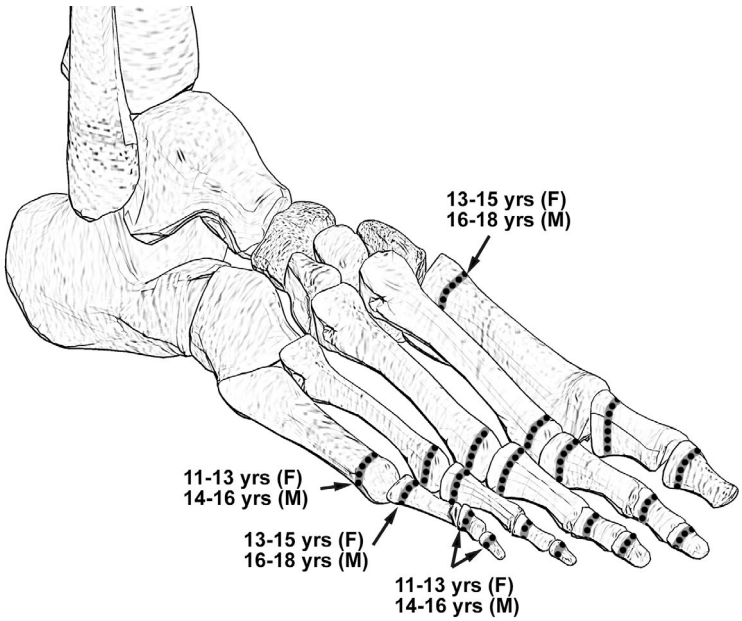

Figure 45. Fusion time of foot ossification centres | Adapted from Cunningham et al. 2016 and Nikita 2017

Long Bone Length

Metric analysis in the estimation of age-at-death for nonadult skeletal remains is based on the rate of skeletal growth prior to the fusion of the ossification centres. Note that this growth depends on environmental, nutritional and genetic factors; thus, this method should be used as a rough guide to age estimation. Figure 46 is based on data from the seminal work of Fazekas and Kósa (1978) for fetal remains, **Table 14** is drawn from Scheuer et al. (1980) for nonadults between 24 weeks in utero and 6 weeks postnatal, and Figures 47 and 48 are drawn from Maresh (1970) for nonadults from two months to 17 years. In Figures 47-48 the average of the male and female values published by Maresh (1970) is given since it is not possible to accurately determine the sex of nonadults. The reader is strongly advised to consult Cunningham et al. (2016) for published metrics from different assemblages and for various skeletal elements.

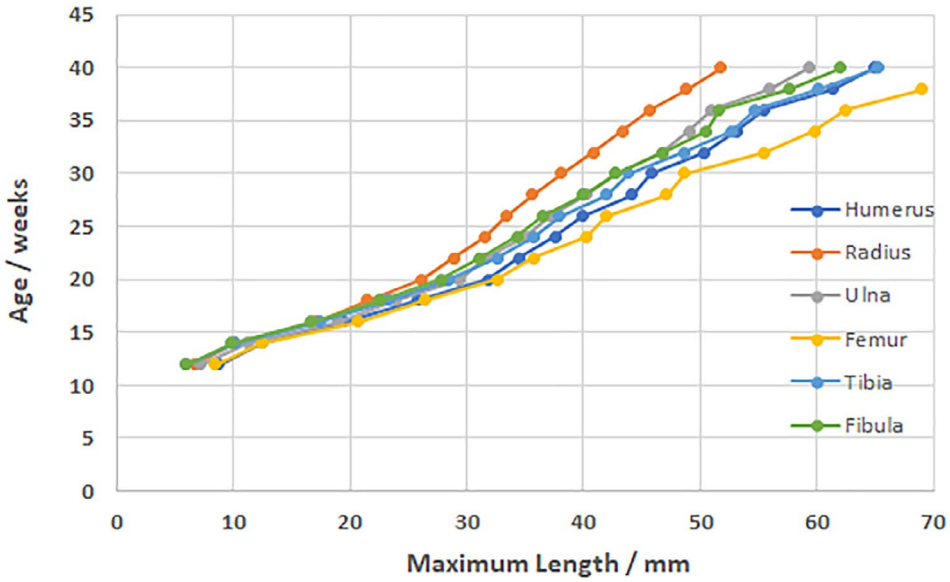

Figure 46. Length of foetal long bone diaphysis per age | Drawn from Fazekas and Kósa 1978

Table 14. Regression equations for age prediction for individuals 24 weeks in utero to 6 weeks postnatal (Scheuer et al. 1980)

Skeletal element	Type of equation	Regression equation	SEE
Humerus	linear	(0.4585 × length) + 8.6563	2.33
	logarithmic	(25.069 $\log_e$ × length) – 66.4655	2.26
Radius	linear	(0.5850 × length) + 7.7100	2.29
	logarithmic	(25.695 $\log_e$ × length) – 63.6541	2.24
Ulna	linear	(0.5072 × length) + 7.8208	2.20
	logarithmic	(26.078 $\log_e$ × length) – 68.7222	2.10
Femur	linear	(0.3303 × length) + 13.5583	2.08
	logarithmic	(19.7271 $\log_e$ × length) – 47.1909	2.04
Tibia	linear	(0.4207 × length) + 11.4724	2.12
	logarithmic	(21.2071 $\log_e$ × length) – 50.2331	2.11

Key: length = maximum length (mm); The logarithmic regression should be preferred for skeletons falling within the third trimester. Note that the standard error of estimate (SEE) is lower for the logarithmic regression, showing a better fitting

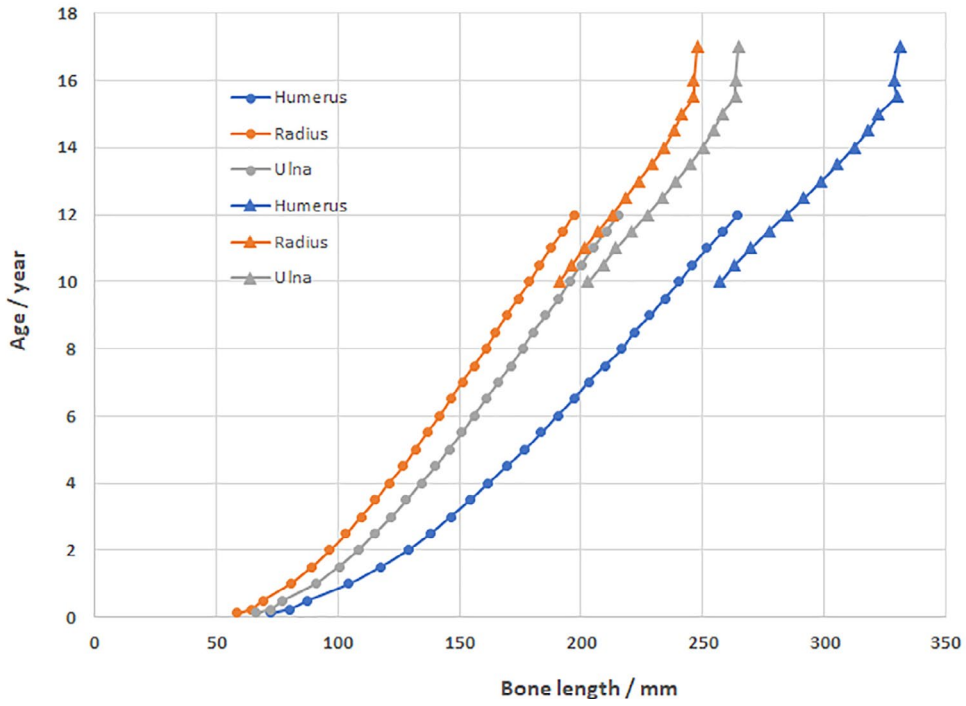

Figure 47. Bone length (in mm) per year; upper limbs | Drawn from Maresh 1970

Note: Circles stand for diaphyseal length, while triangles for total bone length (including the epiphyses)

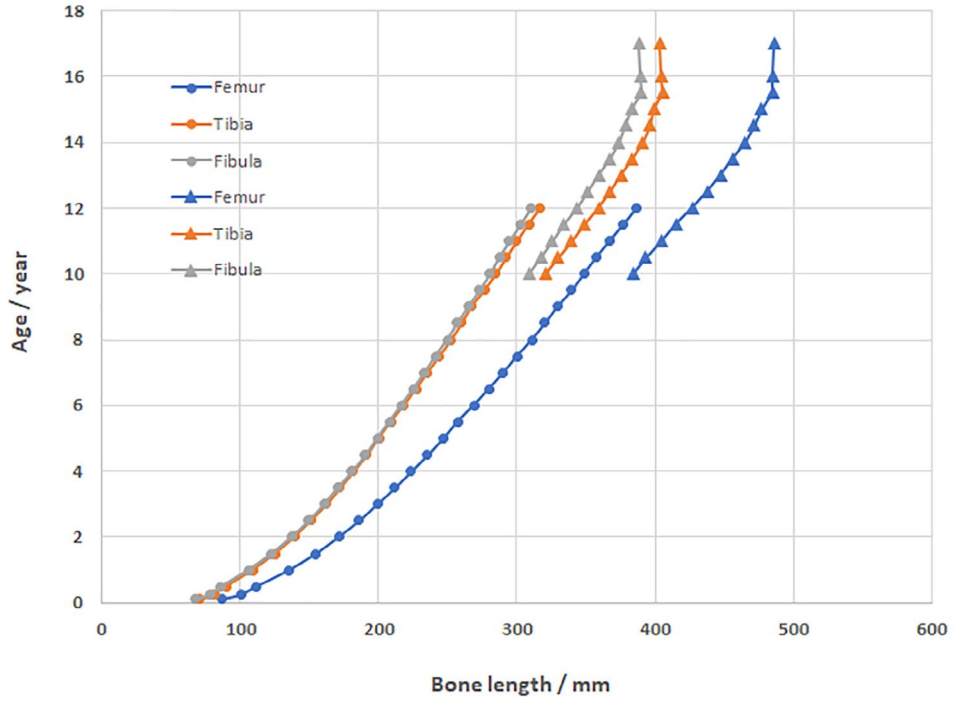

Figure 48. Bone length (in mm) per year; lower limbs | Drawn from Maresh 1970

Note: Circles stand for diaphyseal length, while triangles for total bone length (including the epiphyses)

ADULTS

For young adults, the final stages of skeletal maturation may provide important ageing information. If full skeletal maturity has been reached, age-at-death estimation is based on the degeneration and remodelling of the skeleton. The most widely used methods in the latter category focus on the morphology of the pubic symphysis, the auricular surface of the ilium and the sternal rib end.

Final stages of skeletal maturation

The iliac crest, vertebral annular rings, and medial clavicle complete maturation during the late second and third decades of life and, consequently, can be used for ageing young adults. In specific, the iliac crest fuses at 17 to 23 years, while complete fusion of the medial clavicle occurs by 30 years (Cunningham et al. 2016). Regarding the pattern of fusion of annular rings to the vertebral bodies, in individuals younger than 16 years there is no ring, in those aged 16 to 20 years the ring is fusing, and in adults 20-29 years old the ring has fused (Albert and Maples 1995). Finally, as shown in Figure 37, the first and second sacral vertebrae complete fusion over the age of 25 years, so they are also useful in ageing adults.

Pubic symphysis morphology

Different methods have been proposed for using the morphology of the pubic symphysis in age-at-death estimation (Berg 2008; Brooks and Suchey 1990; Gilbert and McKern 1973; Katz and Suchey 1986; Todd 1920, 1921). The Brooks and Suchey (1990) method will be presented here because it is the most broadly adopted in the literature; however, the reader is advised to consult the variants of this method to determine if they are more appropriate for his/her sample. **Table 15** presents the mean age that corresponds to the stages of morphological change and other descriptive statistics, **Table 16** describes the main age-related changes on the pubic symphysis, while Figures 49 and 50 visualise these changes.

Table 15. Mean age and standard deviation (SD) for each phase of the Suchey-Brooks scheme (Brooks and Suchey 1990)

	FEMALES		MALES	
Phase	**Mean age**	**SD**	**Mean age**	**SD**
I	19.4	2.6	18.5	2.1
II	25	4.9	23.4	3.6
III	30.7	8.1	28.7	6.5
IV	38.2	10.9	35.2	9.4
V	48.1	14.6	45.6	10.4
VI	60	12.4	61.2	12.2

Table 16. Age-related features of the pubic symphysis (Brooks and Suchey 1990)

Phase / **Feature**	**I**	**II**	**III**	**IV**	**V**	**VI**
Symphyseal face	Billowing (well-marked horizontal ridges and furrows)	Ridges may still be visible	Distinct ridges may be present or smooth surface	Fine grained; residual ridges and furrows may be present	Some depression of the surface	Depressed, perhaps pitted or porous with erratic ossification
Symphyseal rim	No rim			Oval outline complete (may be hiatus at ventral rim)	Complete rim; no or little erosion	Erosion and crenulation of the margins
Upper extremity	Not delimited	Commencing delimitation	Ossific nodules fusing	Fully defined, separate face from pubic tubercle		
Lower extremity	Not delimited	Commencing delimitation	Completing delimitation			
Dorsal margin			Dorsal plateau complete, no lipping	Slight lipping may be present	Moderate lipping may be present	
Ventral margin	Bevelling may be commencing	Ventral rampart may start to extend from either or both extremities	Ventral rampart in process of completion	Osteophytes may be present inferiorly	More prominent osteophytes and some breakdown of superior margin	Marked osteophytes present
Others						Prominent pubic tubercle may be present

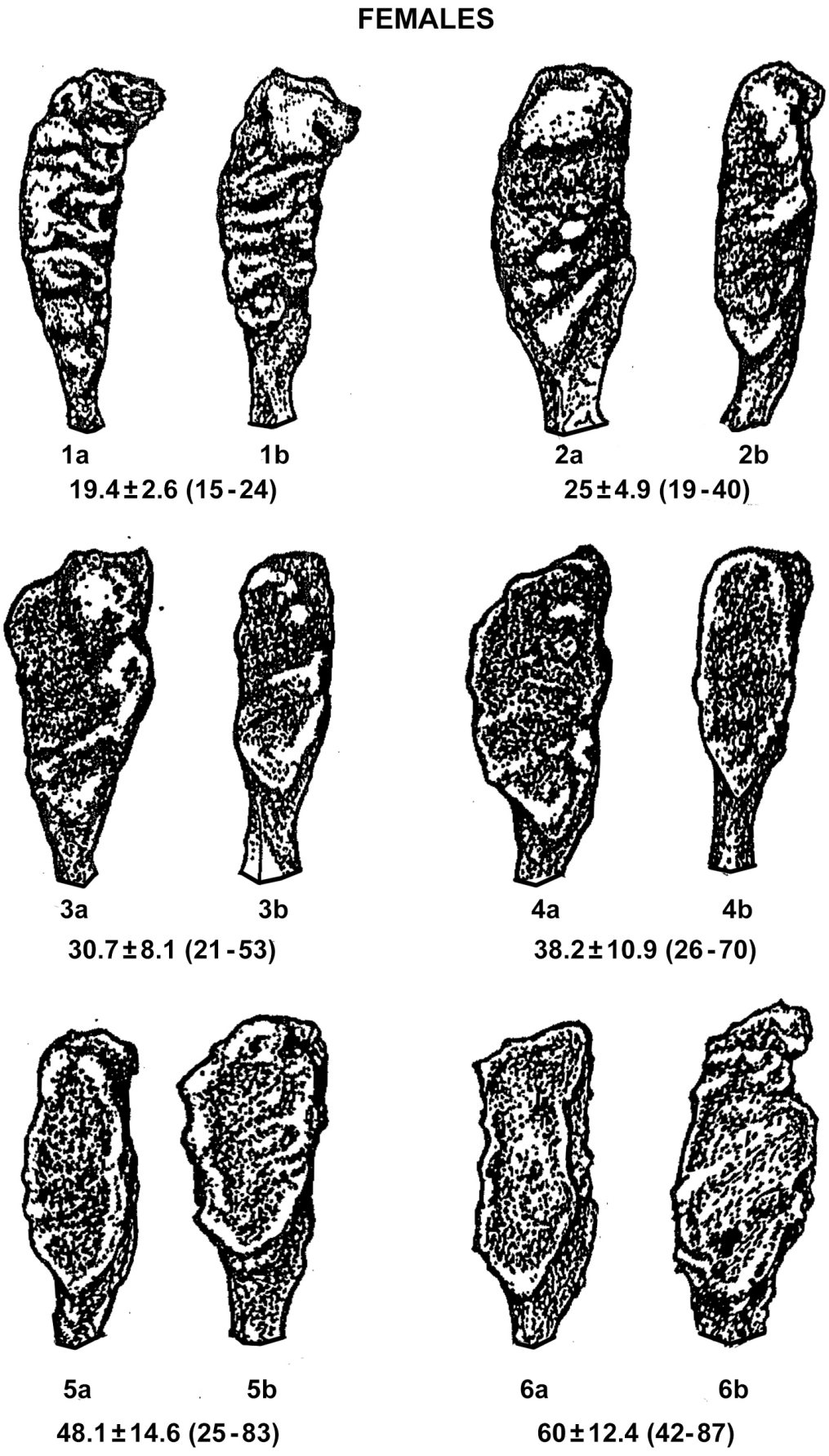

Figure 49. Morphological changes on the pubic symphysis per stage in females
Adapted from P. Walker's drawing in Buikstra and Ubelaker 1994

Key: mean age ± standard deviation (range); (a) indicates the pubic symphyseal morphology at the beginning of each stage and (b) its morphology at the end of the stage

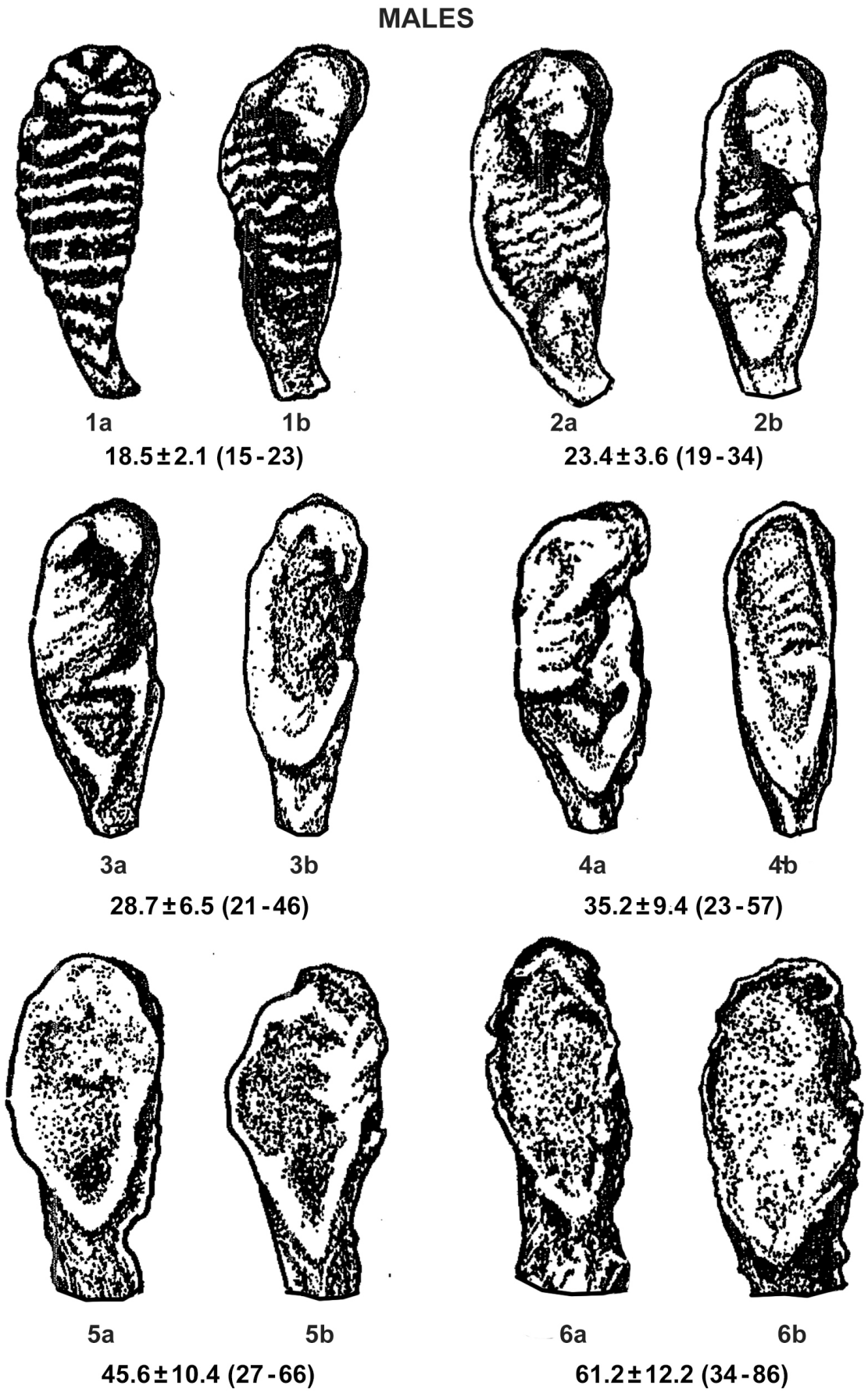

Figure 50. Morphological changes on the pubic symphysis per stage in males
Adapted from P. Walker's drawing in Buikstra and Ubelaker 1994
Key: mean age ± standard deviation (range); (a) indicates the pubic symphyseal morphology at the beginning of each stage and (b) its morphology at the end of the stage

Auricular surface morphology

Similarly to the pubic symphysis, various methods have been proposed that adopt morphological changes on the iliac auricular surface as a means of estimating age-at-death (Buckberry and Chamberlain 2002; Igarashi et al. 2005; Lovejoy et al. 1985; Osborne et al. 2004; Rougé-Maillart et al. 2009). The methods by Lovejoy et al. (1985) and Buckberry and Chamberlain (2002) will be presented here, but again the reader is advised to check the literature for more appropriate options depending on the sample. Figure 51 presents the main anatomical regions examined when the auricular surface is employed in age-at-death estimation, **Table 17** describes the main age-related changes on this surface based on Lovejoy et al. (1985), Figure 52 depicts representative auricular surfaces for young, middle and old adults, while **Tables 18-19** present the Buckberry and Chamberlain (2002) method. Note that in the Buckberry and Chamberlain (2002) method, different traits are independently recorded on the auricular surface (**Table 18**) and then all scores are summed to obtain a composite score. Subsequently, age-at-death is estimated based on this composite score (**Table 19**).

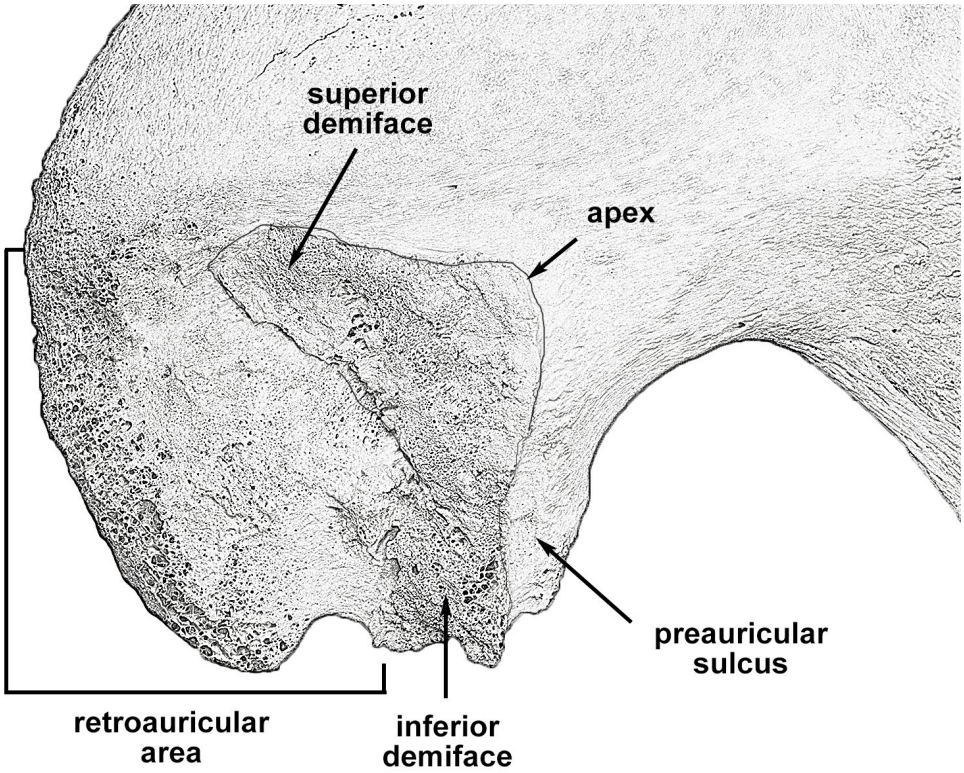

Figure 51. Regions of the ilium used for auricular surface ageing | Adapted from Nikita 2017

Table 17. Age-related features of the auricular surface (Lovejoy et al. 1985)

Stage / **Feature**	**1** 20-24 yrs	**2** 25-29 yrs	**3** 30-34 yrs	**4** 35-39 yrs	**5** 40-44 yrs	**6** 45-49 yrs	**7** 50-60 yrs	**8** 60+ yrs
Billowing	Well defined transverse billows over most surface	Slight to moderate loss/ replacement by striae	Reduced and replaced by fine striae	Marked reduction (still present but poorly defined)	None	None	None	None
Striae	None	Slight	Definite	Marked reduction but still present	May be present but very vague	None	None	None

Stage / Feature	1 20-24 yrs	2 25-29 yrs	3 30-34 yrs	4 35-39 yrs	5 40-44 yrs	6 45-49 yrs	7 50-60 yrs	8 60+ yrs
Surface texture	Fine granularity	Slightly more coarse granularity	Coarse and granular	Uniformly coarse granularity	Coarsely granular with partial densification	Loss of granularity and replacement by dense bone	Marked irregularity and densification	Non-granular, irregular with areas of sub-chondral destruction
Micro-porosity	None	None	In small areas	Slight	Slightly increased	Disappearing	None	None
Macro-porosity	None	None	None	None	Occasional	Little or none	Occasional	Occasional
Apical activity	None	None	None	Minimal	Slight (minor lipping)	Slight to moderate	Moderate to marked	Marked (though not a requisite)
Joint margins	Regular	Regular	Regular	Regular	Slight irregularity	Increased irregularity	Marked irregularity	Very irregular and lipped
Retro-auricular activity	None	None	Slight	Slight	Slight to moderate	Moderate	Moderate to marked	Well defined with profuse osteophytes

Young adult Middle adult Old adult

Figure 52. Representative auricular surface morphological phases (Madden 2011a: https://osteoware.si.edu/content/software-downloads)

Table 18. Scoring system for the Buckberry and Chamberlain (2002) method

Trait	Score	Description
Transverse organization	1	Transverse organization in ≥ 90% of auricular surface
	2	Transverse organization in 50-89% of auricular surface
	3	Transverse organization in 25-49% of auricular surface
	4	Transverse organization in < 25% of auricular surface
	5	No transverse organization

Trait	Score	Description
Surface texture	1	Fine granularity in ⩾ 90% of auricular surface
	2	Fine granularity in 50-89% of auricular surface; partial replacement of finely granular by coarsely granular bone; no dense bone
	3	Coarse granularity in ⩾ 50% of auricular surface; no dense bone
	4	Dense bone present but in < 50% of auricular surface
	5	Dense bone in ⩾ 50% of auricular surface
Microporosity	1	No microporosity
	2	Microporosity on one demiface
	3	Microporosity on both demifaces
Macroporosity	1	No macroporosity
	2	Macroporosity on one demiface
	3	Macroporosity on both demifaces
Apical changes	1	Sharp apex; possible slight auricular surface elevation relative to adjacent bone
	2	Limited lipping, the articular margin is smooth and of distinct shape
	3	Irregular contours of articular margin

Table 19. Age estimates from composite scores and age stages (Buckberry and Chamberlain 2002)

Composite score	Auricular surface stage	Mean age	Standard deviation	Median age	Range
5-6	I	17.33	1.53	17	16-19
7-8	II	29.33	6.71	27	21-38
9-10	III	37.86	13.08	37	16-65
11-12	IV	51.41	14.47	52	29-81
13-14	V	59.94	12.95	62	29-88
15-16	VI	66.71	11.88	66	39-91
17-19	VII	72.25	12.73	73	53-92

Sternal rib end morphology

Age-related changes at the sternal rib end have also been explored as age markers (DiGangi et al. 2009; Hartnett 2010; İşcan et al. 1984, 1985; Kunos et al. 1999; Oettlé and Steyn 2000; Yoder et al. 2001). Brief descriptions of sternal rib end morphological changes observed with age are given in **Tables 20** and **21**, following the İşcan et al. (1984, 1985) method, while Figure 53 depicts representative rib end morphological phases. Note that although this method was designed based on the fourth rib, it has been shown that it is applicable on any rib from the third to the ninth (Dudar 1993; Loth and İşcan 1989). Validation studies have produced mixed results (Cerezo-Román and Hernández Espinoza 2014; Loth 1995; Saunders et al. 1992), thus it should be used cautiously.

Table 20. Age-related features of the sternal rib end in males (İşcan et al. 1984)

Stage / Feature	0-1 <19 yrs	2-4 20-32 yrs	5-6 33-55 yrs	7-8 55+ yrs
Pit	Originally flat or billowy, deepening in later stages	Increased depth, V shaped but gradually turning moderately wide U shaped	Markedly deep and wide U shaped	Very deep and wide U shaped; floor absent or filled with projections
Walls		Originally thick but growing thinner in later stages	Thin with sharp edges	Extremely thin with sharp irregular edges and bony projections; occasional "window" formation
Rim	Regular with occasional scalloping in later stages	Initially scalloped or wavy but more irregular in later stages	Irregular with projections but no scalloping	Very irregular
Bone	Smooth and solid	Overall solid	Increased porosity	Very brittle and porous

Young adult | Middle adult | Old adult

Figure 53. Representative rib end morphological phases (Madden 2011a: https://osteoware.si.edu/content/software-downloads)

Table 21. Age-related features of the sternal rib end in females (İşcan et al. 1985)

Stage / Feature	0-1 <15 yrs	2-4 16-32 yrs	5-6 33-58 yrs	7-8 59+ yrs
Pit	Initially flat surface with ridges or billows; slight deepening and partial loss of ridges and billows in later stages	Increased depth, initially V shaped but gradually turning narrow U shaped, ridges or billowing possibly still present	Increased depth, wider V or U shaped; lined by a plaque-like deposit	Slight decrease in depth; flared U shaped, with eroded floor, occasionally filled with bony growths
Walls		Thick but growing thinner in later stages	Thin	Very thin, "window" formation in later stages
Rim	Regular with rounded edges and slight waviness in later stages	Wavy with some scalloping	Irregular, with sharp edges, projections, and no scalloping	Irregular with sharp edges and projections
Bone	Smooth and solid	Firm and solid with slight loss of density later	Lighter and brittle	Very thin and brittle

Cranial Suture Closure

At birth the cranium consists of several bones, interconnected via sutures. With increasing age, the sutures gradually close and the cranial bones fuse together. Different authors have proposed methods of skeletal ageing based on this property (Nemeskéri et al. 1960; Todd and Lyon 1924, 1925). The most widely used ageing method based on ectocranial suture closure was devised by Meindl and Lovejoy (1985). In implementing this method:

1. Score the degree of suture closure for each site for the lateral-anterior and vault systems (Figure 54)
2. Sum the scores for each system to get a composite score
3. Find the age-at-death that corresponds to the composite score (**Table 22**)

A number of studies evaluated ageing methods based on suture closure, and their results are not encouraging (e.g., Hershkovitz et al. 1997; Key et al. 1994). Therefore, this method should be used only when other criteria are not available or in association with other methods.

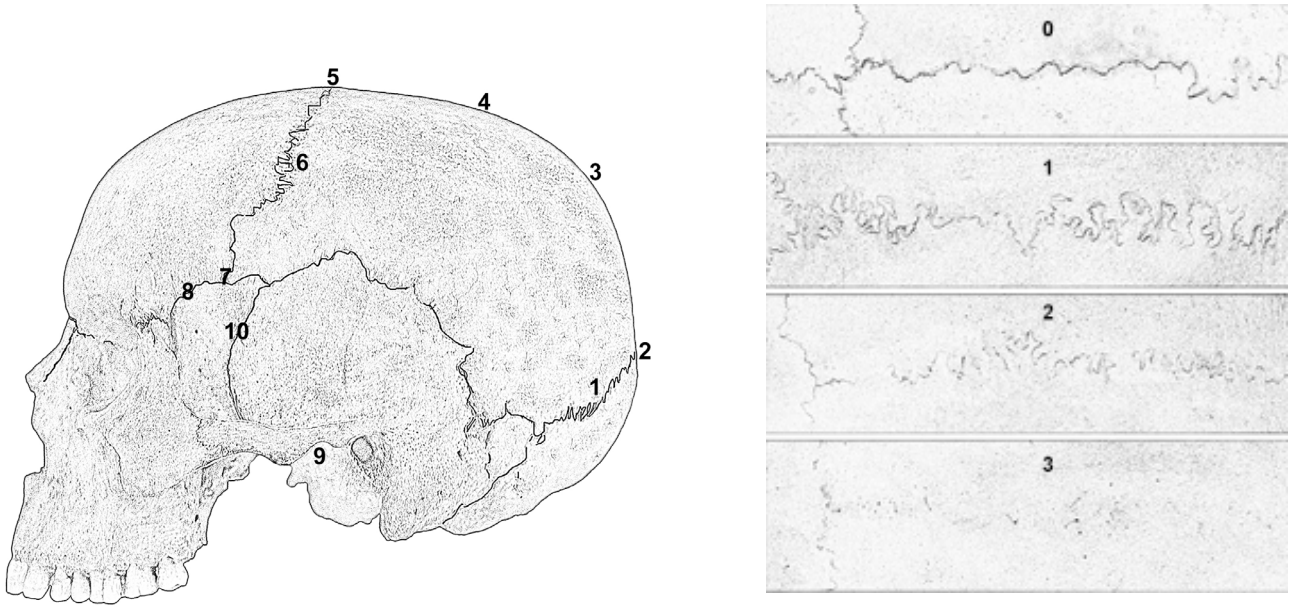

Figure 54. Cranial sutures (left) and degrees of obliteration (right) | Adapted from Nikita 2017
Note: Sutures 1-7 comprise the vault system, while sutures 6-10 the lateral-anterior system

Table 22. Composite scores and corresponding ages (Meindl and Lovejoy 1985)

Vault system				Lateral-anterior system			
Composite score	**Mean age**	**SD**	**Inter-decile range**	**Composite score**	**Mean age**	**SD**	**Inter-decile range**
0	-	-	-35	0	-	-	-43
1-2	30.5	9.6	19-44	1	32	8.3	21-42
3-6	34.7	7.8	23-45	2	36.2	6.2	29-44
7-11	39.4	9.1	28-44	3-5	41.1	10	28-52
12-15	45.2	12.6	31-65	6	43.4	10.7	30-54
16-18	48.8	10.5	35-60	7-8	45.5	8.9	35-57
19-20	51.5	12.6	34-63	9-10	51.9	12.5	39-69
21	-	-	43-	11-14	56.2	8.5	49-65
				15	-	-	-

PATHOLOGICAL LESIONS

Osseous modifications due to pathology will generally appear as:

1. Abnormal bone formation
2. Abnormal bone absence
3. Abnormal bone size
4. Abnormal bone shape (Buikstra 2019; Ortner 2011)

In this section, we follow the pathology categories proposed by Wilczak and Jones (2011a) because these are given per osseous expression category, thus they are applicable both to entire skeletons as well as to isolated skeletal elements. The scoring scheme per condition provided below also comes from Wilczak and Jones (2011a) and the contributions therein; thus, it follows the free software Osteoware data entry system (https://osteoware.si.edu/). The only exception are dental diseases, for which information was obtained from Nikita (2017) and references therein. The reader is advised to consult the original sources for rich photographic documentation of different skeletal lesions, as well as seminal palaeopathology textbooks, such as Aufderheide and Rodriguez-Martin (1998), Buikstra (2019), and Waldron (2008).

Pathological lesions should be described in the following order:

- First, the anatomical location of the lesion must be recorded
- Second, the lesion must be described using unambiguous and descriptive terminology
- Next, the distribution of the lesions on the skeleton is recorded and relationships to other pathologies are discussed
- Finally, a diagnosis may be undertaken (Barker et al. 2008b)

Size abnormalities (Madden 2011b)

Hydrocephaly	**Microcephaly**	**Acromegaly**
• Enlarged vault • Thinned cranial bones • Widely open sutures • Wormian bones • Flat cranial base	• Cranial circumference < 46 cm or capacity < 1000cc • Face enlarged compared to cranial vault	• Prominent facial bones and prognathism • Dental crowding and malocclusion • Elongated ribs and beaded costrochondral junctions • Enlarged vertebrae • Tufted digits • Enlarged or eroded sella turcica • New bone formation at prominent osseous structures (e.g., trochanters) and entheses
Achondroplastic Dwarfism	**Gigantism**	
• Shortened and abnormally thick limbs • Not particularly affected axial skeleton	• Height three or more standard deviations higher than the population mean • Too long but normally proportioned bones	

Shape abnormalities (Madden 2011b)

Premature Suture Closure	**Bowing***	**Angulation**
• Abnormal cranial shape as continuous brain growth expands the vault in the direction of open sutures	• Abnormal curvature of long bone diaphysis * Important to distinguish true bowing from pseudobowing (e.g., "saber shin")	• Angulation of bone diaphysis
Flaring Metaphyses	**Uniform Widening**	**Fusiform (Spindle-Shaped)**
• Abnormal bone building on the external surface of the metaphyses	• Uniform widening of tubular bones due to abnormal bone deposition	• Thickened diaphysis with tapering at one or both epiphyses

Abnormal bone loss (Mulhern 2011)

Location	Extent of Involvement
• Periosteal surface or external table • Cortex, trabeculae or diploë • Endosteal surface or inner table • At entheses	• < 1/3 of the area involved • 1/3 - 2/3 of the area involved • > 2/3 of the area involved
Number of Foci	**Size of Focal Bone Loss**
• 1 • 2 • 3-5 • 6-10 • > 10	• < 1 cm • 1-5 cm • > 5 cm
Bony Response to Local Bone Loss	
• Localized destruction, circumscription, sclerotic reaction • Localized destruction, boundaries well-defined but no sclerosis • Localized destruction, margins not sharply defined • Moth-eaten destruction • Permeated destruction	

Abnormal bone formation (Wilczak and Jones 2011b)

General category	Extent of Involvement
• Surface bone formation • Abnormal matrix formation	• < 1/3 of the area involved • 1/3 - 2/3 of the area involved • 2/3 of the area involved
Periosteal Surface	**Productive Reaction Type**
• Woven bone • Sclerotic reaction • Compact/remodeled	• Solid • Lamellated • Shell-type • Parallel spiculated • Sunburst • Cauliflower
Surface Appearance	**Endosteal Surface**
• Porous • Striated • Undulating • Vascular impressions • Pitted • Smooth • Nodular • Other/Irregular	• Lamellae visible • Medullary cavity narrowed but no visible lamellae
Abnormal Matrix	**Ossified Tissue**
• Deposition of woven bone • Extensions of cancellous bone • Trabecular coarsening	• Myositis ossificans • Ossification of ligaments • Ossification of cartilage • Enthesophytes • Other
Specific structures	
• Button osteoma • Stellate scars • Sequestrum • Involucrum • Cloaca	

Trauma (O'Brien and Dudar 2011)

Fracture Type	Characteristics
• Partial • Simple • Comminuted/butterfly • Spiral • Compression • Depressed skull fracture • Other	• Pathological • Blunt round/Blunt oval • Edged/sharp force trauma • Projectile entry • Projectile exit • Projectile embedded • Radiating/stellate • Amputation • Other
Timing of Perimortem Fractures	**Dislocations**
• Clearly perimortem • Ambiguous (likely postmortem)	• Traumatic • Congenital • Cause ambiguous
Trauma Complications	**Healing stage of Antemortem Fractures**
• Nonunion • Tissue necrosis • Infection • Traumatic arthritis • Joint fusion • Traumatic myositis ossificans • Deformation • Traumatic enthesopathy	• Callus formation (woven bone) • Callus formation (sclerotic bone) • Healing/fracture obliteration

Fracture timing

Bone that breaks while green tends to produce smooth fracture lines with sharp, linear edges, while dry bone fractures have rough, jagged edges.

Porosity and Channel Formation (Wilczak 2011)

Degree of Porosity	Other Features
1. Pore size: • Pinpoint • Between pinpoint and 0.5 mm • > 0.5 mm • Coalesced 2. Pore density (number of pores per cm^2) • <15; low • 15-24; moderate • 25-50; high • >50; extreme	• Pitting • Striations • Undulations/irregular thickening • Rounded thickening along sutures
Location of Ectocranial Porosity	**Vascular Channel Locations**
• Orbits • Superior vault near sutures • Superior vault in non-sutural areas • Other	• Orbits • Endocranial • Other cranial
Activity	**Vascular Channel Appearance**
• Active • Healing	• Very fine and shallow • Deep with sharp edges and flattened interchannel surfaces • Deep with rounded interchannel surfaces
Diploic Hyperostosis	**Vascular Channel Density**
• Possible • Definite • Absent	• Channels disrupt <25% of the lamina in the affected area • Channels disrupt 25%-50% of the lamina in the affected area • Channels disrupt >50% of the lamina in the affected area

Pathological conditions of the vertebrae (Mulhern and Jones 2011)

Vertebral Pathologies	Spondylolysis
• Schmorl's depressions • Spondylolisthesis	• Complete fracture • Partial or complete reattachment • Partial fracture (elements never fully separated)

Vertebral Osteophytes	Porosities around Margins of Vertebral Osteophytes
• Barely discernible • With elevated rim • Curved spicules • With fusion of spicules	• Porosities around margins • Porosities within end plates
Syndesmophytes	**Vertebral Body Fractures**
• Barely discernible • With elevated rim • Extended spicules • With fusion of spicules	• Compression • Single end-plate depression without wedging • Single end-plate depression with wedging • Biconcave bodies
Cleft Sacra and Spina Bifida	**Abnormal Shape of Spinal Column**
• Partial cleft sacra • Completely cleft sacra • Complete spina bifida	• Kyphosis • Scoliosis • Kyphosis/scoliosis

Arthritis (Dudar 2011)

Surface Porosity	Marginal Lipping
• Barely discernible • Clearly present • Coalesced	• Barely discernible • Rounded ridge • Sharp ridge, sometimes with curled spicules • Initial fusion • Fused
Surface Osteophytes	**Erosion**
• Barely discernible • Clearly present	• Barely discernible • Clearly present
Eburnation	**Extent of Surface or Margin Affected***
• Barely discernible • Polish only • Polish with grooves	• <1/3 • 1/3 to 2/3 • >2/3

* Each of the five articular surface alterations (Porosity, Marginal Lipping, Surface Osteophytes, Erosion, and Eburnation) should be scored for the extent of the joint surface or circumference affected

Dental diseases | Adapted from Nikita 2017 and references therein

Periodontal Disease	**Periapical Cavities**
A. Cementoenamel junction - alveolar crest distance • 0-2 mm • 2-5 mm • >5 mm B. Extent of alveolar bone resorption • None • <1/2 of the root exposed • >1/2 of the root exposed • Complete resorption	A. Location • Buccal/labial • Lingual B. Size • <3 mm diameter • >3 mm diameter C. Cavity wall • Smooth • Rough
Dental Caries	**Enamel Hypoplasia**
A. Location • Absent • Occlusal • Interproximal • Buccal/labial • Lingual • Root • Gross B. Degree of expression • No caries • Small cavity; no penetration to dentine • Cavity penetrates the dentine • Cavity penetrates the pulp chamber	A. Type of defect • Absence • Enamel opacity • Linear horizontal grooves • Linear horizontal pits • Altogether missing enamel • Other B. Location • Cusp • Midcrown • Neck
Dental Calculus	**Antemortem Tooth Loss**
A. Location • Supragingival • Subgingival B. Size • Absent • <1/3 of the crown covered • 1/3 to 2/3 of the crown covered • >2/3 of the crown covered	A. Degree of expression • None • Socket depth >2 mm, irregular socket walls • Socket depth <2 mm, irregular socket walls, large pores on alveolar bone • Complete socket obliteration

ACTIVITY MARKERS

As a living tissue, bone adapts its form when mechanical loading is imposed on it, while teeth document the masticatory and extra-masticatory activities that involved the mouth. As such, the study of skeletal remains can provide insights to past repetitive activity patterns. The main osteological methods used for the study of activity patterns include long bone cross-sectional geometric properties, entheseal changes, dental wear and osteoarthritis.

Long bone cross-sectional geometric properties

During physical activity, the skeleton deposits new bone tissue along the axes subjected to stress, altering the cross-sectional geometry (CSG) of long-bone diaphyses and other elements (Ruff et al. 2006). Biomechanics, the application of mechanical principles to biological systems, can contribute to the assessment of mechanical loading on the skeleton based on the CSG of the long bones (Ruff 2008). The CSG can be assessed using different techniques, some of which allow the visualization of both the periosteal and the endosteal contours, while others capture only periosteal diaphyseal shape (for a brief review of methods see Moore 2012). The former require specialised equipment (CT or radiographs), while the latter use moulds of sub periosteal contours and are more easily applicable (Stock and Shaw 2007). Among the estimated cross-sectional geometric properties, TA, the total subperiosteal area, is related to bending/torsional strength. Second moments of area express resistance to bending loads applied antero-posteriorly (Ix) and mediolaterally (Iy), while the maximum (Imax) and the minimum (Imin) second moments of area are measures of the maximum and minimum bending rigidity, respectively. Finally, the sum of the perpendicular second moments of area (Ix + Iy) produces the polar moment of area (J), which reflects torsional and (twice) average bending rigidity (Ruff 2008 and references therein). Biomechanical properties should be standardized according to body size, and body mass is often used for this purpose (Ruff 2008; Ruff et al. 1993). If body mass cannot be estimated, powers of bone length may be used: for second moments of area the recommended power is $(\text{bone length})^{5.33}$, whereas for the total subperiosteal area it is $(\text{bone length})^{3}$ (Ruff et al. 1993).

Entheseal changes

Entheses are specialized interfaces where muscles, tendons or ligaments attach on bone (Figures 55-61: light brown represents muscle origins and blue muscle insertions). During muscle activity, the skeleton responds to the increased mechanical loading by new bone formation and/or bone resorption at the entheses. Entheses may be fibrous or fibrocartilaginous (Benjamin et al. 2006).

In fibrous entheses the soft tissues attach to the bone either directly or via a layer of periosteum, while fibrocartilaginous entheses have four histological zones:

1. tendon or ligament,
2. uncalcified fibrocartilage,
3. calcified fibrocartilage, and
4. subchondral bone.

Between the zones of uncalcified and calcified fibrocartilage lies the tidemark, a regular calcification front (Benjamin et al. 1986, 2002). The expression of entheseal changes is affected by many factors besides activity, such as sex, diet, age, body size, genetics, and pathological conditions (e.g. Jurmain et al. 2011; Michopoulou et al. 2015; Milella et al. 2012; Niinimäki 2011; Weiss 2004; Weiss et al. 2012). For this reason, entheseal changes should be used cautiously as skeletal activity markers. Many researchers have examined the most efficient way to record ECs. Some opt for simple presence/absence (**Table 23**) and others propose ordinal schemes (**Tables 24-25**).

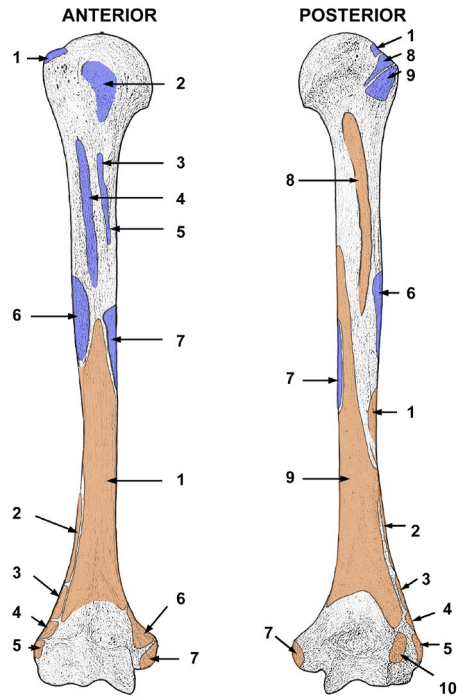

Figure 56. Humeral entheses | Adapted from Nikita 2017
Origins: 1 = brachialis, 2 = brachioradialis, 3 = extensor carpi radialis longus, 4 = extensor carpi radialis brevis, 5 = common origin of extensors, 6 = pronator teres, 7 = common origin of flexors, 8 = triceps brachii (lateral head), 9 = triceps brachii (medial head), 10 = anconeus
Insertions: 1 = supraspinatus, 2 = subscapularis, 3 = latissimus dorsi, 4 = pectoralis major, 5 = teres major, 6 = deltoideus, 7 = coracobrachialis, 8 = infraspinatus, 9 = teres minor

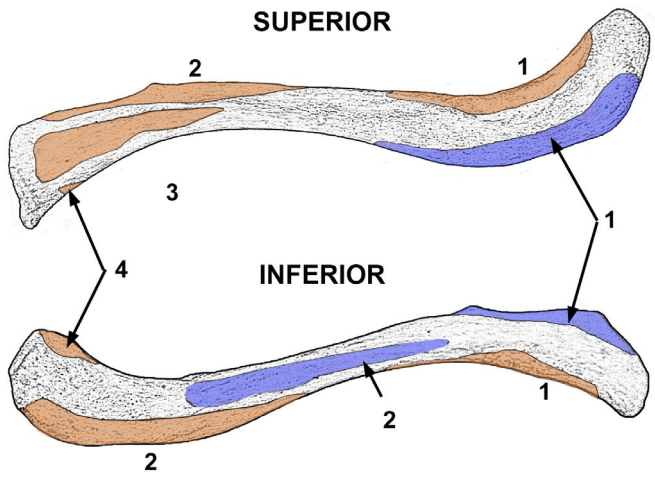

Figure 55. Clavicular entheses | Adapted from Nikita 2017
Origins: 1 = deltoideus, 2 = pectoralis major, 3 = sternocleidomastoideus, 4 = sternohyoid
Insertions: 1 = trapezius, 2 = subclavius

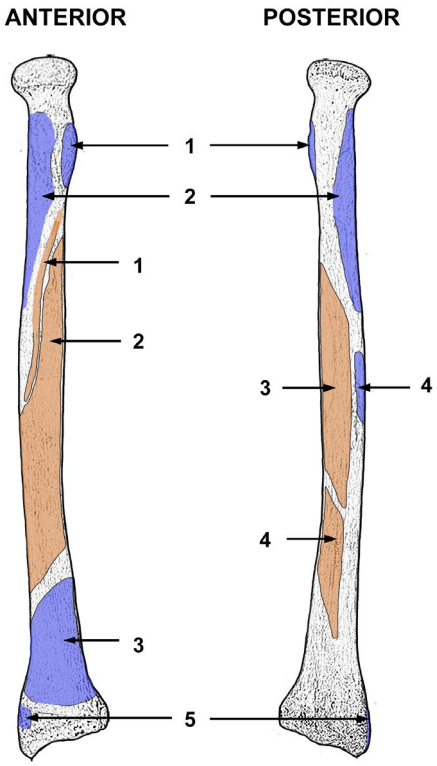

Figure 57. Radial entheses | Adapted from Nikita 2017
Origins: 1 = flexor digitorum superficialis, 2 = flexor pollicis longus, 3 = abductor pollicis longus, 4 = extensor pollicis brevis
Insertions: 1 = biceps brachii, 2 = supinator, 3 = pronator quadratus, 4 = pronator teres, 5 = brachioradialis

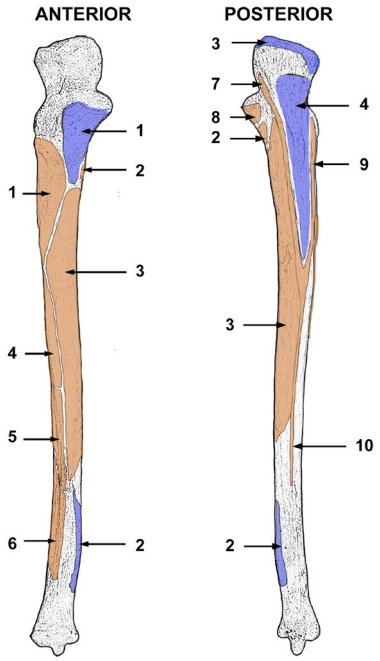

Figure 58. Ulnar entheses | Adapted from Nikita 2017
Origins: 1 = supinator, 2 = pronator teres, 3 = flexor digitorum profundus, 4 = abductor pollicis longus, 5 = extensor pollicis longus, 6 = extensor indicis, 7 = flexor carpi ulnaris, 8 = flexor digitorum superficialis, 9 = extensor carpi ulnaris, 10 = common origin of flexor digitorum profundus, flexor carpi ulnaris, and extensor carpi ulnaris. **Insertions:** 1 = brachialis, 2 = pronator quadratus, 3 = triceps brachii, 4 = anconeus

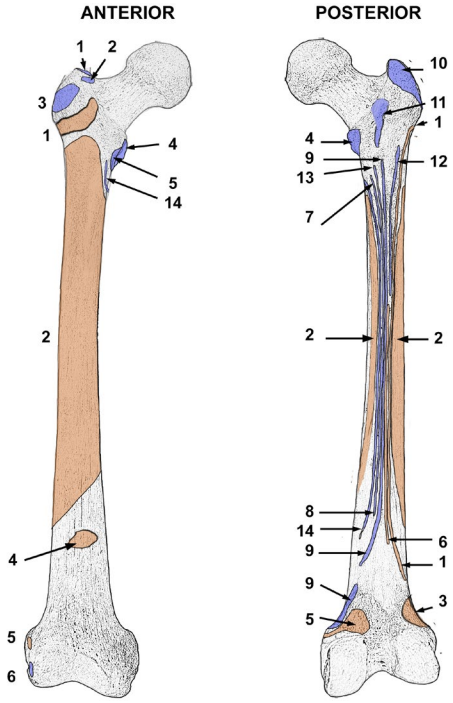

Figure 59. Femoral entheses | Adapted from Nikita 2017
Origins: 1 = vastus lateralis, 2 = vastus intermedius, 3 = gastrocnemius (lateral head), 4 = articularis genu, 5 = gastrocnemius (medial head), 6 = biceps femoris (short head). **Insertions:** 1 = piriformis, 2 = obturator internus and gemelli, 3 = gluteus minimus, 4 = psoas major, 5 = iliacus, 6 = popliteus, 7 = pectineus, 8 = adductor magnus, 9 = biceps femoris, 10 = gluteus medius, 11 = quadratus femoris, 12 = gluteus maximus, 13 = adductor longus, 14 = adductor brevis

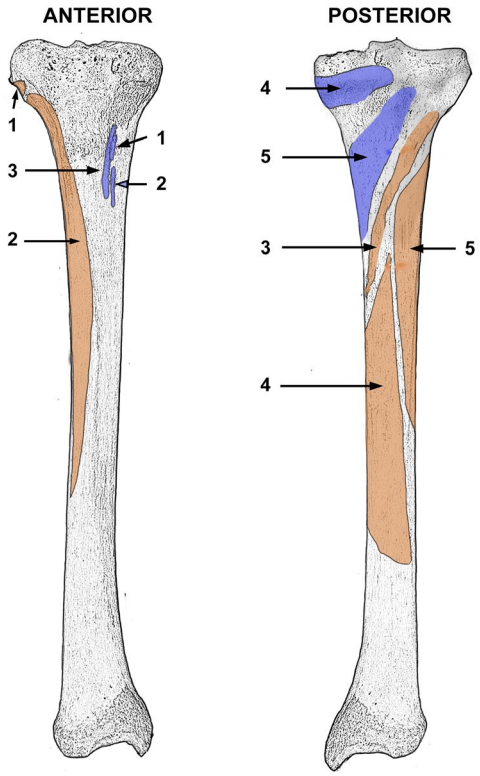

Figure 60. Tibial entheses | Adapted from Nikita 2017
Origins: 1 = extensor digitorum longus, 2 = tibialis anterior, 3 = soleus, 4 = flexor digitorum longus, 5 = tibialis posterior
Insertions: 1 = gracilis, 2 = semitendinosus, 3 = sartorius, 4 = semimembranosus, 5 = popliteus

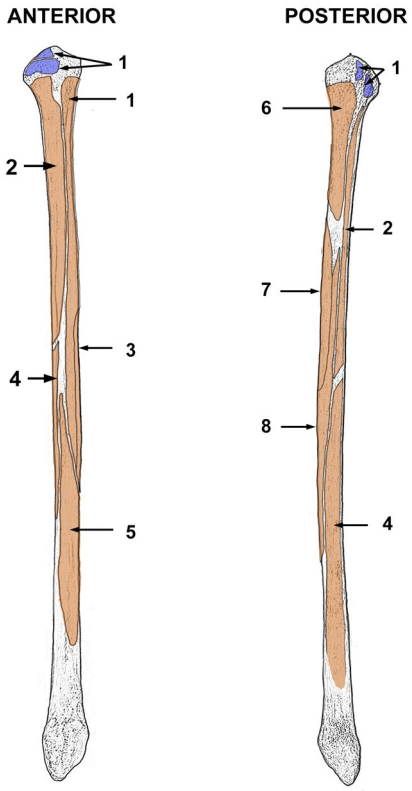

Figure 61. Fibular entheses | Adapted from Nikita 2017
Origins: 1 = extensor digitorum longus, 2 = fibularis longus, 3 = extensor hallucis longus, 4 = fibularis brevis, 5 = fibularis tertius, 6 = soleus, 7 = tibialis posterior, 8 = flexor hallucis longus. **Insertions:** 1 = biceps femoris

Table 23. Recording Scheme by Villotte et al. (2010) for fibrocartilaginous entheses

Present	Absent
• Irregular entheseal surface • Enthesophytes • >3 foramina • Cystic changes • Calcification deposits • Osseous defects	• None of the 'Present' traits

Table 24. Recording Scheme by Hawkey and Merbs (1995)

Robusticity	Stress
0. None 1. Slight elevation of bone surface but no crests or ridges 2. Mound-shaped elevation but no crests or ridges 3. Sharp crests and/or ridges with occasional grooves between them	0. None 1. Shallow pitting (depth <1 mm) 2. Deeper pitting (pit depth 1-3 mm, pit length <5 mm) 3. Marked pitting (pit depth >3 mm, pit length >5 mm)
Ossification	
0. None 1. Slight exostosis (<2 mm protrusion) 2. Distinct exostosis (2-5 mm protrusion) 3. Pronounced exostosis (>5 mm protrusion and/or covering large part of the bone surface)	

Notes:

1. In tendinous attachment sites, the robusticity categories are slightly different: 0, absent; 1, slight indentation; 2, rough bone surface; 3, deep indentation, often with bone crests
2. Ossification markers are mostly due to traumatic episodes rather than daily activity patterns; thus, they are rarely used in entheseal change studies (Hawkey 1998)
3. This scheme has been criticized that it does not consider the anatomical differences between fibrous and fibrocartilaginous entheses (Alves Cardoso and Henderson 2010)

Table 25. Coimbra Method for fibrocartilaginous entheses (Drawn from Henderson et al. 2013, 2016)

Zone 1*	
Bone formation	**Erosion**
0. Absent 1. Osseous projection < 1mm in elevation & covering <50% of zone 1 2. Osseous projection ⩾ 1mm in elevation & covering ⩾ 50% of zone 1	0. Absent 1. Covering <25% of zone 1 2. Covering ⩾25% of zone 1
Zone 2*	
Textural change	**Bone formation**
0. Absent 1. Covering >50% of zone 2	0. Absent 1. Distinct formation >1mm in any direction and covering <50% of zone 2 2. Distinct formation >1mm in any direction and covering ⩾50% of zone 2
Erosion	**Fine porosity**
0. Absent 1. Covering <25% of zone 2 2. Covering ⩾25% of zone 2	0. Absent 1. Covering <50% of zone 2 2. Covering ⩾50% of zone 2
Macroporosity	**Cavitation**
0. Absent 1. 1-2 pores 2. >2 pores	0. Absent 1. 1 cavity 2. >1 cavities

* Each enthesis is divided into two zones, as shown in Figure 62, and the features described in Table 25 are recorded per zone

Figure 62. Coimbra method zones in M. subscapularis. Bone with unmarked zones (top); solid black line showing zone 1 and beige semi-transparent surface is zone 2 (bottom)

Osteoarthritis

See recording standards in the pathology section for arthritis.

Dental wear

Dental wear is the outcome of three interacting mechanisms: attrition, abrasion, and erosion. Attrition is the result of the direct contact between teeth, abrasion is produced by the contact between teeth and (non)dietary objects, while dental erosion is caused by chemical processes (Arnadottir et al. 2010; Hillson 2005).

The two most common approaches for recording dental wear involve:

1. using an ordinal scheme to express the extent of exposed dentine, and
2. calculating the area of exposed dentine in relation to the total occlusal/biting surface area.

Figure 63 presents the Smith (1984) method for recording dental wear using ordinal categories.

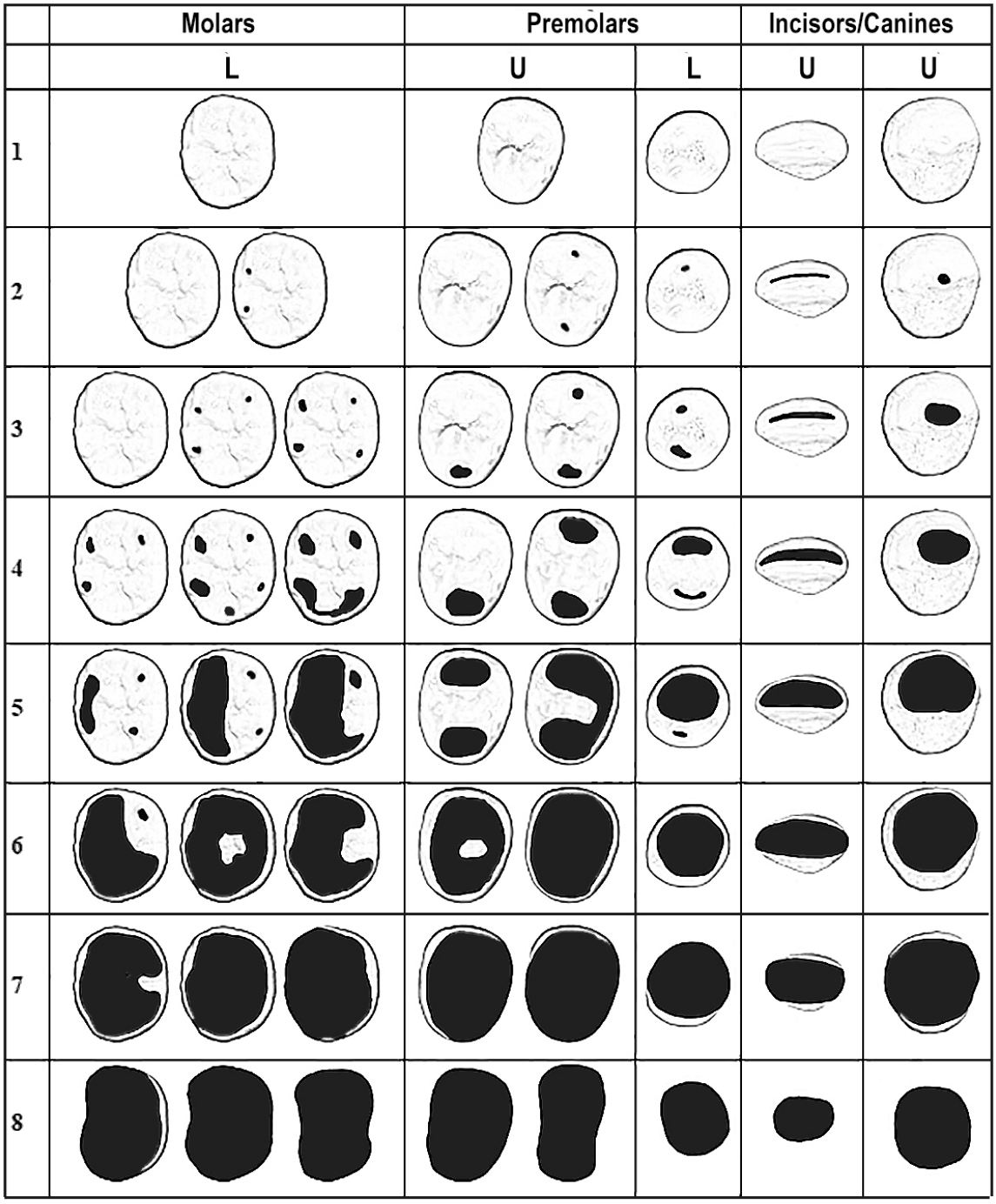

Figure 63. Smith (1984) dental wear stages | Adapted from Nikita 2017

NONMETRIC TRAITS

Nonmetric traits represent normal skeletal anatomical variants that cannot be measured in a continuous/metric manner (Tyrrell 2000). What makes them useful in osteoarchaeological studies is the fact that their expression is largely controlled genetically (e.g. Cheverud and Buikstra 1981; Grüneberg 1952; Herrera et al. 2014; Hubbard et al. 2015; Ricaut et al. 2010; Velemínský and Dobisíková 2005); thus, they have been used in kinship and biodistance studies (e.g. Godde and Jantz 2017; Hanihara 2008; Nikita et al. 2012; Rathmann et al. 2017). In addition to genes, environmental factors also affect the expression of nonmetric traits, but there does not appear to be a significant impact on population trait frequencies (Scott and Turner 1997).

Cranial traits (Berry and Berry 1967; Hauser and DeStefano 1989; Mann et al. 2016)

Cranial nonmetric traits can be recorded simply as present/absent. Representative thresholds for presence/absence are given in **Table 26**. If time permits it, a more detailed ordinal scheme may be adopted. Hauser and DeStefano (1989) provide a very detailed scheme, simplified in Nikita (2017). Figures 64-68 visualise many of these traits, while the photographic atlas by Mann et al. (2016) provides many more illustrations.

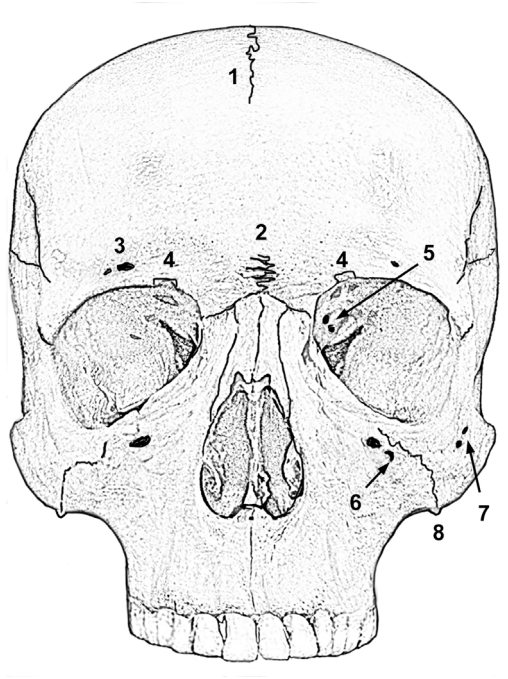

Figure 64. Cranial nonmetric traits; anterior view | Adapted from Nikita 2017: 1 = metopic suture; 2 = supranasal suture; 3 = supraorbital foramina; 4 = supraorbital notches; 5 = ethmoidal foramina; 6 = infraorbital foramina; 7 = zygomatico-facial foramina; 8 = zygomaxillary tubercle

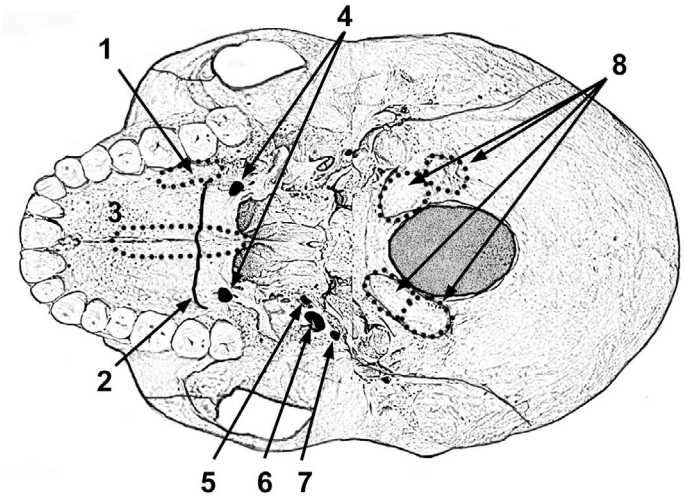

Figure 65. Cranial nonmetric traits; inferior view | Adapted from Nikita 2017: 1 = maxillary torus; 2 = transverse palatine suture; 3 = palatine torus; 4 = lesser palatine foramina; 5 = foramen of Vesalius; 6 = oval foramen; 7 = spinous foramen; 8 = divided occipital condyles

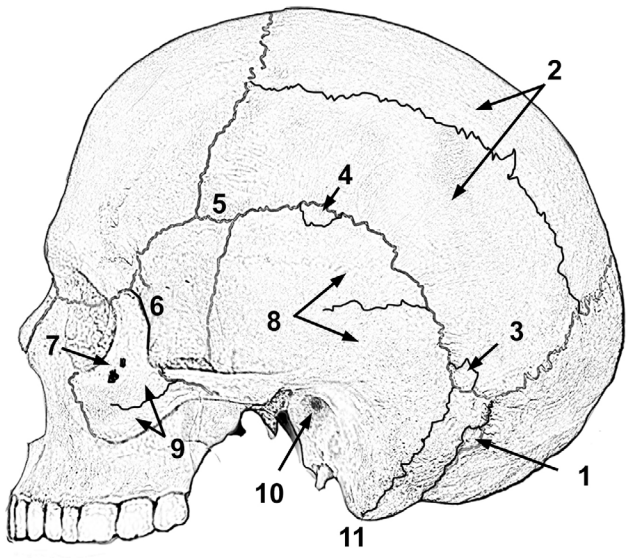

Figure 66. Cranial nonmetric traits; lateral view | Adapted from Nikita 2017: 1 = occipitomastoid ossicle; 2 = divided parietal bone; 3 = parietal notch bone; 4 = squamous ossicle; 5 = frontotemporal articulation; 6 = marginal tubercle; 7 = zygomatico-facial foramen; 8 = divided temporal squama; 9 = divided zygomatic bone; 10 = external auditory torus/exostosis; 11 = squamomastoid suture

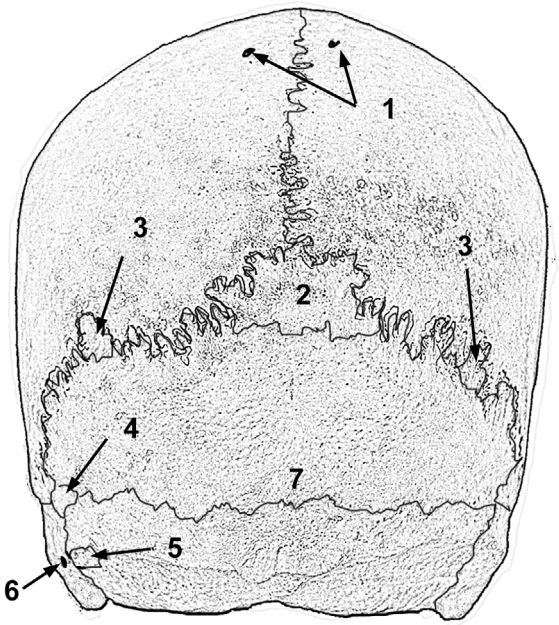

Figure 67. Cranial nonmetric traits; posterior view | Adapted from Nikita 2017: 1 = parietal foramina; 2 = ossicle at lambda; 3 = lambdoid ossicles; 4 = ossicle at asterion; 5 = occipitomastoid ossicle; 6 = mastoid foramen; 7 = inca bone

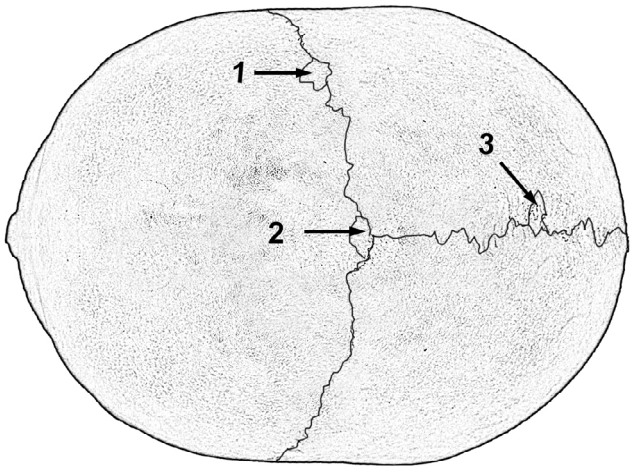

Figure 68. Cranial nonmetric traits; superior view | Adapted from Nikita 2017: 1 = coronal ossicle; 2 = ossicle at bregma; 3 = sagittal ossicle

Table 26. Thresholds for presence/absence recording of cranial nonmetric traits | Adapted from Nikita et al. 2012

Trait	Presence threshold
Metopic suture	Extending along >1/2 of the frontal arc
Metopic fissure	Observable in any variant
Supranasal suture	Observable irrespective of shape and degree of expression
Supraorbital osseous structures	Notches and foramina open to the orbital cavity
Divided infraorbital foramina	Complete bridging
Parietal foramina	Observable irrespective of position, size or number
Divided mental foramina	Complete division
Ethmoidal foramina	If posterior foramen is absent
Lesser palatine foramina	Observable irrespective of position, size, shape or number
Squamous ossicles	Observable irrespective of size or number
Parietal notch bone	Observable irrespective of position, size or number
Epipteric bone	Observable irrespective of size, type of articulation with neighbouring bones or number
Ossicle at asterion	Observable irrespective of position, size, shape or number
Occipitomastoid wormians	Observable irrespective of position, size or number
Coronal ossicles	Observable irrespective of position, size or number
Sagittal ossicles	Observable irrespective of position, size or number
Lambdoid ossicles	Observable irrespective of position, size or number
Inca bone	Suture longer than 10 mm
Divided occipital condyles	Furrow dividing the facet from both sides, even if the separation of the condyle is incomplete

Trait	Presence threshold
Hypoglossal canal bridging	Complete division
Mandibular torus	Any degree of expression
Maxillary torus	Any degree of expression
Auditory torus	Any degree of expression
Palatine torus	Any degree of expression
Apertures at the floor of the acoustic meatus	At least pinhole sized apertures
Divided parietal bone	Suture longer than 1 cm
Divided temporal squama	Suture longer than 5 mm
Os japonicum	Suture longer than 5 mm
Marginal tubercle	Projection longer than 4 mm
Mylohyoid bridging	Osseous bridge irrespective of location and degree of expression
Foramen of Vesalius	Complete division
Foramen ovale incomplete	Any communication between the two foramina except for suture-like gap
Zygomaxillary tubercle	Projection longer than 2 mm
Symmetrical thinness of parietal bones	Any expression from slight flattening to saucer-shaped appearance

Post-cranial traits (Finnegan 1978; Mann et al. 2016)

Post-cranial nonmetric traits are generally recorded simply as present/absent. Figures 69-89 visualise such traits, while Mann et al. (2016) provide many more illustrations.

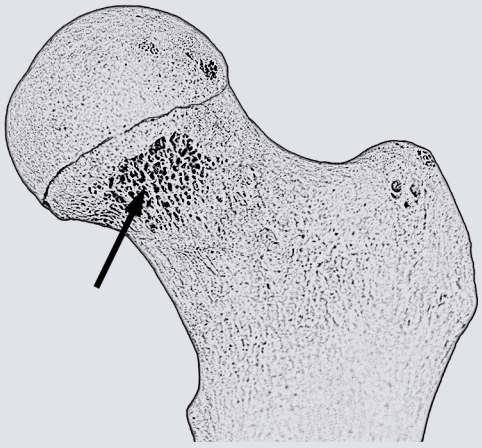

Figure 69. Allen's fossa | Adapted from Nikita 2017
Region of exposed trabeculae, at the anterior side of the femoral neck, close to the head

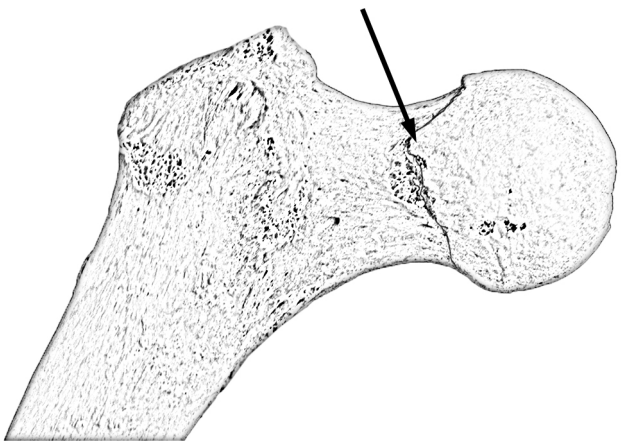

Figure 70. Poirier's facet | Adapted from Nikita 2017
Extension of the articular surface of the femoral head toward the neck; located at the anterior part of the femur

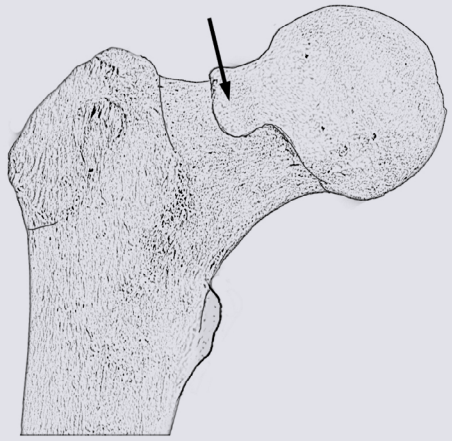

Figure 71. Plaque | Adapted from Nikita 2017
Bone growth starting from Poirier's facet and extending onto the femoral neck

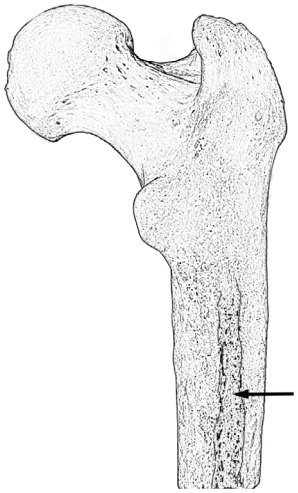

Figure 72. Hypotrochanteric fossa | Adapted from Nikita 2017
Vertical groove on the femoral diaphysis, between the gluteal ridge and the lateral margin

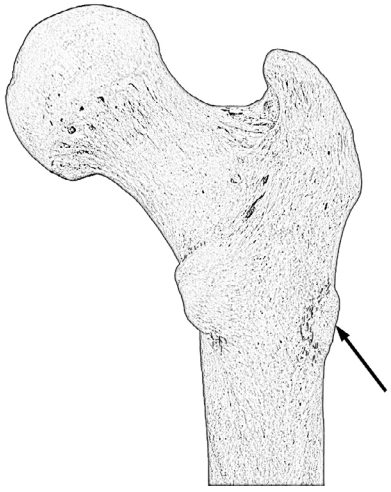

Figure 73. Third trochanter | Adapted from Nikita 2017
Tubercle at the superior part of the gluteal crest

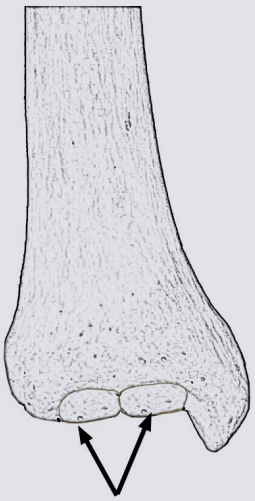

Figure 74. Tibial squatting facets | Adapted from Nikita 2017
Medial tibial squatting facet: extension of the inferior articular surface of the tibia onto the medial part of the anterior aspect of the tibia | **Lateral tibial squatting facet:** extension of the inferior articular surface of the tibia onto the lateral part of the anterior aspect of the tibia

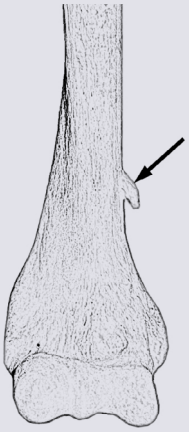

Figure 75. Supracondyloid process | Adapted from Nikita 2017
Bony process above the medial epicondyle

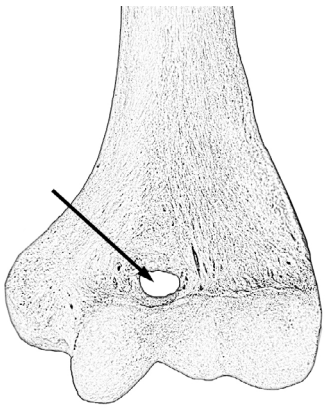

Figure 76. Septal aperture | Adapted from Nikita 2017
Aperture in the bony septum between the olecranon and the coronoid fossa on the distal humerus

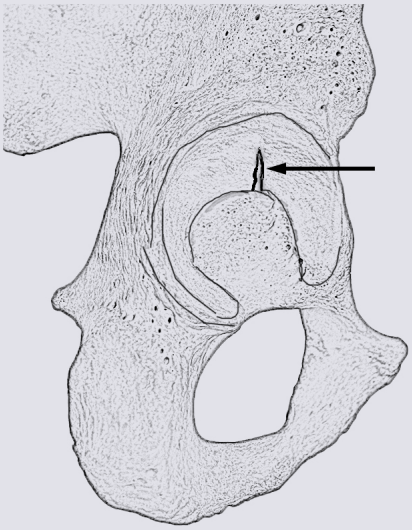

Figure 77. Acetabular crease | Adapted from Nikita 2017
Fold, pleat or crease on the acetabular articular surface

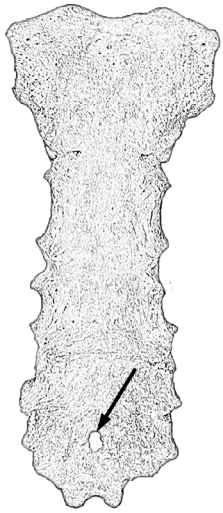

Figure 78. Sternal foramen | Adapted from Nikita 2017
Foramen in the lower part of the body of the sternum

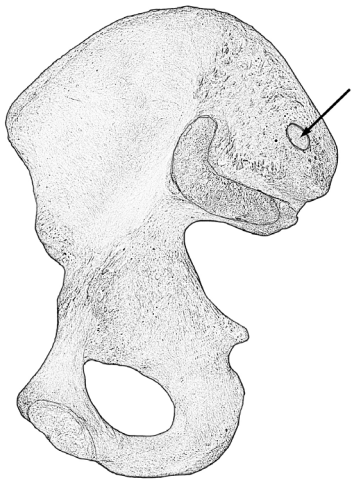

Figure 79. Accessory sacral facets | Adapted from Nikita 2017
Additional articular facets on the sacrum or ilium, posterior to the auricular surface

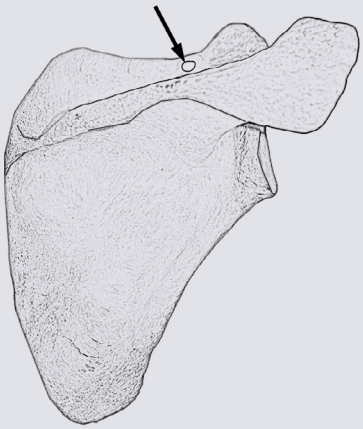

Figure 80. Bridging of suprascapular notch | Adapted from Nikita 2017
Conversion of the notch into a foramen by ossification of the suprascapular ligament

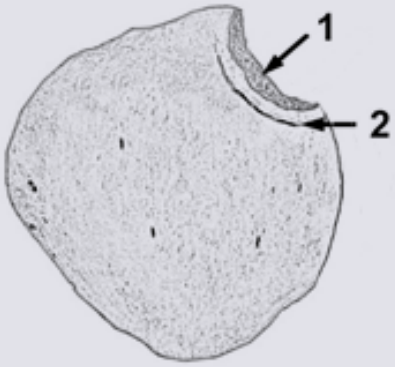

Figure 81. Vastus notch (1) and Vastus fossa (2) | Adapted from Nikita 2017
Vastus notch: small, smooth-bordered notch in the superolateral angle of the patella | **Vastus fossa:** slight depression anterior to the vastus notch

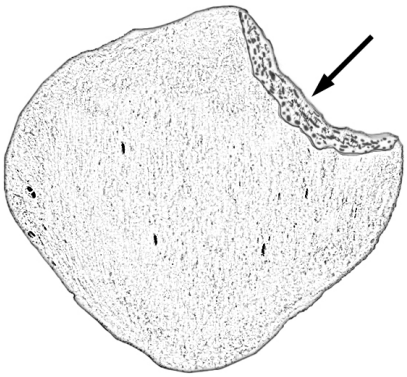

Figure 82. Emarginate patella | Adapted from Nikita 2017
Large rough-bordered notch in the superolateral angle of the patella

Figure 83. Medial talar facet | Adapted from Nikita 2017
Distinct facet on the superior medial surface of the talar neck

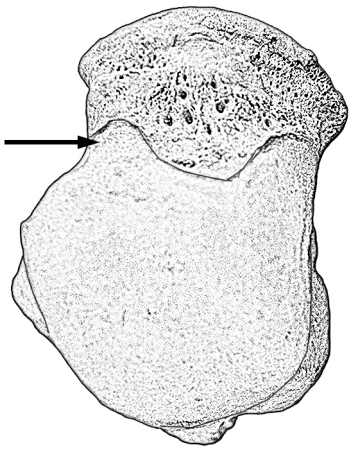

Figure 84. Lateral talar extension | Adapted from Nikita 2017
Extension of the lateral part of the anterior trochlear margin towards the talar neck

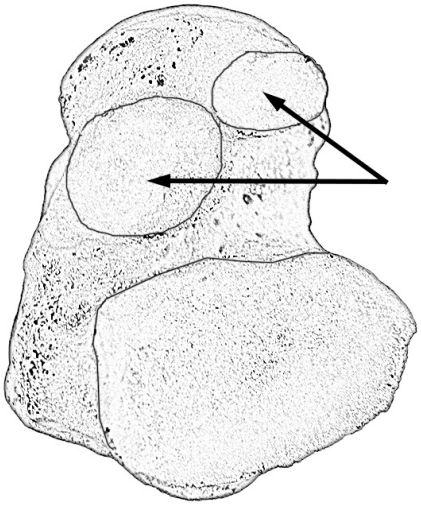

Figure 85. Double inferior anterior talar facet | Adapted from Nikita 2017
Division of the inferior surface of the head of the talus into discrete facets

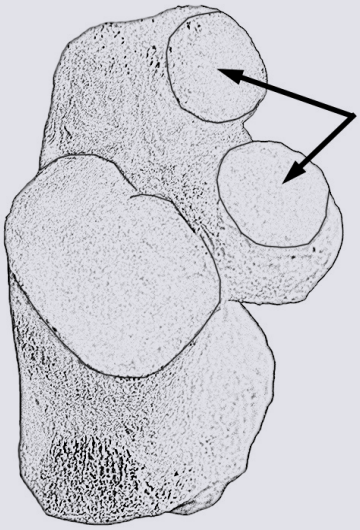

Figure 86. Double anterior calcaneal facet | Adapted from Nikita 2017
Discrete anterior and middle facets on the superior surface of the calcaneus

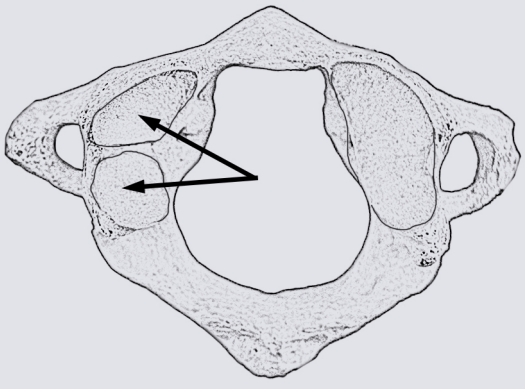

Figure 87. Double atlas facet | Adapted from Nikita 2017
Two distinct facets on the superior articular surface

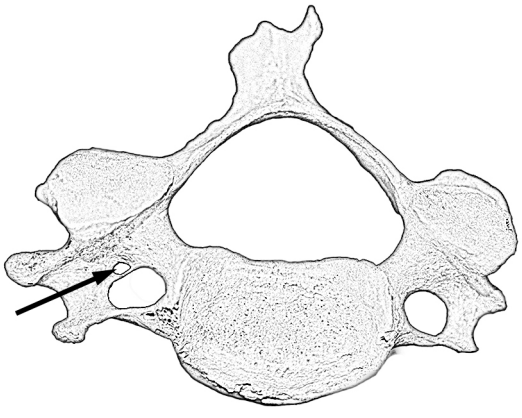

Figure 88. Transverse foramen bipartite | Adapted from Nikita 2017
Division of the transverse foramina of any of the third to seventh cervical vertebrae

Dental traits (Turner et al. 1991)

Dental nonmetric traits are considered among the most accurate in biodistance analysis as they exhibit higher heritability compared to cranial and post-cranial traits (Ansorge 2001). Their degree of expression is recorded along an ordinal scale, as described below (Scott and Turner 1997; Turner et al. 1991). Subsequently, their expression is dichotomised into presence/absence. For this dichotomy, different thresholds have been proposed by different scholars depending on the dental traits and the skeletal assemblages under study (e.g. Turner 1987). For more detailed descriptions and photographs of dental nonmetric traits, as well as for additional traits to the ones given below, the reader is advised to consult Scott et al. (2016).

Incisors (Turner et al. 1991)

Winging Outward rotation of the distal end of the labial surface of maxillary central incisors	**Shovel-shaped incisors** Prominent mesial and distal ridges lingually, and deep lingual fossa
1. Bilateral 2. Unilateral 3. None 4. Counter-winging	0. Absent 1. Very slight elevations 2. Easily seen elevations 3. Stronger ridging; tendency for ridge convergence at cingulum 4. Convergence and ridging stronger than in grade 3 5. Ridges almost in contact at cingulum 6. Ridges sometimes in contact at cingulum 7. Barrel-shaped
Double shoveling Mesial and distal ridges present on the labial surface of maxillary incisors and canines	**Labial curvature** The labial surface of upper incisors ranges from flat to markedly convex
0. Absent 1. Ridging visible under strong contrasting light 2. Ridging more clearly visible and palpated 3. Ridging readily palpated 4. Ridging pronounced on at least half of the crown height 5. Ridging very prominent 6. Extreme double shovel	0. Flat 1. Trace convexity 2. Weak convexity 3. Moderate convexity 4. Pronounced convexity

Interruption groove Grooves crossing the mesial or distal marginal ridges, or the cingulum of the lingual surface of maxillary incisors	**Tuberculum dentale** Tuberculum on the lingual surface of maxillary incisors and canines
0. Absent M. Groove on mesiolingual border D. Groove on distolingual border MD. Grooves on mesiolingual and distolingual borders Med. Groove on cingulum	0. Absent 1. Faint ridge 2. Trace ridge 3. Strong ridge 4. Pronounced ridge 5-. Weakly developed cuspule (no free apex) 5. Weakly developed cuspule (free apex) 6. Cusp
Peg-shaped incisors Maxillary lateral incisors of particularly small size and abnormal crown morphology	
0. Normal 1. Abnormally small but with normal crown morphology 2. Abnormally small and without normal crown morphology	

Canines (Turner et al. 1991)

Distal accessory ridge Ridge on the lingual surface between the median ridge and the distal marginal ridge	**Lower canine root number** Mandibular canines may exhibit two roots instead of one
0. Absent 1. Very faint 2. Weakly developed 3. Moderately developed 4. Strongly developed 5. Very pronounced	1. One root 2. Two roots (separated along more than 1/4 to 1/3 of the total root length)
Bushman canine (mesial canine ridge) Mesiolingual marginal ridge of maxillary canines larger than distolingual ridge	
0. Mesiolingual and distolingual ridges of equal size, neither attached to tuberculum dentale 1. Mesiolingual ridge larger than distolingual, weakly attached to tuberculum dentale 2. Mesiolingual ridge larger than distolingual, moderately attached to tuberculum dentale 3. Mesiolingual ridge much larger than distolingual, fully merged with tuberculum dentale	

Premolars (Turner et al. 1991)

Odontome Conical projection on the median occlusal ridge of the buccal cusp	**Upper premolar root number** Maxillary premolars may exhibit one, two, or three roots
0. Absent 1. Present	1. One root 2. Two roots (separated along more than 1/4 to 1/3 of the total root length) 3. Three roots (length defined as in grade 2)
Distosagittal ridge Buccalward rotation of the distal margin of the buccal cusp of maxillary first premolars and associated fossa or pit	**Tome's root** Deep grooving or division of the root of mandibular first premolars
0. Absent 1. Present	0. Absent or shallow groove with rounded indentation 1. Groove with shallow V-shaped cross section 2. Groove with moderately deep V-shaped cross section 3. Groove with deep V-shaped cross section 4. Deep invagination on the mesial and distal borders 5. Two roots (separate for at least 1/4 to 1/3 of total root length)

Lower premolar lingual cusp variation
The lingual aspect of mandibular premolars may exhibit one to three cusps with variable size

A. No lingual cusp
0. One lingual cusp
1. One or two lingual cusps
2. Two lingual cusps; mesial cusp much larger than distal cusp
3. Two lingual cusps; mesial cusp larger than distal cusp
4. Two lingual cusps; mesial and distal cusps equal in size
5. Two lingual cusps; distal cusp larger than mesial cusp
6. Two lingual cusps; distal cusp much larger than mesial cusp
7. Two lingual cusps; distal cusp very much larger than mesial cusp
8. Three lingual cusps of equal size
9. Three lingual cusps; mesial cusp much larger than medial and/or distal cusp

Molars (Turner et al. 1991)

Carabelli's trait Cusp on the lingual surface of the mesiolingual cusp of maxillary molars	**Hypocone** Distolingual cusp on maxillary molars
0. Absent 1. Groove 2. Pit 3. Small depression 4. Large depression 5. Small cusp 6. Medium-sized cusp 7. Large cusp	0. Absent 1. Faint ridging 2. Faint cuspule 3. Small cusp 4. Medium-sized cusp 5. Large cusp 6. Very large cusp
Enamel extensions Apical enamel projections	**Upper molar root number** Upper molars may have one or two roots, instead of three
0. Absent 1. ~ 1-mm-long projection toward the root 2. ~ 2-mm-long projection 3. >4 mm projection	1. One root 2. Two roots (separated along more than 1/4 to 1/3 of the total root length) 3. Three roots (length defined as in grade 2) 4. Four roots (length defined as in grade 2)
Metaconule Occlusal tubercle between the metacone and hypocone	**Deflecting wrinkle** Angulation on the median occlusal ridge of the mesiolingual cusp of mandibular molars
0. Absent 1. Faint cuspule 2. Trace cuspule 3. Small cuspule 4. Small cusp 5. Medium-sized cusp	0. Absent 1. Straight ridge, but with midpoint constriction 2. Ridge deflected distally, but no contact with distolingual cusp 3. Ridge deflected distally, forming L shape; it contacts distolingual cusp
Anterior fovea Triangular depression distal to the mesial marginal ridge of mandibular molars	**Tuberculum intermedium** Seventh cusp in the lingual groove between the mesiolingual and distolingual cusps of mandibular molars
0. Absent 1. Faint groove 2. Groove deeper than in grade 1 3. Groove longer than in grade 2 4. Groove very long	0. Absent 1. Faint cusp 2. Small cusp 3. Medium-sized cusp 4. Large cusp

Tuberculum sextum Additional cusp between the hypoconulid and entoconid	**Lower molar root number** Lower molars may have one to three roots
0. Absent 1. Cusp 6 much smaller than cusp 5 2. Cusp 6 smaller than cusp 5 3. Cusp 6 equal to cusp 5 4. Cusp 6 larger than cusp 5 5. Cusp 6 much larger than cusp 5	1. One root 2. Two roots (separated along more than 1/4 to 1/3 of the total root length) 3. Three roots (third root usually 1/3 the size of a normal root)
Hypoconulid A distal or distobuccal cusp on mandibular molars	**Groove pattern** Variable pattern of grooves on the occlusal surface of mandibular molars
0. Absent 1. Very small cusp 2. Small cusp 3. Medium-sized cusp 4. Large cusp 5. Very large cusp	Y. Metaconid and hypoconid in contact +. All four cusps in contact X. Protoconid and entoconid in contact

MORPHOSCOPIC TRAITS

Morphoscopic traits are recorded as a means of assessing ancestry, whereby ancestry is defined as an individual's geographic region of origin. They are principally used in forensic anthropology rather than in bioarchaeology. Various craniofacial traits have been proposed for visually assessing ancestry.

Hefner (2009) proposed a scoring system for cranial traits that fall into five categories:

1. Assessing bone shape
2. Assessing bony feature morphology
3. Assessing suture shape
4. Presence/absence data, and
5. Assessing feature prominence
   (for examples see Figures 89-99)

Morphoscopic traits versus nonmetric traits

Morphoscopic traits are found in all skeletons but in different morphological expressions, while nonmetric traits are characters that may be present or absent.

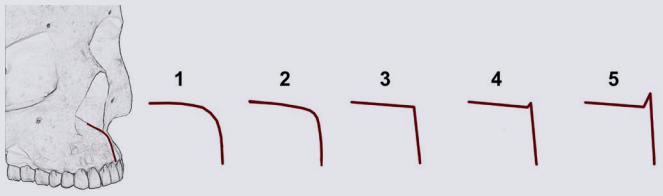

Figure 89. Inferior nasal aperture morphology (INA) | Adapted from Hefner 2009 and Nikita 2017

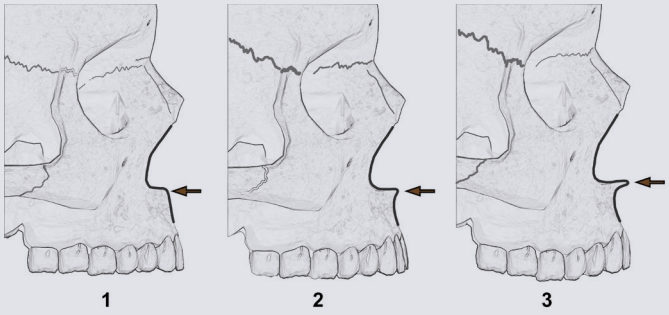

Figure 90. Anterior nasal spine (ANS) | Adapted from Hefner 2009 and Nikita 2017

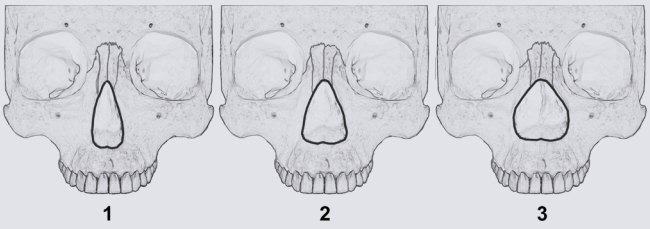

Figure 91. Nasal aperture width (NAW) | Adapted from Hefner 2009 and Nikita 2017

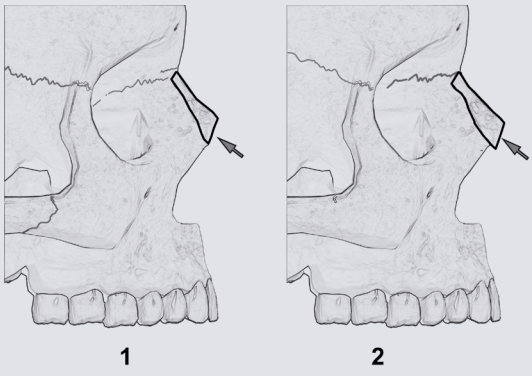

Figure 92. Nasal overgrowth (NO) | Adapted from Hefner 2009 and Nikita 2017

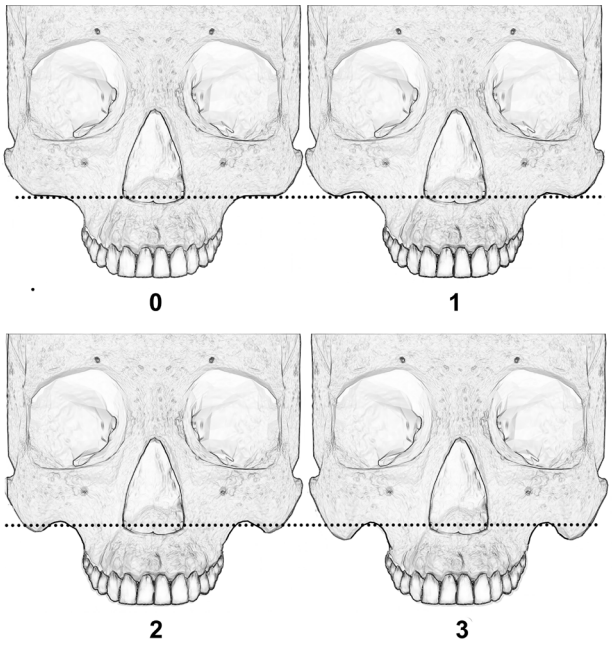

Figure 93. Malar tubercle (MT) | Adapted from Hefner 2009 and Nikita 2017

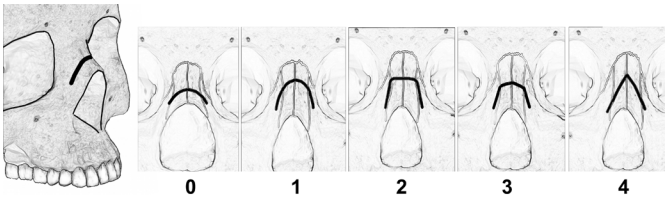

Figure 94. Nasal bone contour (NBC) | Adapted from Hefner 2009 and Nikita 2017

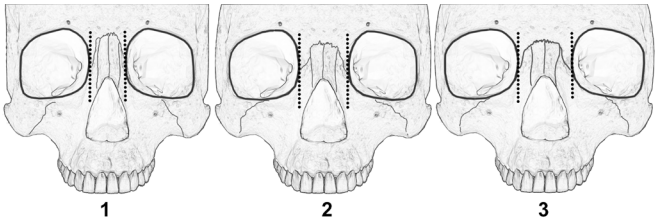

Figure 95. Interorbital breadth (IOB) | Adapted from Hefner 2009 and Nikita 2017

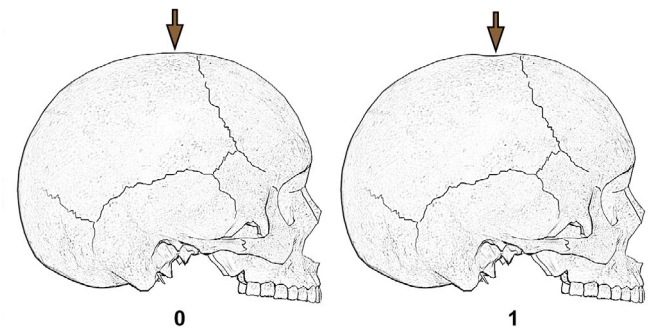

Figure 96. Postbregmatic depression (PBD) | Adapted from Hefner 2009 and Nikita 2017

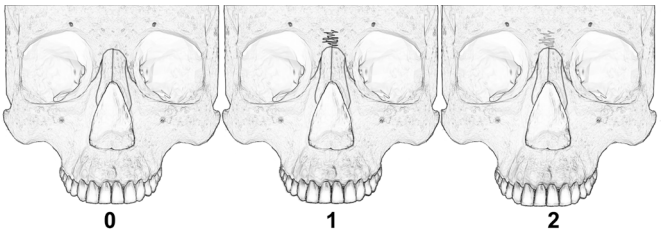

Figure 97. Supranasal suture (SPS) | Adapted from Hefner 2009 and Nikita 2017

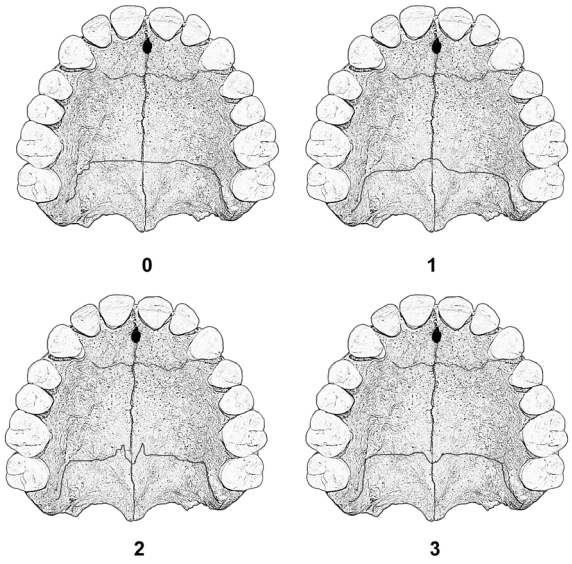

Figure 98. Transverse palatine suture (TPS) shape | Adapted from Hefner 2009 and Nikita 2017

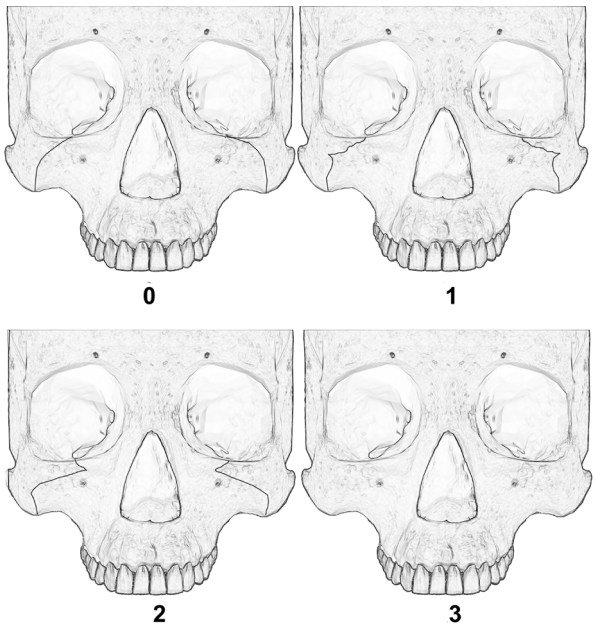

Figure 99. Zygomaticomaxillary suture (ZS) shape | Adapted from Hefner 2009 and Nikita 2017

METRICS

Figures 100-113 visualise standard measurements from Moore-Jansen and Jantz (1989) that may be obtained from fully formed (adult) bones, and Figure 114 depicts dental measurements. For measurements obtained from nonadult bones, see Buikstra and Ubelaker (1994). Long bone lengths should be taken using an osteometric board, while a sliding caliper should be used to collect all other measurements. For teeth, the use of a dental caliper is advised.

ADULTS

Cranium

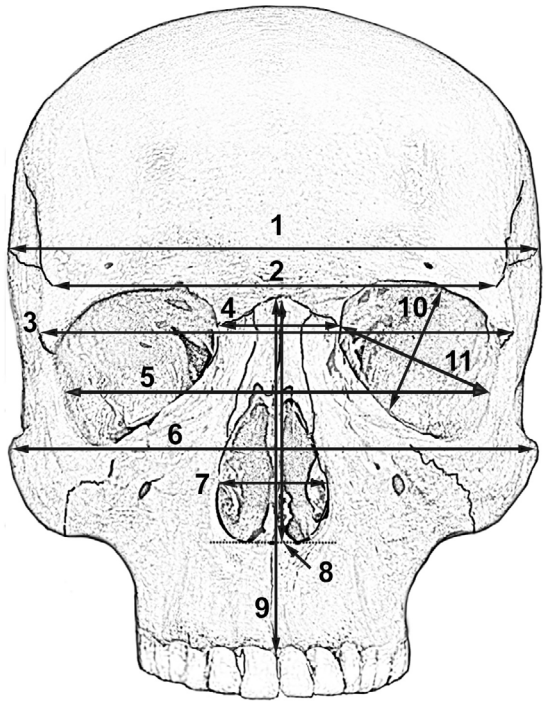

Figure 100. Cranial measurements; anterior view | Adapted from Nikita 2017

1. Maximum cranial breadth (#2 Moore-Jansen and Jantz 1989)
2. Minimum frontal breadth (#11 Moore-Jansen and Jantz 1989)
3. Upper facial breadth (#12 Moore-Jansen and Jantz 1989)
4. Interorbital breadth (#18 Moore-Jansen and Jantz 1989)
5. Biorbital breadth (#17 Moore-Jansen and Jantz 1989)
6. Bizygomatic diameter (#3 Moore-Jansen and Jantz 1989)
7. Nasal breadth (#14 Moore-Jansen and Jantz 1989)
8. Nasal height (#13 Moore-Jansen and Jantz 1989)
9. Upper facial height (#10 Moore-Jansen and Jantz 1989)
10. Orbital height (#16 Moore-Jansen and Jantz 1989)
11. Orbital breadth (#15 Moore-Jansen and Jantz 1989)

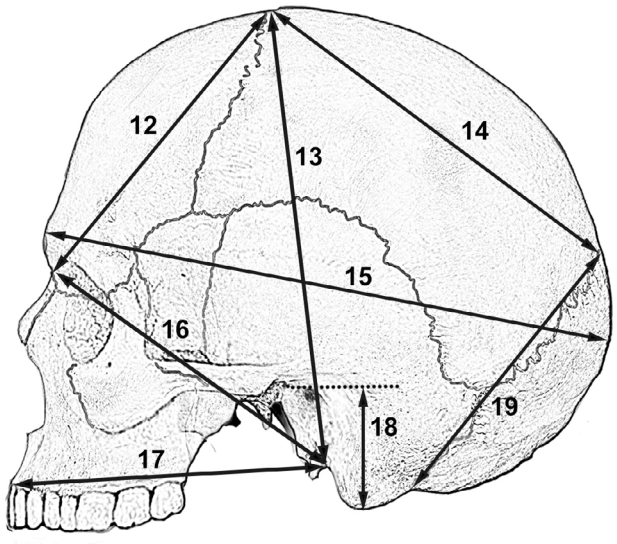

Figure 101. Cranial measurements; lateral view | Adapted from Nikita 2017

12. Frontal chord (#19 Moore-Jansen and Jantz 1989)
13. Basion-bregma height (#4 Moore-Jansen and Jantz 1989)
14. Parietal chord (#20 Moore-Jansen and Jantz 1989)
15. Maximum cranial length (#1 Moore-Jansen and Jantz 1989)
16. Cranial base length (#5 Moore-Jansen and Jantz 1989)
17. Basion-prosthion length (#6 Moore-Jansen and Jantz 1989)
18. Mastoid length (#24 Moore-Jansen and Jantz 1989)
19. Occipital chord (#21 Moore-Jansen and Jantz 1989)

Important note:
The arrows that end at the anterior of the mastoid process for measurements 13, 16 & 17 point to basion, while the arrow that ends at the posterior of the mastoid process for measurement 19 points to the opisthion

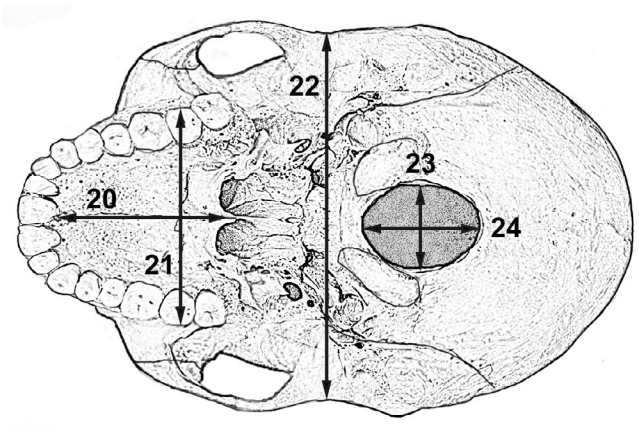

Figure 102. Cranial measurements; inferior view | Adapted from Nikita 2017

20. Maxillo-alveolar length (#8 Moore-Jansen and Jantz 1989)
21. Maxillo-alveolar breadth (#7 Moore-Jansen and Jantz 1989)
22. Biauricular breadth (#9 Moore-Jansen and Jantz 1989)
23. Foramen magnum breadth (#22 Moore-Jansen and Jantz 1989)
24. Foramen magnum length (#23 Moore-Jansen and Jantz 1989)

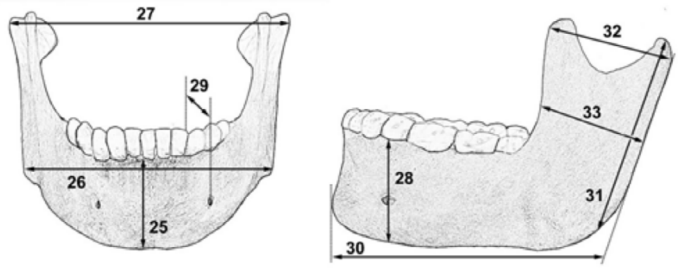

Figure 103. Mandibular measurements | Adapted from Nikita 2017

25. Chin height (#25 Moore-Jansen and Jantz 1989)
26. Bigonial width (#28 Moore-Jansen and Jantz 1989)
27. Bicondylar breadth (#29 Moore-Jansen and Jantz 1989)
28. Height of the mandibular body (#26 Moore-Jansen and Jantz 1989)
29. Breadth of the mandibular body (#27 Moore-Jansen and Jantz 1989)
30. Mandibular length (#33 Moore-Jansen and Jantz 1989)
31. Maximum ramus height (#32 Moore-Jansen and Jantz 1989)
32. Maximum ramus breadth (#30 Moore-Jansen and Jantz 1989)
33. Minimum ramus breadth (#31 Moore-Jansen and Jantz 1989)

Clavicle

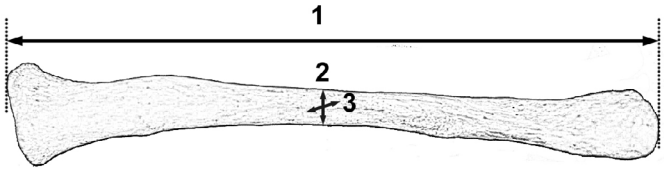

Figure 104. Clavicular measurements | Adapted from Nikita 2017

1. Maximum length (#35 Moore-Jansen and Jantz 1989)
2. Superior-inferior (vertical) diameter at midshaft (#37 Moore-Jansen and Jantz 1989)
3. Anterior-posterior (sagittal) diameter at midshaft (#36 Moore-Jansen and Jantz 1989)

Scapula

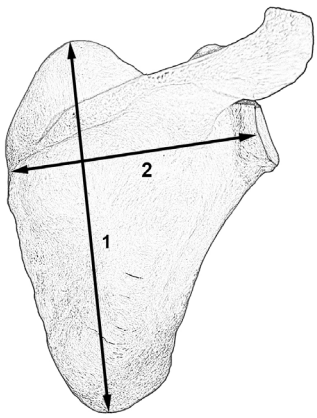

Figure 105. Scapular measurements | Adapted from Nikita 2017

1. Height (#38 Moore-Jansen and Jantz 1989)
2. Breadth (#39 Moore-Jansen and Jantz 1989)

Humerus

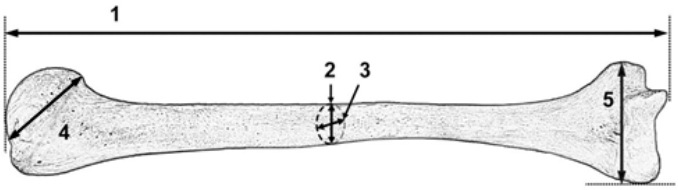

Figure 106. Humeral measurements | Adapted from Nikita 2017

1. Maximum length (#40 Moore-Jansen and Jantz 1989)
2. Maximum midshaft diameter (#43 Moore-Jansen and Jantz 1989)
3. Minimum midshaft diameter (#44 Moore-Jansen and Jantz 1989)
4. Vertical head diameter (#42 Moore-Jansen and Jantz 1989)
5. Epicondylar breadth (#41 Moore-Jansen and Jantz 1989)

Ulna

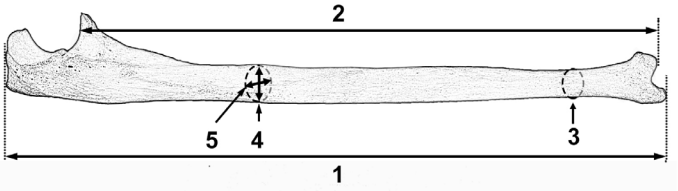

Figure 107. Ulnar measurements | Adapted from Nikita 2017

1. Maximum length (#48 Moore-Jansen and Jantz 1989)
2. Physiological length (#51 Moore-Jansen and Jantz 1989)
3. Minimum circumference (#52 Moore-Jansen and Jantz 1989)
4. Anteroposterior (dorsovolar) diameter (#49 Moore-Jansen and Jantz 1989)
5. Mediolateral (transverse) diameter (#50 Moore-Jansen and Jantz 1989)

Radius

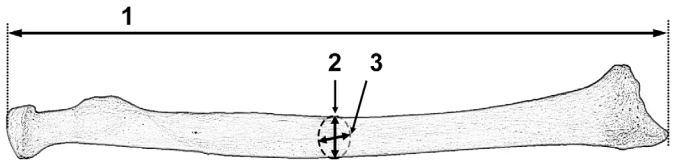

Figure 108. Radial measurements | Adapted from Nikita 2017

1. Maximum length (#45 Moore-Jansen and Jantz 1989)
2. Mediolateral (transverse) midshaft diameter (#47 Moore-Jansen and Jantz 1989)
3. Anteroposterior (sagittal) midshaft diameter (#46 Moore-Jansen and Jantz 1989)

Os Coxa

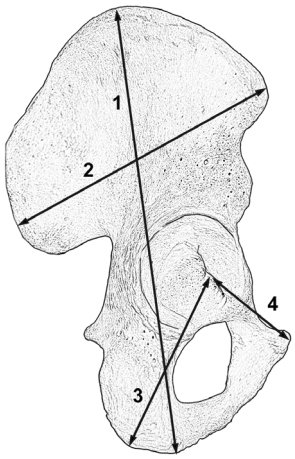

Figure 109. Os coxal measurements | Adapted from Nikita 2017

1. Height (#56 Moore-Jansen and Jantz 1989)
2. Iliac breadth (#57 Moore-Jansen and Jantz 1989)
3. Ischium length (#59 Moore-Jansen and Jantz 1989)
4. Pubis length (#58 Moore-Jansen and Jantz 1989)

Sacrum

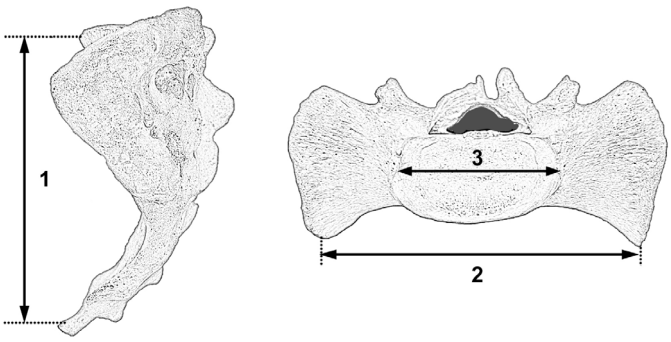

Figure 110. Sacral measurements | Adapted from Nikita 2017

1. Anterior length (#53 Moore-Jansen and Jantz 1989)
2. Anterosuperior breadth (#54 Moore-Jansen and Jantz 1989)
3. Maximum transverse base diameter (#55 Moore-Jansen and Jantz 1989)

Femur

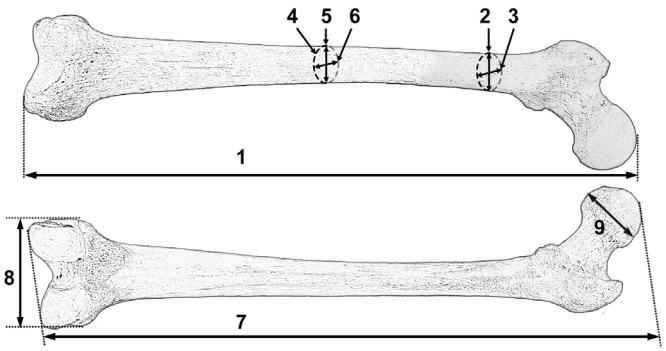

Figure 111. Femoral measurements | Adapted from Nikita 2017

1. Maximum length (#60 Moore-Jansen and Jantz 1989)
2. Subtrochanteric mediolateral (transverse) diameter (#65 Moore-Jansen and Jantz 1989)
3. Subtrochanteric anteroposterior (sagittal) diameter (#64 Moore-Jansen and Jantz 1989)
4. Midshaft circumference (#68 Moore-Jansen and Jantz 1989)
5. Mediolateral (transverse) midshaft diameter (#67 Moore-Jansen and Jantz 1989)
6. Anteroposterior (sagittal) midshaft diameter (#66 Moore-Jansen and Jantz 1989)
7. Bicondylar length (#61 Moore-Jansen and Jantz 1989)
8. Epicondylar breadth (#62 Moore-Jansen and Jantz 1989)
9. Maximum head diameter (#63 Moore-Jansen and Jantz 1989)

Tibia

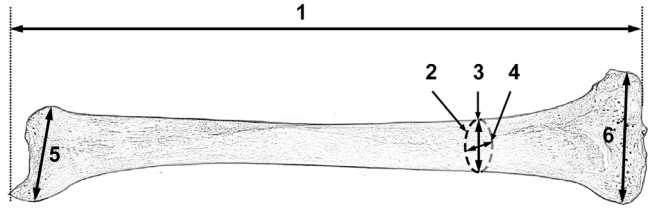

Figure 112. Tibial measurements | Adapted from Nikita 2017

1. Length (#69 Moore-Jansen and Jantz 1989)
2. Circumference at nutrient foramen (#74 Moore-Jansen and Jantz 1989)
3. Mediolateral (transverse) diameter at nutrient foramen (#73 Moore-Jansen and Jantz 1989)
4. Maximum diameter at nutrient foramen (#72 Moore-Jansen and Jantz 1989)
5. Maximum distal epiphyseal breadth (#71 Moore-Jansen and Jantz 1989)
6. Maximum proximal epiphyseal breadth (#70 Moore-Jansen and Jantz 1989)

Fibula

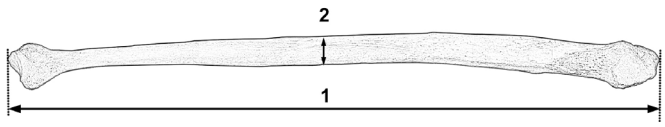

Figure 113. Fibular measurements | Adapted from Nikita 2017
1. Maximum length (#75 Moore-Jansen and Jantz 1989)
2. Maximum midshaft diameter (#76 Moore-Jansen and Jantz 1989)

Teeth (Aubry 2014; Hillson et al. 2005; White et al. 2011)

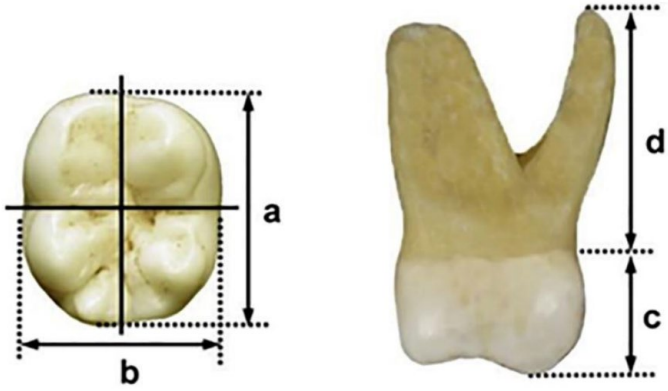

Figure 114. Dental measurements | Adapted from Nikita 2017
1. Maximum mesiodistal crown diameter (a)
2. Maximum buccolingual crown diameter (b)
3. Crown height (c)
4. Root length (d)

STATURE ESTIMATION

Stature estimation from skeletal remains is based on anatomical and mathematical methods. Anatomical methods measure the height/length of skeletal elements from the tarsals to the cranium, sum these measurements and add a correction factor for the missing soft tissues (Fully 1956; Raxter et al. 2006). The method by Raxter et al. (2006) is the most frequently adopted one. According to this method, the measurements shown in Figure 115 are obtained, they are summed to get the skeletal height, and then the living stature is estimated as: living stature = 1.009 × skeletal height – 0.0426 × age + 12.1 (when the age of the individual is known) or living stature = 0.996 × skeletal height + 11.7 (when the age of the individual is unknown). In these equations stature/height is in cm and age in years. Anatomical methods are robust to population and individual variation in body proportions and generally provide more accurate estimates compared to mathematical methods; however, they are only applicable to well-preserved skeletons.

Mathematical methods involve regression equations for stature estimation based on specific bone dimensions. They are based on the correlation between stature and individual bone dimensions, mostly long-bone lengths. After the bones are measured, the measurements are put into the appropriate regression formula. In general, the linear regression equation for stature estimation from a skeletal measurement has the following form:

$$\text{Stature} = a + bx$$

where a is the y intercept of the line, b is the slope, and x is the bone measurement.

Regression equations for stature estimation have been published for different populations across the world. Nikita (2017) provides a compilation of population-specific studies, which use not only long bones but also other skeletal elements. **Tables 27-28** provide representative stature estimation equations for European and American populations, respectively. These tables are based on long bone lengths, which will be difficult to obtain in highly fragmented assemblages. In such assemblages, stature estimation equations based on smaller elements (e.g. metacarpals, phalanges etc.) could be used though the margin of error is much higher when using such elements (see Byers et al. 1989; Musgrave and Harneja 1978, and other references in Nikita 2017).

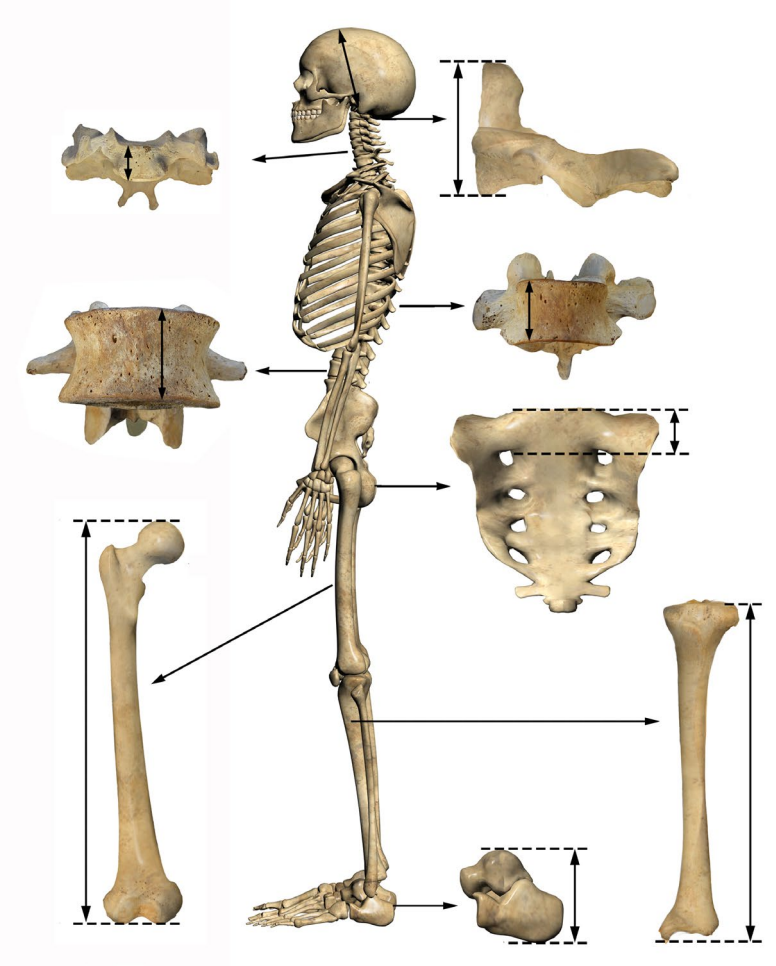

Figure 115. Measurements for anatomical stature estimation | Adapted from Nikita 2017

Table 27. Stature estimation equations – European populations (Ruff et al. 2012)

Element	**Region**	**Sex**	**Equation** (lengths in cm)
Femur	All	Males	2.72*maximum length + 42.85
		Females	2.69*maximum length + 43.56
		Combined	2.77*maximum length + 40.50
Tibia	North	Males	3.09*maximum length + 52.04
		Females	2.92*maximum length + 56.94
		Combined	3.13*maximum length + 50.11
	South	Males	2.78*maximum length + 60.76
		Females	3.05*maximum length + 49.68
		Combined	3.02*maximum length + 51.36
Humerus	All	Males	3.83*maximum length + 41.42
		Females	3.38*maximum length + 54.60
		Combined	3.72*maximum length + 44.86
Radius	All	Males	4.85*maximum length + 47.46
		Females	4.20*maximum length + 63.08
		Combined	4.46*maximum length + 56.94

Table 28. Stature estimation equations – American populations (Wilson et al. 2010)

Element	Ethnic group	Sex	Stature*	Equation (lengths in cm)
Humerus	White	Males	FSTAT	3.541*maximum length + 58.389
		Females	FSTAT	2.527*maximum length + 86.587
		Males	ASTAT	3.574*maximum length + 57.208
		Females	ASTAT	2.534*maximum length + 86.622
	Black	Males	FSTAT	3.371*maximum length + 62.046
		Females	FSTAT	5.010*maximum length + 9.777
		Males	ASTAT	3.277*maximum length + 65.455
		Females	ASTAT	3.785*maximum length + 47.347
Radius	White	Males	FSTAT	4.480*maximum length + 62.835
		Females	FSTAT	3.870*maximum length + 75.621
		Males	ASTAT	4.525*maximum length + 61.218
		Females	ASTAT	3.530*maximum length + 83.293
	Black	Males	FSTAT	5.168*maximum length + 38.372
		Females	FSTAT	5.198*maximum length + 40.624
		Males	ASTAT	4.235*maximum length + 63.463
		Females	ASTAT	3.781*maximum length + 75.200
Ulna	White	Males	FSTAT	4.632*maximum length + 51.051
		Females	FSTAT	3.540*maximum length + 77.889
		Males	ASTAT	4.534*maximum length + 53.331
		Females	ASTAT	3.346*maximum length + 82.815
	Black	Males	FSTAT	5.015*maximum length + 33.641
		Females	FSTAT	3.136*maximum length + 83.054
		Males	ASTAT	3.979*maximum length + 62.953
		Females	ASTAT	3.285*maximum length + 80.696
Femur	White	Males	FSTAT	2.835*maximum length + 41.967
		Females	FSTAT	2.637*maximum length + 48.549
		Males	ASTAT	2.701*maximum length + 48.057
		Females	ASTAT	2.624*maximum length + 49.263
	Black	Males	FSTAT	2.410*maximum length + 58.483
		Females	FSTAT	2.802*maximum length + 37.852
		Males	ASTAT	2.455*maximum length + 56.661
		Females	ASTAT	2.449*maximum length + 54.863

Tibia	White	Males	FSTAT	2.962*maximum length + 68.205
		Females	FSTAT	2.311*maximum length + 81.485
		Males	ASTAT	2.891*maximum length + 62.953
		Females	ASTAT	2.351*maximum length + 80.108
	Black	Males	FSTAT	2.628*maximum length + 68.205
		Females	FSTAT	3.217*maximum length + 43.660
		Males	ASTAT	2.455*maximum length + 75.477
		Females	ASTAT	2.855*maximum length + 58.204
Fibula	White	Males	FSTAT	2.916*maximum length + 64.052
		Females	FSTAT	2.559*maximum length + 73.747
		Males	ASTAT	2.832*maximum length + 66.958
		Females	ASTAT	2.487*maximum length + 76.508
	Black	Males	FSTAT	2.916*maximum length + 60.030
		Females	FSTAT	3.569*maximum length + 33.128
		Males	ASTAT	2.665*maximum length + 69.392
		Females	ASTAT	2.993*maximum length + 55.826

* Stature formulae calculated using forensic stature (FSTAT) and a combined dataset of forensic, cadaver, and measured statures referred to as Any Stature (ASTAT)

POST-MORTEM BONE ALTERATION

By the examination of the distribution of post-mortem bone alteration (fracture patterning, burning, tool marks etc.), it is possible to reconstruct the behaviours leading to the creation of an assemblage, that is, how the human body was disassembled at each site (Fernández-Jalvo and Andrews 2016). However, the same bone alteration may be due to a number of causative factors, while one taphonomic change may overlay another.

In **Tables 29-35**, we follow the distinction of bone alterations given in Fernández-Jalvo and Andrews (2016) because these start from morphological attributes rather than from the causative agents, which, as highlighted above, may be difficult or even impossible to identify. Finally, **Table 36** presents the Anatomical Preservation Index, Bone Representation Index and Qualitative Bone Index, as defined by Andrews and Bello (2006) and Bello and Andrews (2006).

Table 29. Linear marks (Fernández-Jalvo and Andrews 2016)

Type	Agent	Characteristics	Other categories/agents
Inorganic Linear Marks with V Shaped Cross-Section Made by Stone	Human tool use Movement of rock against bone (abrasion) Movement of bone against hard surface (trampling, transport)	Tissue accumulation in front of the cutting edge Asymmetric cross-section Displaced bone may form a raised shoulder alongside the linear mark	**Scrapes** Broad areas of linear marks caused either by movement of stone across a bone surface or by movement of the bone against a hard surface

Type	Agent	Characteristics	Other categories/agents
Organic Linear Marks with U Shaped Cross-Section Made by Animals	Animal gnawing	More abrasive compared to cut marks and trampling marks	**Rodent gnawing incisor marks** Multiple, parallel, broad, shallow, and flat-bottomed **Carnivore chewing canine/premolar/molar marks** Small, single, U-shaped in cross-section, and without internal striations **Raptor beak marks** Superficial, broad and flat-bottomed, of variable length **Insect marks** Punctures and linear marks **Plant root marks** With U-shaped cross-section and smooth contours, often curved, branched and multiple

Table 30. Pits and Perforations* (Fernández-Jalvo and Andrews 2016)

Type	Agent	Characteristics	Other categories/agents
Organic Processes Producing Pits or Cone-Shaped Perforations	Carnivore chewing or gripping	Conical or cone-shaped perforations	**Insect damage** Perforations with no floor, penetrating deep inside the bone **Plant root marks** Smooth edged and abundant
Inorganic Processes Producing Broad-Based Perforations	• Trampling • Butchery or carcass dismemberment	**Trampling** Superficial, irregular perforations with broad base, numerous and scattered across the bone surface	**Percussion marks** Broader and more variable in size than carnivore tooth marks
Organic Processes Producing Broad-Based Perforations	Large birds	Large and irregular perforations on thin bone	**Lichen** **Plant roots** **Carnivore tooth marks** **Wind erosion**
Perforations from Chemical Attack	• Cave corrosion • Digestion • Diatoms	**Cave corrosion** Perforations that thin out the bone to the extent that the bone surface begins to collapse **Digestion** Bone surface destruction and pitting **Diatoms** Perforations with a lineal trajectory	

* Pits are superficial marks on the bone surface, while perforations penetrate the underlying bone tissue. Pits and perforations have lengths less than 4 times their breadth to distinguish them from linear marks

Table 31. Discoloration and Staining (Fernández-Jalvo and Andrews 2016)

Type	Agent	Characteristics	Other categories/agents
Black Staining	Manganese dioxide	• Overall or patchy surface staining • Dendritic patterns	• Carbon deposition • Fungal attack • Fire
Brown and Black Variable Staining	• Humic acids • Fire		
Red Staining	• Iron rich soils • Red ochre		

Table 32. Flaking and Cracking (Fernández-Jalvo and Andrews 2016)

Type	Agent
Inorganic Cracking of Surface Bone	• Thermal exposure • Highly alkaline or acidic environmental conditions • Weathering*
Inorganic Flaking of Surface Bone	• Weathering • Boiling • Highly alkaline environmental conditions
Organic Cracking	• Digestion • Root marks

*Weathering results from the exposure of skeletal elements to fluctuating temperatures, humidity, solar radiation and other weather conditions. Representative recording schemes are given in Table 33

Table 33. Weathering recording schemes | Adapted from McKinley 2004

Stage	Description
0	No surface erosion
1	Slight and patchy erosion
2	More extensive erosion with deeper penetration
3	Erosion affecting most of bone surface; general bone morphology preserved but some bone surface details masked by erosive action
4	Erosion affecting the entire bone surface, variable penetration depth, overall bone profile maintained
5	Heavy erosion affecting the entire bone surface, some modification of the bone profile
5+	As grade 5 but with modification of the bone profile

Table 34. Corrosion and Digestion (Fernández-Jalvo and Andrews 2016)

Definition	Agent	Characteristics
Corrosion Bone surface modifications due to chemical attack by biological or geochemical agents	Moist, chemically reactive conditions and removal from direct contact with the air	Unsystematic loss of bone tissue
Digestion Bone surface modification and internal bone structure chemical modification	High acidity in predator stomachs due to digestive enzymes	Bone surface etching

Table 35. Breakage and Deformation (Fernández-Jalvo and Andrews 2016)

Morphology of Breaks	Fragmentation	Deformation
Fracture Outline • Curved or spiral (usually on fresh/ green bone; often due to human action or carnivore chewing) • Transverse (sediment movement; trampling; diagenesis; local micro-faulting) **Fracture Angle** • Oblique (on green bone) • Perpendicular (on buried bone) • Mixed (on dry bone) **Fracture Edge** • Smooth (on green bone) • Jagged (on dry bone)	Number of fragments into which bones have been broken	Bone of distorted morphology but not broken

Table 36. General preservation (Andrews and Bello 2006; Bello and Andrews 2006)

Anatomical Preservation Index	Bone Representation Index	Qualitative Bone Index
Ratio between how much of each bone is preserved and the total number of bones in the skeleton	Ratio between number of bones retrieved and total number of bones that should have been present if all skeletons had been intact	Ratio between each bone's intact cortical surface and damaged surface
Class 1: 0% Class 2: 1–24% Class 3: 25–49% Class 4: 50–74% Class 5: 75–99% Class 6: 100%		Class 1: 0% Class 2: 1–24% Class 3: 25–49% Class 4: 50–74% Class 5: 75–99% Class 6: 100%

REFERENCES

Adams BJ, Crabtree PJ, Santucci G. 2008. ***Comparative Skeletal Anatomy: A Photographic Atlas for Medical Examiners, Coroners, Forensic Anthropologists, and Archaeologists***. Totowa, FL: Humana Press

Aerssens J, Boonen S, Lowet G, Dequeker J. 1998. Interspecies differences in bone composition, density, and quality: Potential implications for in vivo bone research. ***Endocrinology*** 139: 663–670

Albert AM, Maples WR. 1995. Stages of epiphyseal union for thoracic and lumbar vertebral centra as a method of age determination for teenage and young adult skeletons. ***Journal of Forensic Science*** 40: 623-633

AlQahtani SJ, Hector MP, Liversidge HM. 2010. Brief communication: The London atlas of human tooth development and eruption. ***American Journal of Physical Anthropology*** 142: 481-490

Alves Cardoso FA, Henderson CY. 2010. Enthesopathy formation in the humerus: Data from known age-at-death and known occupation skeletal collections. ***American Journal of Physical Anthropology*** 141: 550-560

Anastasiou E, Papathanasiou A, Schepartz LA, Mitchell PD. 2018. Infectious disease in the ancient Aegean: Intestinal parasitic worms in the Neolithic to Roman period inhabitants of Kea, Greece. ***Journal of Archaeological Science: Reports*** 17: 860-864

Andrews P, Bello S. 2006. Pattern in human burial practice. In: Gowland R, Knüsel C (eds.) ***Social Archaeology of Funerary Remains***. Oxford: Oxbow Books; p. 14–29

Ansorge H. 2001. Assessing non-metric skeleton characters as a morphological tool. ***Zoology*** 104: 268-277

Arnadottir IB, Holbrook WP, Eggertsson H, Gudmundsdottir H, Jonsson SH, Gudlaugsson JO, Saemundsson SR, Eliasson ST, Agustsdottir H. 2010. Prevalence of dental erosion in children: a national survey. ***Community Dentistry and Oral Epidemiology*** 38: 521-526

Atici L. 2014. Commingled bone assemblages: Insights from zooarchaeology and taphonomy of a bone bed at Karain B Cave, SW Turkey. In: Osterholz AJ, Baustian KM, Martin DL (eds.) ***Commingled and Disarticulated Human Remains***. New York: Springer; p. 213-253

Aubry BS. 2014. Technical note: cervical dimensions for in situ and loose teeth: a critique of the Hillson et al. (2005) method. ***American Journal of Physical Anthropology*** 154: 159-164

Aufderheide AC, Rodriguez-Martin C. 1998. ***The Cambridge Encyclopedia of Human Paleopathology***. Cambridge: Cambridge University Press

Barker P. 2003. ***Techniques of Archaeological Excavation***. London: Routledge

Barker C, Cox M, Flavel A, Laver J, Loe L. 2008a. Mortuary procedures II – Skeletal analysis I: Basic procedures and demographic assessment. In: Cox M, Flavel A, Hanson I, Laver J, Wessling R (eds.) ***The Scientific Investigation of Mass Graves: Towards Protocols and Standard Operating Procedures***. Cambridge: Cambridge University Press; p. 295-382

Barker C, Cox M, Flavel A, Laver J, Lewis M, McKinley J. 2008b. Mortuary procedures III – Skeletal analysis 2: Techniques for determining identity. In: Cox M, Flavel A, Hanson I, Laver J, Wessling R (eds.) ***The Scientific Investigation of Mass Graves: Towards Protocols and Standard Operating Procedures***. Cambridge: Cambridge University Press; p. 383-498

Barone R. 1976. ***Anatomie Comparée des Mammiferes Domestiques. III Splachnologie***. Laboratorie d' Anatomie Ecole Vétérinare de Lyon

Bartelink EJ, Milligan CF, Sturdy Colls C. 2016. The role of forensic archaeology in missing persons investigations. In: Morewitz SJ, Sturdy Colls C (eds.) ***Handbook of Missing Persons***. New York: Springer; p. 271-284

Bass WM. 1995. ***Human Osteology: A Laboratory and Field Method***. Springfield, IL: Charles C. Thomas

Beckett S, Rogers K, Clement JG. 2011. Inter-species variation in bone mineral behaviour upon heating. ***Journal of Forensic Sciences*** 56: 571–579

Bello S, Andrews P. 2006. The intrinsic pattern of preservation of human skeletons and its influence on the interpretation of funerary behaviours. In: Gowland R, Knüsel C (eds.) ***Social Archaeology of Funerary Remains***. Oxford: Oxbow Books; p. 1-13

Benjamin M, Evans EJ, Copp L. 1986. The histology of tendon attachments to bone in man. *Journal of Anatomy* 149: 89-100

Benjamin M, Kumai T, Milz S, Boszczyk BM, Boszczyk AA, Ralphs JR. 2002. The skeletal attachment of tendons-tendon "entheses". *Comparative Biochemistry and Physiology Part A: Physiology* 133: 931-945

Benjamin M, Toumi H, Ralphs JR, Bydder G, Best TM, Milz S. 2006. Where tendons and ligaments meet bone: attachment sites ("entheses") in relation to exercise and/or mechanical load. *Journal of Anatomy* 208: 471-490

Berg GE. 2008. Pubic bone age estimation in adult women. *Journal of Forensic Sciences* 53: 569-577

Berg GE. 2012. Determining the sex of unknown human skeletal remains. In: Tersigni-Tarrant MA, Shirley NR (eds.) *Forensic Anthropology: An Introduction*. Boca Raton, FL: CRC Press; p. 139-160

Berry AC, Berry RJ. 1967. Epigenetic variation in the human cranium. *Journal of Anatomy* 101: 361-379

Bilfeld MF, Dedouit F, Sans N, Rousseau H, Rougé D, Telmon N. 2015. Ontogeny of size and shape sexual dimorphism in the pubis: A multislice Computed Tomography study by geometric morphometry. *Journal of Forensic Sciences* 60: 1121-1128

Biltz RM, Pellegrino ED. 1969. The chemical anatomy of bone: a comparative study of bone composition in sixteen vertebrates. *The Journal of Bone and Joint Surgery* 31A: 456–466

Boucher BJ. 1955. Sex differences in the foetal sciatic notch. *Journal of Forensic Medicine* 2: 51–54

Bratter P, Gawlik D, Lausch J, Rosick U. 1977. On the distribution of trace elements in human skeleton. *Journal of Radioanalytical Chemistry* 37: 393–403

Brody RH, Edwards HGM, Pollard AM. 2001. Chemometric methods applied to the differentiation of Fourier-transform Raman spectra of ivories. *Analytica Chimica Acta* 427: 223–232

Brooks S, Suchey JM. 1990. Skeletal age determination based on the os pubis: a comparison of the Acsádi-Nemeskéri and Suchey-Brooks methods. *Human Evolution* 5: 227-238

Buckberry JL, Chamberlain AT. 2002. Age estimation from the auricular surface of the ilium: a revised method. *American Journal of Physical Anthropology* 119: 231-239

Buikstra JE, Ubelaker DH (eds.) 1994. *Standards for Data Collection from Human Skeletal Remains*. Fayetteville: Arkansas Archaeological Survey Research Series No 44

Buikstra JE (ed.) 2019. *Ortner's Identification of Pathological Conditions in Human Skeletal Remains, 3rd edition*. San Diego: Academic Press

Byers S, Akoshima K, Curran B. 1989. Determination of adult stature from metatarsal length. *American Journal of Physical Anthropology* 79: 275-279

Cabo LL, Dirkmaat DC, Adovasio JM, Rozas VC. 2012. Archaeology, mass graves, and resolving commingling issues through spatial analysis. In: Dirkmaat DC (ed.) *A Companion to Forensic Anthropology*. New York: Blackwell Publishing; p. 175-196

Cardoso HF. 2008. Sample-specific (universal) metric approaches for determining the sex of immature human skeletal remains using permanent tooth dimensions. *Journal of Archaeological Science* 35: 158-168

Cardoso HF. 2007. Environmental effects on skeletal versus dental development: Using a documented subadult skeletal sample to test a basic assumption in human osteological research. *American Journal of Physical Anthropology* 132: 223-233

Carver M. 2013. *Archaeological Investigation*. London: Routledge

Cassman V, Odegaard N. 2007. Examination and analysis. In: Cassman V, Odegaard N, Powell J (eds.) *Human Remains: Guide for Museums and Academic Institutions*. Toronto: Altamira Press; p. 49-75

Cattaneo C, DiMartino S, Scali S, Craig OE, Grandi M, Sokol R. 1999. Determining the human origin of fragments of burnt bone: a comparative study of histological, immunological and DNA techniques. *Forensic Science International* 102: 181-191

Cerezo-Román JI, Hernández Espinoza PO. 2014. Estimating age at death using the sternal end of the fourth ribs from Mexican males. *Forensic Science International* 236: 196.e1-196.e6

Cheetham P, Cox M, Flavel A, Hanson I, Haynie T, Oxlee D, Wessling R. 2008. Search, location, excavation, and recovery. In: Cox M, Flavel A, Hanson I, Laver J, Wessling R (eds.) *The Scientific Investigation of Mass Graves: Towards Protocols and Standard Operating Procedures*. Cambridge: Cambridge University Press; p. 183-267

Cheverud JM, Buikstra JE. 1981. Quantitative genetics of skeletal nonmetric traits in the rhesus macaques on Cayo Santiago. I. Single trait heritabilities. *American Journal of Physical Anthropology* 54: 43-49

Christensen AM, Smith MA, Thomas RM. 2012. Validation of X-ray fluorescence spectrometry for determining osseous or dental origin of unknown material. *Journal of Forensic Sciences* 57: 47–51

Christensen AM, Passalacqua NV, Bartelink EJ. 2014. *Forensic Anthropology: Current Methods and Practice*. San Diego: Academic Press

Connor MA. 2007. *Forensic Methods: Excavation for the Archaeologist and Investigator*. Rowman: Altamira

Coquerelle M, Bookstein FL, Braga J, Halazonetis DJ, Weber GW, Mitteroecker P. 2011. Sexual dimorphism of the human mandible and its association with dental development. *American Journal of Physical Anthropology* 145: 192-202

Courtaud P. 1996. Anthropologie de sauvetage: vers une optimisation des méthodes d' enregistrement. Présentation d' une fiche anthropologique. *Bulletins et Mémoires de la Société d'Anthropologie de Paris* 8: 157-167

Cunningham C, Scheuer L, Black S. 2016. *Developmental Juvenile Osteology, 2nd edition*. Amsterdam: Elsevier

Currey JD. 2002. *Bones: Structure and Mechanics*. Princeton: Princeton University Press

De Reu J, Plets G, Verhoeven G, De Smedt P, Bats M, Cherretté B, De Maeyer W, Deconynck J, Herremans D, Laloo P, Van Meirvenne M, De Clercq W. 2013. Towards a three-dimensional cost-effective registration of the archaeological heritage. *Journal of Archaeological Science* 40: 1108-1121

DiGangi EA, Bethard JD, Kimmerle EH, Konigsberg LW. 2009. A new method for estimating age-at-death from the first rib. *American Journal of Physical Anthropology* 138: 164-176

Dirkmaat DC. 2012. Documenting context at the outdoor crime scene: Why bother? In: Dirkmaat DC (ed.) *A Companion to Forensic Anthropology*. New York: Blackwell Publishing; p. 48-65

Dobney KM, Rielly K. 1988. A method for recording archaeological animal bones: the use of diagnostic zones. *Circaea* 5: 79-96

Dudar CJ. 1993. Identification of rib number and assessment of intercostal variation at the sternal rib end. *Journal of Forensic Sciences* 38: 788-797

Dudar CJ. 2011. Arthritis. In: Wilczak CA, Jones EB (eds.) *OsteowareTM Software Manual: Volume II*. Washington, D.C.: Smithsonian Institution; p. 76-83

Duday H. 2009. *The Archaeology of the Dead: Lectures in Archaeothanatology*. Oxford: Oxford University Press

Dupras TL, Schultz JJ, Wheeler SM, Williams LJ. 2012. *Forensic Recovery of Human Remains. Archaeological Approaches, 2nd edition*. Boca Raton: CRC Press

Edwards HGM, Hassan NF, Arya N. 2006. Evaluation of Raman spectroscopy and application of chemometric methods for the differentiation of contemporary ivory specimens I: elephant and mammalian species. *Journal of Raman Spectroscopy* 37: 353–360

Evis LH, Hanson I, Cheetham PN. 2016. An experimental study of two grave excavation methods: Arbitrary Level Excavation and Stratigraphic Excavation. *STAR: Science & Technology of Archaeological Research* 2: 177-191

Fazekas G, Kósa F. 1978. *Forensic Fetal Osteology*. Budapest: Akadémiai Kiadó

Ferembach D, Schwidetzky I, Stloukal M. 1980. Recommendations for age and sex diagnoses of skeletons. *Journal of Human Evolution* 9: 517-549

Fernández-Jalvo Y, Andrews P. 2016. *Atlas of Taphonomic Identifications: 1001+ Images of Fossil and Recent Mammal Bone Modification*. New York: Springer

Finnegan M. 1978. Non-metric variation of the infracranial skeleton. *Journal of Anatomy* 125: 23-37

France DL. 2009. *Human and Nonhuman Bone Identification: A Color Atlas*. Boca Raton, FL: CRC Press

France CAM, Giaccai JA, Doney CR. 2015. Brief Communication: The effects of Paraloid B-72 and Butvar B-98 treatment and organic solvent removal on d13C, d15N,and d18O values of collagen and hydroxyapatite in a modern bone. *American Journal of Physical Anthropology* 157: 330–338

Fully G. 1956. Une nouvelle méthode de détermination de la taille. *Annales de Médecine Légales* 35: 266–273

Gaudio D, Betto A, Vanin S, De Guio A, Galassi A, Cattaneo C. 2015. Excavation and study of skeletal remains from a World War I mass grave. *International Journal of Osteoarchaeology* 25: 585-592

Gilbert BM. 1973. *Mammalian Osteo-archaeology: North America*. Missouri Archaeological Society

Gilbert BM, McKern TW. 1973. A method of aging the female os pubis. *American Journal of Physical Anthropology* 38: 31–38

Godde K, Jantz RL. 2017. Evaluating Nubian population structure from cranial nonmetric traits: Gene flow, genetic drift, and population history of the Nubian Nile Valley. *Human Biology* 89: 255-280

Grüneberg H. 1952. Genetical studies on the skeleton of the Mouse IV. Quasi-continuous variations. *Journal of Genetics* 51: 95-114

Haglund WD. 2002. Recent mass graves, an introduction. In: Haglund WD, Sorg MH (eds.) *Advances in Forensic Taphonomy: Method, Theory, and Archaeological Perspectives*. Boca Raton, FL: CRC Press; p. 243-261

Haglund WD, Connor M, Scott DD. 2001. The archaeology of contemporary mass graves. *Historical Archaeology* 35: 57-69

Hanihara T. 2008. Morphological variation of major human populations based on nonmetric dental traits. *American Journal of Physical Anthropology* 136: 169-182

Hanson I. 2016. Mass grave investigation and identifying missing persons: Challenges and innovations in archaeology and anthropology in the context of mass death environments. In: Morewitz SJ, Sturdy Colls C (eds.) *Handbook of Missing Persons*. New York: Springer; p. 491-514

Harris E. 1989. *Principles of Archaeological Stratigraphy, 2nd edition*. San Diego: Academic Press

Hartnett KM. 2010. Analysis of age-at-death estimation using data from a new, modern autopsy sample e part II: sternal end of first rib. *Journal of Forensic Sciences* 55: 1152-1156

Hauser G, De Stefano GF. 1989. *Epigenetic Variants of the Human Skull*. Stuttgart: Schweizerbart

Hawkey DE. 1998. Disability, compassion and the skeletal record: using musculoskeletal stress markers (MSM) to construct an osteobiography from early New Mexico. *International Journal of Osteoarchaeology* 8: 326-340

Hawkey DE, Merbs CF. 1995. Activity-induced musculoskeletal stress markers (MSM) and subsistence strategy changes among ancient Hudson Bay Eskimos. *International Journal of Osteoarchaeology* 5: 324-338

Hefner JT. 2009. Cranial nonmetric variation and estimating ancestry. *Journal of Forensic Sciences* 54: 985-995

Henderson CY, Mariotti V, Pany-Kucera D, Villotte S, Wilczak C. 2013. Recording specific entheseal changes of fibrocartilaginous entheses: initial tests using the Coimbra Method. *International Journal of Osteoarchaeology* 23: 152-162

Henderson CY, Mariotti V, Pany-Kucera D, Villotte S, Wilczak C. 2016. The new 'Coimbra Method': a biologically appropriate method for recording specific features of fibrocartilaginous entheseal changes. *International Journal of Osteoarchaeology* 26: 925-932

Herrera B, Hanihara T, Godde K. 2014. Comparability of multiple data types from the Bering strait region: cranial and dental metrics and nonmetrics, mtDNA, and Y-chromosome DNA. *American Journal of Physical Anthropology* 154: 334-348

Hershkovitz I, Latimer B, Dutour O, Jellema LM, Wish-Baratz S, Rothschild C, Rothschild BM. 1997. Why do we fail in ageing the skull from the sagittal suture? *American Journal of Physical Anthropology* 103: 393-399

Hester TR, Shafer HJ, Feder KL. 1997. *Field Methods in Archaeology, 7th edition*. Mayfield: Mountain View

Hillier ML, Bell LS. 2007. Differentiating human bone from animal bone: a review of histological methods. *Journal of Forensic Sciences* 52: 249-263

Hillson S. 1992. *Mammal Bones and Teeth: An Introductory Guide to Methods of Identification*. London: Institute of Archaeology Publications, University College London

Hillson S. 1996. *Dental Anthropology*. Cambridge: Cambridge University Press

Hillson S. 2005. *Teeth, 2nd edition*. Cambridge: Cambridge University Press

Hillson S, FitzGerald C, Flinn H. 2005. Alternative dental measurements: proposals and relationships with other measurements. *American Journal of Physical Anthropology* 126: 413-426

Hochrein MJ. 2002. An autopsy of the grave: Recognizing, collecting, and preserving forensic geotaphonomic evidence. In: Haglund WD, Sorg MH (eds.) *Advances in Forensic Taphonomy: Method, Theory, and Archaeological Perspectives*. Boca Raton, FL: CRC Press; p. 46-66

Hoppa RD, Garlie TN. 1998. Secular changes in the growth of Toronto children during the last century. *Annals of Human Biology* 25: 553–561

Howland MD, Kuester F, Levy TE. 2014. Structure from motion: Twenty-first century field recording with 3D technology. *Near Eastern Archaeology* 77: 187–191

Hubbard AR, Guatelli-Steinberg D, Irish JD. 2015. Do nuclear DNA and dental nonmetric data produce similar reconstructions of regional population history? An example from modern Coastal Kenya. *American Journal of Physical Anthropology* 157: 295-304

Hunter JR. 1996. Recovering Buried Remains. In: Hunter JR, Roberts CA, Martin AL (eds.) *Studies in Crime: An Introduction to Forensic Archaeology*. London: B.Y. Batsford; p. 7-23

Hunter JR, Cox M. 2005. *Forensic Archaeology: Advances in Theory and Practice*. London: Routledge

Igarashi Y, Uesu K, Wakebe T, Kanazawa E. 2005. New method for estimation of adult skeletal age at death from the morphology of the auricular surface of the ilium. *American Journal of Physical Anthropology* 128: 324-339

İşcan MY, Loth SR, Wright RK. 1984. Age estimation from the rib by phase analysis: white males. *Journal of Forensic Sciences* 29: 1094-1104

İşcan MY, Loth SR, Wright RK. 1985. Age estimation from the rib by phase analysis: white females. *Journal of Forensic Sciences* 30: 853-863.

Joukowsky M. 1980. *A complete manual of field archaeology: tools and techniques of field work for archaeologists*. Englewood Cliffs: Prentice-Hall

Jurmain R, Alves Cardoso F, Henderson C, Villotte S. 2011. Bioarchaeology's Holy Grail: the reconstruction of activity. In: Grauer AL (ed.) *A Companion to Paleopathology*. New York: Wiley-Backwell; p. 531-552

Katz D, Suchey JM. 1986. Age determination of the male os pubis. *American Journal of Physical Anthropology* 69: 427–435

Kendell A, Willey P. 2014. Crow Creek bone bed commingling: Relationship between bone mineral density and Minimum Number of Individuals and its effect on paleodemographic analyses. In: Osterholtz AJ, Baustian KM, Martin DL (eds.) *Commingled and Disarticulated Human Remains: Working Toward Improved Theory, Method, and Data*. New York: Springer; p. 85-104

Key CA, Aiello LC, Molleson T. 1994. Cranial suture closure and its implications for age estimation. *International Journal of Osteoarchaeology* 4: 193-207

Klales AR, Ousley SD, Vollner JM. 2012. A revised method of sexing the human innominate using Phenice's nonmetric traits and statistical methods. *American Journal of Physical Anthropology* 149: 104-114

Knüsel CJ, Outram AK. 2004. Fragmentation: The Zonation Method applied to fragmented human remains from archaeological and forensic contexts. *Environmental Archaeology* 9: 85-97

Krogman WM, İşcan MY. 1986. *The Human Skeleton in Forensic Medicine, 2nd edition*. Springfield, IL: Charles C. Thomas

Kunos CA, Simpson SW, Russell KF, Hershkovitz I. 1999. First rib metamorphosis: its possible utility for human age-at-death estimation. *American Journal of Physical Anthropology* 110: 303-323

Lampl M, Veldhuis JD, Johnson ML. 1992. Saltation and stasis: a model of human growth. *Science* 258: 801–803

Levy T, M. Vincent M, Howland et al. 2014. The art of implementing SfM for reconstruction of archaeological sites in Greece: Preliminary applications of cyber-archaeological recording at Corinth. *Mediterranean Archaeology and Archaeometry* 14: 125–133

Liversidge HM, Dean MC, Molleson TI. 1993. Increasing human tooth length between birth and 5.4 years. *American Journal of Physical Anthropology* 90: 307-313

Loth SR. 1995. Age assessment of the Spitalfields cemetery population by rib phase analysis. *American Journal of Human Biology* 7: 465-471

Loth SR, İşcan MY. 1989. Morphological assessment of age in the adult: the thoracic region. In: İşcan MY (ed.) *Age Markers in the Human Skeleton*. Springfield: Charles C. Thomas; p. 105-135

Loth SR, Henneberg M. 1996. Mandibular ramus flexure: a new morphologic indicator of sexual dimorphism in the human skeleton. *American Journal of Physical Anthropology* 99: 473-485

Lovejoy CO, Meindl RS, Pryzbeck TR, Mensforth RP. 1985. Chronological metamorphosis of the auricular surface of the ilium: a new method for the determination of adult skeletal age at death. *American Journal of Physical Anthropology* 68: 15-28

Mack JE, Waterman AJ, Racila A-M, Artz JA, Lillios KT. 2016. Applying zooarchaeological methods to interpret mortuary behaviour and taphonomy in commingled burials: The case study of the Late Neolithic site of Bolores, Portugal. *International Journal of Osteoarchaeology* 26: 524-536

Madden G. 2011a. Age and sex. In: Wilczak CA, Dudar JC (eds). *OsteowareTM Software Manual, Volume I.* Washington, D.C.: Smithsonian Institution; p. 19-44

Madden G. 2011b. Size, shape, and bone-specific abnormality. In: Wilczak CA, Jones EB (eds). *OsteowareTM Software Manual, Volume II.* Washington, D.C.: Smithsonian Institution; p. 10-25

Mann RW, Hunt DR, Scott Lozanoff S. 2016. *Photographic Regional Atlas of Non-Metric Traits and Anatomical Variants in the Human Skeleton*. San Diego: Academic Press

Maresh MM. 1970. Measurements from roentgenograms. In: McCammon RW (ed.) *Human Growth and Development*. Springfield, IL: Charles C. Thomas; p. 157-200

McKinley JI. 2004. Compiling a skeletal inventory: disarticulated and co-mingled remains. In: Brickley M, McKinley JI (eds.) *Guidelines to the Standards for Recording Human Remains*. Institute of Field Archaeologists Paper No 7; p. 14-17.

McLaughlin G, Lednev IK. 2012. Spectroscopic discrimination of bone samples from various species. *American Journal of Analytical Chemistry* 3: 161–167.

Meindl RS, Lovejoy CO. 1985. Ectocranial suture closure: a revised method for the determination of skeletal age at death based on the lateral anterior sutures. *American Journal of Physical Anthropology* 68: 57-66

Meizel-Lambert CJ, Schultz JJ, Sigman ME. 2015. Chemical differentiation of osseous and nonosseous materials using scanning electron microscopy-energy-dispersive X-ray spectrometry and multi-step statistical analysis. *Journal of Forensic Sciences* 60: 1534-1541

Michopoulou E, Nikita E, Valakos ED. 2015. Evaluating the efficiency of different recording protocols for entheseal changes in regards to expressing activity patterns using archival data and cross-sectional geometric properties. *American Journal of Physical Anthropology* 158: 557-568

Milella M, Belcastro MG, Zollikofer CPE, Mariotti V. 2012. The effect of age, sex and physical activity on entheseal morphology in a contemporary Italian skeletal collection. *American Journal of Physical Anthropology* 148: 379-388

Moore MK. 2012. Functional morphology and medical imaging. In: DiGangi EA, Moore MK (eds.) *Research Methods in Human Skeletal Biology*. San Diego: Academic Press; p. 397-424

Moore-Jansen PH, Jantz RL. 1989. *Data Collection Procedures for Forensic Skeletal Material.* Knoxville: Report of Investigations 48

Moorrees CF, Fanning EA, Hunt Jr EE. 1963a. Formation and resorption of three deciduous teeth in children. *American Journal of Physical Anthropology* 21: 205-213

Moorrees CFA, Fanning EA, Hunt EE Jr. 1963b. Age variation of formation stages for ten permanent teeth. *Journal of Dental Research* 42: 1490–1502

Mulhern DM, Ubelaker DH. 2001. Differences in osteon banding between human and nonhuman bone. *Journal of Forensic Sciences* 46: 220–222

Mulhern DM. 2011. Abnormal bone loss. In: Wilczak CA, Jones EB (eds). *OsteowareTM Software Manual, Volume II.* Washington, D.C.: Smithsonian Institution; p. 26-31

Mulhern DM, Jones EB. 2011. Pathological condition of the vertebrae. In: Wilczak CA, Jones EB (eds). *OsteowareTM Software Manual, Volume II*. Washington, D.C.: Smithsonian Institution; p. 61-68

Musgrave JH, Harneja NK. 1978. The estimation of adult stature from metacarpal bone length. *American Journal of Physical Anthropology* 48: 113-119

Nawrocki SP. 1996. *An Outline of Forensic Archaeology*. University of Indianapolis Archeology & Forensics Laboratory

Nemeskéri J, Harsányi L, Acsádi G. 1960. Methoden zur diagnose des lebensalters von skelettfunden. *Anthropologischer Anzeiger* 24: 70-95

Niinimäki S. 2011. What do muscle marker ruggedness scores actually tell us? *International Journal of Osteoarchaeology* 21: 292-299

Nikita E. 2017. *Osteoarchaeology: A Guide to the Macroscopic Study of Human Skeletal Remains*. San Diego: Academic Press

Nikita E, Mattingly D, Lahr MM. 2012. Sahara: barrier or corridor? Nonmetric cranial traits and biological affinities of North African Late Holocene populations. *American Journal of Physical Anthropology* 147: 280-292

Oakley K. 2005. Forensic archaeology and anthropology. *Forensic Science, Medicine, and Pathology* 1: 169-172

O'Brien C, Dudar JC. 2011. Trauma. In: Wilczak CA, Jones EB (eds.) *OsteowareTM Software Manual: Volume II*. Washington, D.C.: Smithsonian Institution; p. 44-54

Oettlé AC, Steyn M. 2000. Age estimation from sternal ends of ribs by phase analysis in South African blacks. *Journal of Forensic Sciences* 45: 1071-1079

Oikonomopoulou EK, Valakos E, Nikita E. 2017. Population-specificity of sexual dimorphism in cranial and pelvic traits: evaluation of existing and proposal of new functions for sex assessment in a Greek assemblage. *International Journal of Legal Medicine* 131: 1731-1738

Ortner DJ. 2003. *Identification of Pathological Conditions in Human Skeletal Remains*. San Diego: Academic Press

Ortner DJ. 2011. Human skeletal paleopathology. *International Journal of Paleopathology* 1: 4-11

Osborne D, Simmons T, Nawrocki S. 2004. Reconsidering the auricular surface as an indicator of age at death. *Journal of Forensic Sciences* 49: 905-911

Osterholtz AJ. 2018. *A FileMaker Pro database for use in the recording of Commingled and/or Fragmentary Human Remains*. Mississippi State University: Department of Anthropology and Middle Eastern Cultures. *http://hdl.handle.net/11668/14276*

Osterholtz AJ. 2019. Advances in documentation of commingled and fragmentary remains. *Advances in Archaeological Practice* 7: 77–86

Osterholtz AJ, Baustian KM, Martin DL (eds.) 2014. *Commingled and Disarticulated Human Remains: Working Toward Improved Theory, Method, and Data*. New York: Springer

Outram AK. 2001. A new approach to identifying bone marrow and grease exploitation: why the "indeterminate" fragments should not be ignored. *Journal of Archaeological Science* 28: 401-410

Pales L, Garcia MA. 1981. *Atlas ostéologique pour servir à l' identification des mammifères du quaternaire: II. Tête-rachis, ceintures scapulaire et pelvienne: membres*. Paris: Éditions du Centre National de la Recherche Scientifique

Phenice TW. 1969. A newly developed visual method of sexing the os pubis. *American Journal of Physical Anthropology* 30: 297-301

Rathmann H, Saltini Semerari G, Harvati K. 2017. Evidence for migration influx into the ancient Greek colony of Metaponto: A population genetics approach using dental nonmetric traits. *International Journal of Osteoarchaeology* 27: 453-464

Rautray TR, Mishra S, Patnaik SK, Vijayan V, Panigrahi S. 2007. Analysis of human bone and teeth. *Indian Journal of Physics* 81: 99–102

Raxter MH, Auerbach BM, Ruff CB. 2006. Revision of the Fully technique for estimating statures. *American Journal of Physical Anthropology* 130: 374-384

Reinhard K, Confalonieri U, Ferreira LF, Herrmann B, Araújo A. 1986. Recovery of parasite remains from coprolites and latrines: aspects of palaeoparasitological technique. *Homo* 37: 217-239

Ricaut F, Auriol V, von Cramon-Taubadel N, Keyser C, Murail P, Ludes B, Crubézy E. 2010. Comparison between morphological and genetic data to estimate biological relationship: the case of the Egyin Gol necropolis (Mongolia). *American Journal of Physical Anthropology* 143: 355-364

Roskams S. 2001. ***Excavation***. Cambridge: Cambridge University Press

Rougé-Maillart C, Vielle B, Jousset N, Chappard D, Telmon N, Cunha E. 2009. Development of a method to estimate skeletal age at death in adults using the acetabulum and the auricular surface on a Portuguese population. ***Forensic Science International*** 188: 91-95

Ruff CB. 2008. Biomechanical analyses of archaeological human skeletons. In: Katzenberg MA, Saunders SR (eds.) ***Biological Anthropology of the Human Skeleton***. New York: Wiley Liss; p. 183-206

Ruff CB, Trinkaus E, Walker A, Larsen CS. 1993. Postcranial robusticity in Homo. I. Temporal trends and mechanical interpretation. ***American Journal of Physical Anthropology*** 91: 21-53

Ruff C, Holt B, Trinkaus E. 2006. Who's afraid of the big bad Wolff?: "Wolff's Law" and bone functional adaptation. ***American Journal of Physical Anthropology*** 129: 484-498

Ruff CB, Holt BM, Niskanen M, Sladék V, Berner M, Garofalo E, Garvin HM, Hora M, Maijanen H, Niinimäki S, Salo K, Schuplerová E, Tompkins D. 2012. Stature and body mass estimation from skeletal remains in the European Holocene. ***American Journal of Physical Anthropology*** 148: 601-617

Saunders SR, Fitzgerald C, Rogers T, Dudar C, McKillop H. 1992. A test of several methods of skeletal age estimation using a documented archaeological sample. ***Canadian Society of Forensic Science Journal*** 25: 97-118

Scheuer JL, Musgrave JH, Evans SR. 1980. The estimation of late fetal and perinatal age from limb bone length by linear and logarithmic regression. ***Annals of Human Biology*** 7: 257–265

Schmid E. 1972. ***Atlas of Animal Bones***. Amsterdam: Elsevier

Schwartz JH. 1995. ***Skeleton Keys***. New York: Oxford University Press

Scott GR, Turner CG. 1997. ***The Anthropology of Modern Teeth: Dental Morphology and its Variation in Recent Human Populations***. Cambridge: Cambridge University Press

Scott GR, Maier C, Heim K. 2016. Identifying and recording key morphological (nonmetric) crown and root traits. In: Irish JD, Scott GR (eds.) ***A Companion to Dental Anthropology***. Chichester: Wiley Blackwell; p. 247-264

Shackelford LL, Harris AES, Konigsberg LW. 2012. Estimating the distribution of probable age-at-death from dental remains of immature human fossils. ***American Journal of Physical Anthropology*** 147: 227-253

Shimoyama M, Maeda H, Sato H, Ninomiya Y, Ozaki Y. 1997. Nondestructive discrimination of biological materials by near-infrared Fourier transform Raman spectroscopy and chemometrics: discrimination among hard and soft ivories of African elephants and mammoth tusks and prediction of specific gravity of the ivories. ***Applied Spectroscopy*** 51: 1154–1158

Sideris A, Liritzis I, Liss B, Howland MD, Levy TE. 2017. At-risk cultural heritage: New excavations and finds from the Mycenaean site of Kastrouli, Phokis, Greece. ***Mediterranean Archaeology and Archaeometry*** 17: 271-285

Siebke I, Campana L, Ramstein M, Furtwängler A, Hafner A, Lösch S. 2018. The application of different 3D-scan-systems and photogrammetry at an excavation - A Neolithic dolmen from Switzerland. ***Digital Applications in Archaeology and Cultural Heritage*** 10: e00078

Smith BH. 1984. Patterns of molar wear in hunter-gatherers and agriculturalists. ***American Journal of Physical Anthropology*** 63: 39-56

Spradley MK, Jantz RL. 2011. Sex estimation in forensic anthropology: skull versus postcranial elements. ***Journal of Forensic Sciences*** 56: 289-296

Stock JT, Shaw CN. 2007. Which measures of diaphyseal robusticity are robust? A comparison of external methods of quantifying the strength of long bone diaphyses to cross-sectional geometric properties. ***American Journal of Physical Anthropology*** 134: 412-423

Stover E, Ryan M. 2001. Breaking bread with the dead. ***Historical Archaeology*** 35: 7–25

Stull KE, Godde K. 2013. Sex estimation of infants between birth and one year through discriminant analysis of the humerus and femur. ***Journal of Forensic Sciences*** 58: 13-20

SWGANTH (Scientific Working Group for Forensic Anthropology). ***Resolving Commingled Human Remains***. Issue date: 01/22/2013 Revision: 2

Thenius E. 1989. ***Zähne und Gebiß der Säugetiere***. Berlin: W. de Gruyter

Todd TW. 1920. Age changes in the pubic bone. I: The male White pubis. ***American Journal of Physical Anthropology*** 3: 285–334

Todd TW. 1921. Age changes in the pubic bone. II: The Pubis of the male Negro-White hybrid, III: The Pubis of the White female. IV: The Pubis of the female Negro-White hybrid. *American Journal of Physical Anthropology* 4: 1–70

Todd TW, Lyon DW. 1924. Endocranial suture closure, its progress and age relationship: part I.-Adult males of the white stock. *American Journal of Physical Anthropology* 7: 325-384

Todd TW, Lyon DW. 1925. Cranial suture closure, its progress and age relationship: part II.-Ectocranial suture closure in adult males of the white stock. *American Journal of Physical Anthropology* 8: 23-45

Tuller HH. 2012. Mass graves and human rights: Latest developments, methods, and lessons learned. In: Dirkmaat DC (ed.) *A Companion to Forensic Anthropology*. New York: Blackwell Publishing; p. 157-174

Tuller H, Đuric M. 2006. Keeping the pieces together: Comparison of mass grave excavation methodology. *Forensic Science International* 156: 192–200

Tuller H, Hofmeister U. 2014. Spatial analysis of mass grave mapping data to assist in the reassociation of disarticulated and commingled human remains. In: Adams BJ, Byrd JE (eds.) *Commingled Human Remains: Methods in Recovery, Analysis, and Identification*. San Diego: Academic Press; p. 7-32

Turner II CG. 1987. Late Pleistocene and Holocene population history of East Asia based on dental variation. *American Journal of Physical Anthropology* 73: 305-321

Turner II CG, Nichol CR, Scott GR. 1991. Scoring procedures for key morphological traits of the permanent dentition: The Arizona State University Dental Anthropology System. In: Kelley MA, Larsen CS (eds.) *Advances in Dental Anthropology*. New York: Wiley-Liss; p. 13–31

Tyrrell A. 2000. Skeletal non-metric traits and the assessment of inter- and intra-population diversity: past problems and future potential. In: Cox M, Mays S (eds.) *Human Osteology in Archaeology and Forensic Science*. London: Greenwich Medical Media, Ltd; p. 289-306

Ubelaker DH. 1989. *Human Skeletal Remains. Excavation, Analysis, Interpretation*. Washington, DC: Taraxacum.

Ubelaker DH, Ward DC, Braz VS, Stewart J. 2002. The use of SEM/EDS analysis to distinguish dental and osseus tissue from other materials. *Journal of Forensic Sciences* 47: 1-4

Vass AA, Madhavi M, Synstelien J, Collins K. 2005. Elemental characterization of skeletal remains using laser-induced breakdown spectroscopy (LIBS). *Proceedings of the American Academy of Forensic Sciences Annual Meeting, New Orleans*, February 21-26, 2005, p. 307–308

Velemínský P, Dobisíková M. 2005. Morphological likeness of the skeletal remains in a Central European family from 17th to 19th century. *HOMO-Journal of Comparative Human Biology* 56: 173-196

Viciano J, López-Lázaro S, Alemán I. 2013. Sex estimation based on deciduous and permanent dentition in a contemporary Spanish population. *American Journal of Physical Anthropology* 152: 31-43

Villotte S, Castex D, Couallier V, Dutour O, Knüsel CJ, Henry-Gambier D. 2010. Enthesopathies as occupational stress markers: evidence from the upper limb. *American Journal of Physical Anthropology* 142: 224-234

Vosselman G, Maas H. 2010. *Airborne and Terrestrial Laser Scanning*. Dunbeath: Whittles Publishing

Waldron T. 2008. *Palaeopathology*. Cambridge: Cambridge University Press

Walker R. 1985. *A Guide to Post-cranial Bones of East African Animals: Mrs. Walker's Bone Book*. Norwich: Hylochoerus Press

Watson J, McClelland J. 2018. *Distinguishing Human from Non-Human Animal Bone*. The University of Arizona: Arizona State Museum

Weiss E. 2004. Understanding muscle markers: lower limbs. *American Journal of Physical Anthropology* 125: 232-238

Weiss E, Corona L, Schultz B. 2012. Sex differences in musculoskeletal stress markers: problems with activity pattern reconstructions. *International Journal of Osteoarchaeology* 22: 70-80

White TD, Black MT, Folkens PA. 2011. *Human Osteology, 3rd edition*. New York: Elsevier

Whitman EJ. 2004. *Differentiating Between Human and Non-human Secondary Osteons in Human, Canine and Bovine Rib Tissue*. Doctoral Dissertation, Michigan State University

Wilczak CA, Jones EB (eds.) 2011a. *OsteowareTM Software Manual: Volume II*. Washington, D.C.: Smithsonian Institution

Wilczak CA, Jones EB (eds.) 2011b. Abnormal bone formation. In: Wilczak CA, Jones EB (eds.) *OsteowareTM Software Manual: Volume II*. Washington, D.C.: Smithsonian Institution; p. 32-43

Wilczak CA. 2011. Porosity and channel formation. In: Wilczak CA, Jones EB (eds.) *OsteowareTM Software Manual: Volume II*. Washington, D.C.: Smithsonian Institution; p. 55-60

Wilson RJ, Herrmann NP, Jantz LM. 2010. Evaluation of stature estimation from the database for forensic anthropology. *Journal of Forensic Sciences* 55: 684-689

Yoder C, Ubelaker DH, Powell JF. 2001. Examination of variation in sternal rib end morphology relevant to age assessment. *Journal of Forensic Sciences* 46: 223-227

Zimmerman HA, Meizel-Lambert CJ, Schultz JJ, Sigman ME. 2015a. Chemical differentiation of osseous, dental, and non-skeletal materials in forensic anthropology using elemental analysis. *Science and Justice* 55: 131-138.

Zimmerman HA, Schultz JJ, Sigman ME. 2015b. Preliminary validation of handheld X-ray fluorescence (HHXRF) spectrometry: distinguishing osseous and dental tissue from non-bone material of similar chemical composition. *Journal of Forensic Sciences* 60: 382-390

RECORDING SHEETS

BURIAL RECORDING SHEET

GENERAL INFORMATION	
Archaeological site (site code):	
Trench:	
Context:	
Recorder:	
Date:	
Burial No:	
Field methods for site excavation:	
Primary or secondary burial:	
Cremation or inhumation:	
Grave type:	
Grave size:	

SKETCH OF BODY POSITION & ORIENTATION

DESCRIPTION & NOTES

SKELETAL ELEMENTS PRESENT [1] | Key: Shade the elements present

[1] All three sketches are from Roksandic M. 2003. New Standardised Visual Forms for Recording the Presence of Human Skeletal Elements in Archaeological and Forensic Contexts. *Internet Archaeology 13*. https://doi.org/10.11141/ia.13.3

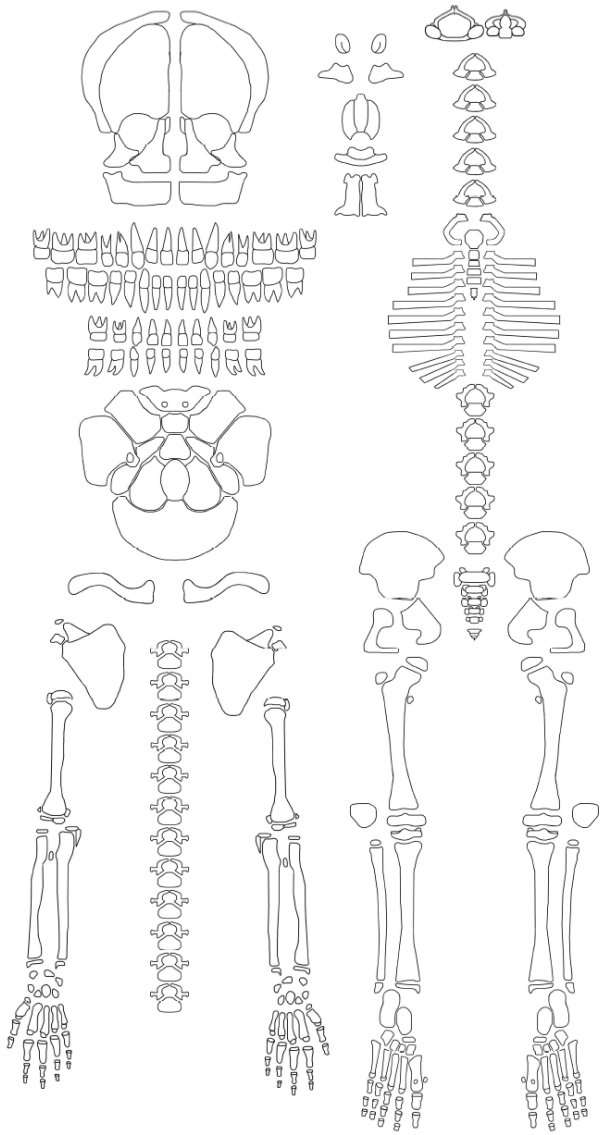

Newborn

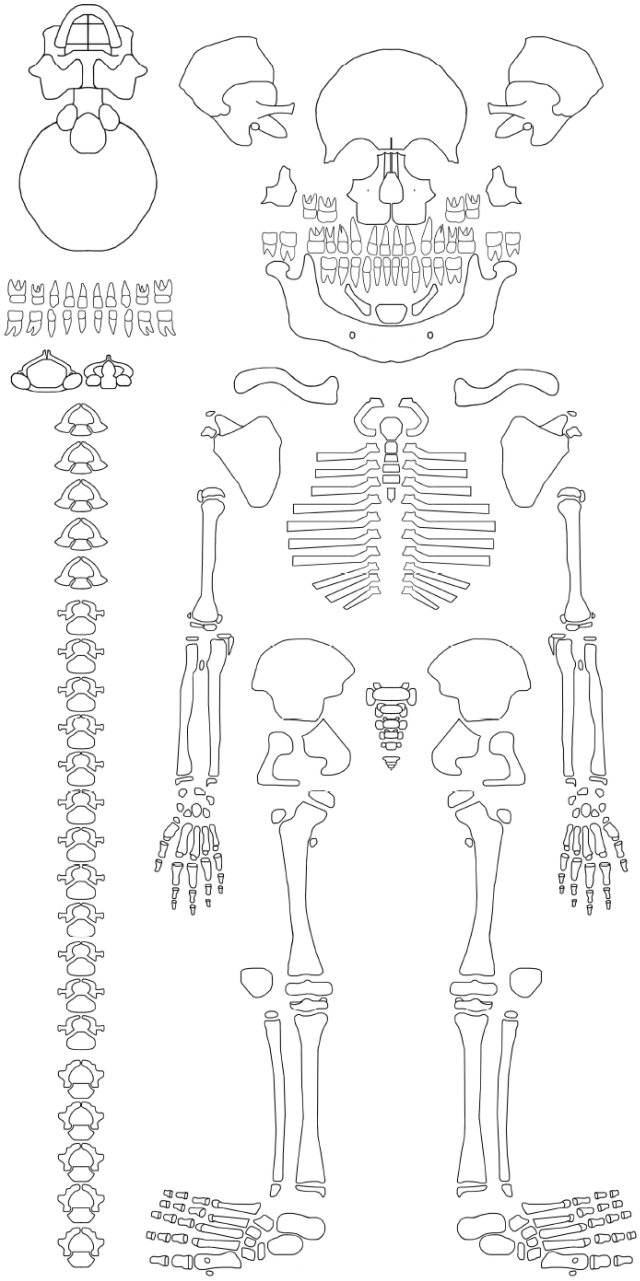

Child

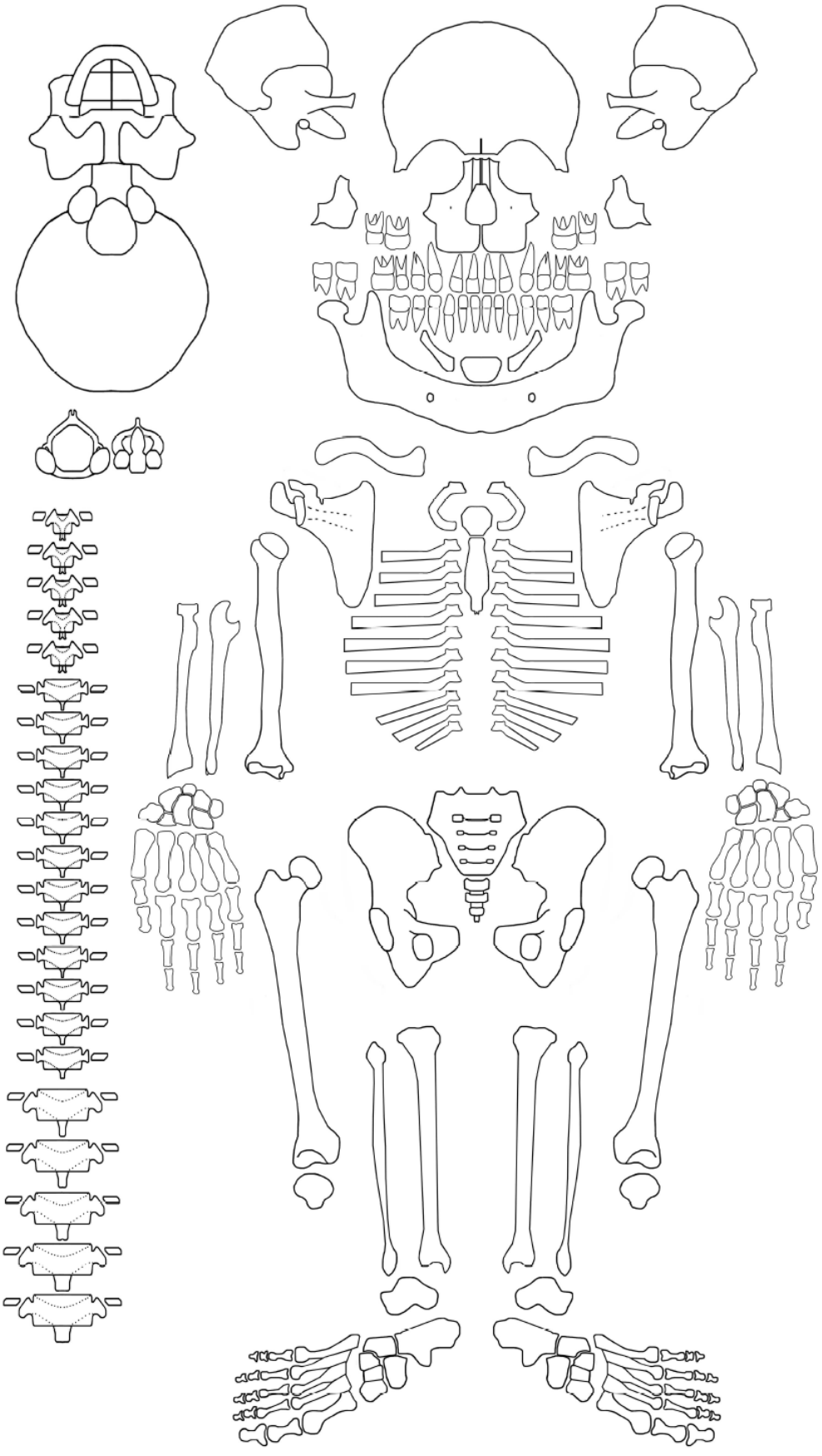

Adult

LEVELS		
Cranium	Sacrum	Feet

CONTEXT				
Above				
			Skeleton	
Below				

SMALL FINDS					

ASSOCIATED FINDS					
Artifacts					
Pottery	Lithics	Wood	Metal	Glass	Other
Organic material					
Animal bone	Shell	Charcoal	Plant remains	Other	

BONE MEASUREMENTS [2]		
Element	Measurement	Value

SAMPLES					
Type					
No					

DOCUMENTATION	
Type	Numbers
Plans	
Photos	
Other	
Other	

[2] Measurements obtained from fragile skeletal elements which will likely fragment upon lifting

RECORDING SHEET FOR ARTICULATED HUMAN SKELETAL REMAINS

GENERAL INFORMATION	
Archaeological site:	
Curation site:	
Recorder:	
Date:	
Skeleton No:	
Burial No:	
Cleaning methods:	
Restoration methods:	

SKELETAL INVENTORY

Key: 0 = absent, 1 = present <25%, 2 = present 26-50%, 3 = present 51-75%,
4 = present >76% (alternatively or additionally, record which zones are present per element)

CRANIUM AND MANDIBLE			
Element	**Part**	**Left**	**Right**
Frontal	-		
Parietal	-		
Occipital	-		
Nasal	-		
Inf. nasal concha	-		
Vomer	-		
Lacrimal	-		
Maxilla	-		
Palatine	-		
Zygomatic	-		
Temporal	Squam. part Petrous part		
Ear ossicles	Malleus Incus Stapes		
Sphenoid	Body Wing		
Ethmoid	-		
Mandible	Corpus Ascend. ramus		

THORACIC CAGE			
Element	**Part**	**Left**	**Right**
Sternum	Manubrium Corpus Xiphoid process		
Rib 1	-		
Rib 2	-		
Rib 3	-		
Rib 4	-		
Rib 5	-		
Rib 6	-		
Rib 7	-		
Rib 8	-		
Rib 9	-		
Rib 10	-		
Rib 11	-		
Rib 12	-		
Extra rib	-		

MISCELLANEA	
Element	
Hyoid	
Ossified cartilage	

SHOULDER GIRDLE			
Element	**Part**	**Left**	**Right**
Clavicle	Med. epiphysis		
	Diaphysis		
	Lat. epiphysis		
Scapula	Body		
	Acromion process		
	Coracoid process		
	Glenoid fossa		

UPPER LIMB LONG BONES			
Element	**Part**	**Left**	**Right**
Humerus	Prox. epiphysis		
	Diaphysis		
	Dist. epiphysis		
Radius	Prox. epiphysis		
	Diaphysis		
	Dist. epiphysis		
Ulna	Prox. epiphysis		
	Diaphysis		
	Dist. epiphysis		

HAND BONES		
Element	**Left**	**Right**
Scaphoid		
Lunate		
Triquetral		
Pisiform		
Trapezium		
Trapezoid		
Capitate		
Hamate		
Sesamoids		
MC 1		
MC 2		
MC 3		
MC 4		
MC 5		
Prox. phalanges		
Middle phalanges		
Dist. phalanges		

VERTEBRAE		
Element	**Body**	**Neural arch**
C1		
C2		
C3		
C4		
C5		
C6		
C7		
T1		
T2		
T3		
T4		
T5		
T6		
T7		
T8		
T9		
T10		
T11		
T12		
L1		
L2		
L3		
L4		
L5		
Extra vertebra		

PELVIC GIRDLE			
Element	**Part**	**Left**	**Right**
Os coxa	Ilium		
	Ischium		
	Pubis		
Sacrum	S1		
	S2		
	S3		
	S4		
	S5		
Coccyx	-		

LOWER LIMB LONG BONES & PATELLA			
Element	**Part**	**Left**	**Right**
Femur	Prox. epiphysis		
	Diaphysis		
	Dist. epiphysis		
Patella	-		
Tibia	Prox. epiphysis		
	Diaphysis		
	Dist. epiphysis		
Fibula	Prox. epiphysis		
	Diaphysis		
	Dist. epiphysis		

UNIDENTIFIED BONE			
Type	**Size class**	**No of fragments**	**Weight**
Cortical	<1 cm		
	1-3 cm		
	3-5 cm		
	>5cm		
Trabecular	<1 cm		
	1-3 cm		
	3-5 cm		
	>5cm		
Cranial	<1 cm		
	1-3 cm		
	3-5 cm		
	>5cm		
Post-cranial	<1 cm		
	1-3 cm		
	3-5 cm		
	>5cm		

FOOT BONES		
Element	**Left**	**Right**
Calcaneus		
Talus		
Navicular		
Cuboid		
First Cuneiform		
Second Cuneiform		
Third Cuneiform		
Sesamoids		
MT 1		
MT 2		
MT 3		
MT 4		
MT 5		
Prox. phalanges		
Middle phalanges		
Dist. phalanges		

DENTAL INVENTORY

Key: 1 = Present, non-erupted, 2 = Present, development completed, in occlusion, 3 = Missing, no associated alveolar bone, 4 = Missing, antemortem loss, 5 = Missing, postmortem loss, 6 = Missing, congenital absence, 7 = Present, damage renders measurement impossible, 8 = Present, unobservable

DECIDUOUS TEETH						
		I1	I2	C	M1	M2
Maxilla	Left					
Maxilla	Right					
Mandible	Left					
Mandible	Right					

PERMANENT TEETH									
		I1	I2	C	P3	P4	M1	M2	M3
Maxilla	Left								
Maxilla	Right								
Mandible	Left								
Mandible	Right								

SEX ASSESSMENT (ONLY FOR ADULT REMAINS)

Key: Record as 1 = Female, 2 = Probable Female, 3 = Ambiguous, 4 = Probable Male, 5 = Male, 0 = Indeterminate

Element		Score/Sex
Pelvis	Subpubic concavity	
	Ventral arc	
	Medial ischiopubic ramus	
	Greater sciatic notch	
	Preauricular sulcus	
	Auricular surface elevation	
	Iliac crest	
	Subpubic arch	
	Pubic ramus	
	Ischial tuberosity	
	Obturator foramen	
	Acetabulum	
	Sacrum	
Cranium	Glabella/supraorbital ridges	
	External occipital protuberance	
	Mastoid process	
	Supraorbital margin	
	Mental eminence	
	Frontal/parietal bossing	
	Suprameatal crest	
	Zygomatic bone	
	Zygomatic process of frontal bone	
	Orbital outline	
	Temporal lines	
	Occipital condyles	
	Palate	
	Canine eminence	
	Chin shape	
	Mandibular ramus flexure	
	Gonial eversion	
	Lower mandibular margin	
	Mandibular angle	
	Mandibular condyles	

METRIC METHODS			
Element	**Method**	**Reference**	**Sex**

FINAL SEX ASSESSMENT	

AGE-AT-DEATH ESTIMATION (FOR NONADULTS)

> Classify individuals in one of the following categories: fetus = before birth, infant = 0-3 yrs, child = 3-12 yrs, adolescent = 12-18 yrs, nonadult = <18 yrs, indeterminate = unable to estimate age-at-death

DENTAL DEVELOPMENT

Key: Record the stage of dental development per tooth using Cunningham et al. (2016) (data drawn from Shackelford et al. 2012) and/or Moorrees et al. (1963a, 1963b)

DECIDUOUS						
		I1	I2	C	M1	M2
Maxilla	Stage					
	Age					
Mandible	Stage					
	Age					

PERMANENT									
		I1	I2	C	P3	P4	M1	M2	M3
Maxilla	Stage								
	Age								
Mandible	Stage								
	Age								

Key: Record the age of the individual based on the overall development of the dentition (tooth formation and eruption) as documented by the London Atlas (AlQahtani et al. 2010)

London Atlas	

Key: Use the equations by Liversidge et al. (1993)

Tooth	**Length**	**Age**

UNION OF OSSIFICATION CENTRES

Key: Record epiphyseal union as 1 = unfused, 2 = fusing, 3 = fused

	Stage	Age
Metopic suture		
Mental symphysis		
Occipital: lateral to basilar		
Occipital: lateral to squamous		
Sphenoid: greater wing to body		
Spheno-occipital synchondrosis		
Temporal: petrous to squamous		
Cervical vert: halves to arch		
Cervical vert: arch to centrum		
Cervical vert: sup. rim		
Cervical vert: inf. rim		
Thoracic vert: halves to arch		
Thoracic vert: arch to centrum		
Thoracic vert: sup. rim		
Thoracic vert: inf. rim		
Lumbar vert: halves to arch		
Lumbar vert: arch to centrum		
Lumbar vert: sup. rim		
Lumbar vert: inf. rim		
Sternum: sternebrae 1-2		
Sternum: sternebrae 2-3		
Sternum: sternebrae 3-4		
Sternum: sternebra 4-xiphoid		
Ribs: head		
Ribs: tubercle		
Scapula: glenoid fossa		
Scapula: acromion		
Scapula: coracoid		
Scapula: inf. angle		
Scapula: medial border		
Clavicle: sternal end		
Clavicle: acromial end		

	Stage	Age
Humerus: proximal epiphysis		
Humerus: distal epiphysis		
Humerus: epicondyle		
Radius: proximal epiphysis		
Radius: distal epiphysis		
Ulna: proximal epiphysis		
Ulna: distal epiphysis		
Hand phalanges		
Metacarpals		
Os coxa: ilium to pubis		
Os coxa: ischium to pubis		
Os coxa: ischium to ilium		
Os coxa: ischial tuberosity		
Os coxa: iliac crest		
Os coxa: pubic symphysis		
Sacrum: S1-S2		
Sacrum: S2-S3		
Sacrum: S3-S4		
Sacrum: S4-S5		
Sacrum: other centres		
Femur: proximal epiphysis		
Femur: distal epiphysis		
Femur: greater troch.		
Femur: lesser troch.		
Tibia: proximal epiphysis		
Tibia: distal epiphysis		
Fibula: proximal epiphysis		
Fibula: distal epiphysis		
Foot phalanges		
Metatarsals		

BONE LENGTH

Key: Use the equations by Scheuer et al. (1980) or Maresh (1970) or other population-specific equations

Element	Length	Age

FINAL AGE ESTIMATION	

AGE-AT-DEATH ESTIMATION (FOR ADULTS)

> Classify individuals in one of the following categories: young adult = 18-35 yrs, middle adult = 35-50 yrs, old adult = 50+ yrs, adult = 18+ yrs, indeterminate = unable to estimate age-at-death

Key: Record epiphyseal union as unfused, fusing, fused

Method		Stage/score	Age
Union of ossification centres	Medial clavicle		
	Iliac crest		
	Vertebral annular rings		
Pubic symphysis	Brooks and Suchey (1990)		
Auricular surface	Lovejoy et al. (1985)		
	Buckberry and Chamberlain (2002)		
Sternal rib end	İşcan et al. (1984, 1985)		
Cranial suture closure – vault system	Meindl and Lovejoy (1985)		
Cranial suture closure – lateral-anterior system	Meindl and Lovejoy (1985)		

FINAL AGE ESTIMATION	

PATHOLOGICAL LESIONS

Key: Record pathological conditions/lesions as 0 = absent or 1 = present (see Madden 2011b)

Type	Pathology/lesion	Element(s) affected	Expression
Bone size abnormalities	Hydrocephaly	-	
	Achondroplastic Dwarfism	-	
	Microcephaly	-	
	Gigantism	-	
	Acromegaly	-	
Bone shape abnormalities	Premature Suture Closure		
	Bowing		
	Angulation		
	Flaring Metaphyses		
	Uniform Widening		
	Fusiform (Spindle-Shaped)		

Key: Follow Osteoware standards (see Mulhern 2011 for abnormal bone loss, Wilczak and Jones 2011b for abnormal bone formation, O'Brien and Dudar 2011 for trauma, Wilczak 2011 for porosity and channel formation, Mulhern and Jones 2011 for vertebral pathology, Dudar 2011 for arthritis)

Type	Variables	Expression
Abnormal bone loss	Element(s) affected	
	Location	
	Extent of Involvement	
	Number of Foci	
	Size of Focal Bone Loss	
	Bony Response to Local Bone Loss	
Abnormal bone formation	Element(s) affected	
	General category	
	Extent of Involvement	
	Periosteal Surface	
	Productive Reaction Type	
	Surface Appearance	
	Endosteal Surface	
	Abnormal Matrix	
	Ossified Tissue	
	Specific structures	

Type	Variables	Expression
Trauma	Element(s) affected	
	Fracture Type	
	Characteristics	
	Timing of Perimortem Fractures	
	Dislocations	
	Trauma Complications	
	Healing stage of Antemortem Fractures	
Porosity and Channel Formation	Element(s) affected	
	Degree	
	Location of Ectocranial Porosity	
	Other Features	
	Diploic Hyperostosis	
	Activity	
	Vascular Channel Locations	
	Vascular Channel Appearance	
	Vascular Channel Density	
Vertebral Pathology	Element(s) affected	
	Type of pathology	
	Vertebral Osteophytes	
	Syndesmophytes	
	Porosities around Margins of Vertebral Osteophytes	
	Cleft Sacra and Spina Bifida	
	Spondylolysis	
	Vertebral Body Fractures	
	Abnormal Shape of Spinal Column	
Arthritis	Surface Porosity	
	Marginal Lipping	
	Surface Osteophytes	
	Erosion	
	Eburnation	
	Extent of Surface or Margin Affected	

Key: See Nikita (2017) and references therein

Type	Variables	Expression
Periodontal Disease	Location	
	Cementoenamel junction - alveolar crest distance	
	Extent of alveolar bone resorption	
Periapical Cavities	Tooth affected	
	Location	
	Size	
	Cavity wall	
Dental Caries	Tooth affected	
	Location	
	Degree of expression	
Enamel Hypoplasia	Tooth affected	
	Type of defect	
	Location	
Dental Calculus	Tooth affected	
	Location	
	Size	
Antemortem Tooth Loss	Tooth affected	
	Degree of expression	

CRANIOMETRICS

Key: All measurements in mm (as defined in Moore-Jansen and Jantz 1989)

Measurement	Value
Maximum cranial breadth	
Minimum frontal breadth	
Upper facial breadth	
Interorbital breadth	
Biorbital breadth	
Bizygomatic diameter	
Nasal breadth	
Nasal height	
Upper facial height	
Orbital height	
Orbital breadth	
Frontal chord	
Basion-bregma height	
Parietal chord	
Maximum cranial length	
Cranial base length	
Basion-prosthion length	
Mastoid length	
Occipital chord	
Maxillo-alveolar length	
Maxillo-alveolar breadth	
Biauricular breadth	
Foramen magnum breadth	
Foramen magnum length	
Chin height	
Bigonial width	
Bicondylar breadth	
Height of mandibular body	
Breadth of mandibular body	
Mandibular length	
Maximum ramus height	
Maximum ramus breadth	
Minimum ramus breadth	

POSTCRANIAL MEASUREMENTS

Key: All measurements in mm (as defined in Moore-Jansen and Jantz 1989)

Element	Measurement	Left	Right
Clavicle	Maximum length		
	Superior-inferior (vertical) diameter at midshaft		
	Anterior-posterior (sagittal) diameter at midshaft		
Scapula	Height		
	Breadth		
Humerus	Maximum length		
	Maximum midshaft diameter		
	Minimum midshaft diameter		
	Vertical head diameter		
	Epicondylar breadth		
Ulna	Maximum length		
	Physiological length		
	Minimum circumference		
	Anteroposterior (dorsovolar) diameter		
	Mediolateral (transverse) diameter		
Radius	Maximum length		
	Mediolateral (transverse) midshaft diameter		
	Anteroposterior (sagittal) midshaft diameter		
Os coxa	Height		
	Iliac breadth		
	Ischium length		
	Pubis length		
Sacrum	Anterior length		
	Anterosuperior breadth		
	Maximum transverse base diameter		
Femur	Maximum length		
	Subtrochanteric mediolateral (transverse) diameter		
	Subtrochanteric anteroposterior (sagittal) diameter		
	Midshaft circumference		
	Mediolateral (transverse) midshaft diameter		
	Anteroposterior (sagittal) midshaft diameter		
	Bicondylar length		
	Epicondylar breadth		
	Maximum head diameter		

Element	Measurement	Left	Right
Tibia	Maximum length		
	Circumference at nutrient foramen		
	Mediolateral (transverse) diameter at nutrient foramen		
	Maximum diameter at nutrient foramen		
	Maximum distal epiphyseal breadth		
	Maximum proximal epiphyseal breadth		
Fibula	Maximum length		
	Maximum midshaft diameter		

CRANIAL NONMETRIC TRAITS

Key: Record as present/absent

Trait	Expression
metopic suture	
supranasal suture	
supraorbital foramina	
supraorbital notches	
ethmoidal foramina	
infraorbital foramina	
zygomatico-facial foramina	
zygomaxillary tubercle	
maxillary torus	
transverse palatine suture	
palatine torus	
lesser palatine foramina	
foramen of Vesalius	
oval foramen	
spinous foramen	
divided occipital condyles	
occipitomastoid ossicle	
divided parietal bone	
parietal notch bone	
squamous ossicle	
frontotemporal articulation	

Trait	Expression
marginal tubercle	
zygomatico-facial foramen	
divided temporal squama	
divided zygomatic bone	
external auditory torus/exostosis	
squamomastoid suture	
parietal foramina	
ossicle at lambda	
lambdoid ossicles	
ossicle at asterion	
occipitomastoid ossicle	
mastoid foramen	
inca bone	
coronal ossicle	
ossicle at bregma	
sagittal ossicle	

MORPHOSCOPIC TRAITS

Key: Record based on Hefner (2009)

Trait	Expression
Inferior nasal aperture	
Anterior nasal spine	
Nasal aperture width	
Nasal overgrowth	
Malar tubercle	
Nasal bone contour	
Interorbital breadth	
Postbregmatic depression	
Supranasal suture	
Transverse palatine suture	
Zygomaticomaxillary suture	

POSTCRANIAL NONMETRIC TRAITS

Key: Record as present/absent

Element	Trait	Expression
Atlas	Double atlas facet	
Cervical vertebrae	Transverse foramen bipartite	
Sternum	Sternal foramen	
Scapula	Bridging of suprascapular notch	
Humerus	Supracondyloid process	
	Septal aperture	
Os coxa	Acetabular crease	
	Accessory sacral facets	
Femur	Allen's fossa	
	Poirier's facet	
	Plaque	
	Hypotrochanteric fossa	
	Third trochanter	
Patella	Vastus notch	
	Emarginate patella	
Tibia	Squatting facets	
Talus	Medial talar facet	
	Lateral talar extension	
	Double inferior anterior talar facet	
Calcaneus	Double anterior calcaneal facet	

DENTAL NONMETRIC TRAITS

Key: Record in an ordinal scale following the ASUDAS system

Tooth	Trait	Expression
Incisors	Winging	
	Shovel-shaped	
	Double shoveling	
	Labial curvature	
	Interruption groove	
	Tuberculum dentale	
	Peg-shaped incisors	
Canines	Distal accessory ridge	
	Lower canine root number	
	Bushman canine	
Premolars	Odontome	
	Upper premolar root number	
	Distosagittal ridge	
	Tome's root	
	Lower premolar lingual cusp variation	
Molars	Carabelli's trait	
	Upper molar root number	
	Enamel extensions	
	Hypocone	
	Metaconule	
	Deflecting wrinkle	
	Anterior fovea	
	Tuberculum intermedium	
	Tuberculum sextum	
	Lower molar root number	
	Hypoconulid	
	Groove pattern	

DENTAL WEAR

Key: Record following Smith (1984)

		I1	I2	C	P3	P4	M1	M2	M3
Maxilla	Left								
	Right								
Mandible	Left								
	Right								

POST-MORTEM BONE ALTERATION

Key: Record based on Fernández-Jalvo and Andrews (2016)

Alteration	Type	Element(s) affected	Possible etiology
Linear marks			
Pits and Perforations			
Discoloration and Staining			
Flaking and Cracking			
Corrosion and Digestion			
Breakage and Deformation			

Key: Record based on Andrews and Bello (2006); Bello and Andrews (2006)

Anatomical Preservation Index	
Bone Representation Index	
Qualitative Bone Index	

ISBN 978-9963-2858-4-6

PROMISE

RESEARCH & INNOVATION FOUNDATION

Structural Funds of the European Union in Cyprus